ENGINEERING EXTRACELLULAR VESICLES FOR GENE-MODULATING COMBINATORIAL THERAPIES

A Dissertation

by

YONG-YU JHAN

Submitted to the Office of Graduate and Professional Studies of
Texas A&M University
in partial fulfillment of the requirements for the degree of

DOCTOR OF PHILOSOPHY

Chair of Committee,	Daniel L. Alge
Co-Chair of Committee,	Corey J. Bishop
Committee Members,	Melissa A. Grunlan
	Carolyn L. Cannon
Head of Department,	Michael J. McShane

May 2021

Major Subject: Biomedical Engineering

ABSTRACT

Extracellular vesicles (EVs) have recently attracted much interest as natural therapeutic agents and promising drug delivery systems. They are important cellular mediators for the transport of various cargo and exhibit a homing ability to specific recipient cells. In addition, they have demonstrated immunomodulatory capabilities. While these findings present exciting opportunities for EV therapeutic applications, technical challenges, specifically low production yield of EVs and inefficient cargo loading, are considerable barriers to successful clinical translation. Manipulating EVs using synthetic biomaterials and surface modification techniques can provide strategies to enhance their therapeutic applicability. In this dissertation, research efforts focused on the development of (1) Semi-artificial, lipid-hybridized EVs for gene-modulating siRNA delivery, (2) a Multi-functional EV platform capable of selective co-delivery of siRNA and doxorubicin (DOX) to cancer cells, and (3) Azide-functionalized EVs enabling surface conjugation *via* bio-orthogonal click chemistry.

To enable mass production of the delivery vesicles, cancer cell-derived EVs were incorporated with various lipids using a sonication and extrusion technique to generate engineered EVs (eEV). Particle number characterization revealed this method produced a 6- to 43-fold increase in numbers of vesicles. Lipid to protein ratio and surface protein expression were evaluated to assess the membrane fusion efficiency. Exogenous siRNA was successfully loaded into eEVs *via* electroporation and effective gene silencing was demonstrated in cancer cells.

Next, a polymer layer-by-layer coated EV complex (LbL-eEV) was developed. Successful co-delivery of siRNA and DOX using LbL-eEV was verified by flow cytometry analysis. Cellular internalization efficiency was investigated and the inherent preferential delivery of LbL-EVs to cancer cells was demonstrated.

In addition to engineering EVs for drug delivery, modification of mesenchymal stem cell-derived EVs with bio-orthogonal functional groups (*e.g.,* azide) to enable surface conjugation *via* click chemistry reaction was also studied. Successful modification of EV producer cells with azide and tetrazine reactive groups through metabolic engineering was demonstrated by fluorescent labelling. In summary, these studies demonstrate the surface composition and functionality of EVs can be tuned by multiple approaches, including membrane fusion with lipid-based materials, polymer coating, and natural biosynthetic pathways in cells. This work provided the proof-of-concept that EVs can be engineered to fill the needs of different therapeutic applications.

DEDICATION

To my undergraduate advisors, who encouraged me to go abroad;

and my family, who indulged me with freedom.

ACKNOWLEDGEMENTS

For me, the Ph.D. study isn't about beginning or achieving the success of career. I see it instead as more like a process of finding a space that allows me for self-cultivation and self-reflection in life journey. In 2016, I came to Texas alone, where I knew no one before I landed. I was fortunate to meet many good friends and neighbors during these years. I would like to thank each and every individual that has interacted with me during my Ph.D. period in providing me the professional guidance and emotional support. Without these special people in my life, I would not have been able to continue my study every time I faced a choice. Each of you has contributed to my completion of this dissertation.

I would like to first sincerely thank my committee chair, Dr. Daniel Alge. He is an exceptionally supportive, understanding and caring advisor, who always arranged things with care and by the gentlest way. His guidance and assistance were essential to my completion of this dissertation. Without such a gradual adaptation process for lab transition, I would not have been able to go through it in times of uncertainty. The mentorship from Dr. Alge is like a long-acting medicine, which brought me back to my focus and reassured me to continue moving forward. I would like to thank my committee co-chair Dr. Corey Bishop, who guided me since the beginning of my Ph.D. journey. He always patiently responded to my various questions and doubts, even they were basic. Having worked with Dr. Bishop over the past years, I learned from him of becoming a hard-working researcher while preserving a sense of humor to life. I would also like to thank my committee members, Dr. Melissa Grunlan and Dr. Carolyn Cannon, for their

time and valuable feedback from preliminary exam, yearly meetings, to the final defense. I genuinely appreciate their constant support and encouragement to me during these years.

I would also like to express my gratitude to all my colleagues who gave me inputs on my projects and supported me as friends: Shreedevi Arun Kumar, Samantha Holt, Sara Abasi, Thomas Tigner, Kanwar Abhay Singh, Giriraj Lokhande, Aparna Murali, Navaneeth Krishna, Kaivalya Deo, Ping Dong, Jun Ma, and Patrick Lee. Thanks also to many undergraduate students who worked in labs day and night together: Amanda Rakoski, Guillermo Palou Zuniga, David Hendrix, David Mitchell Moore, and many others in Pharmacoengineering Lab. I am especially grateful to all lab mates in Alge lab, who created such a welcoming environment for me. The lab has become my second home in the last year. I also want to thank Amanda Myatt as the lab manager, who provided tremendous technical support for all the equipment in the shared labs.

Special thanks to my friends outside of the lab who indirectly helped me through my Ph.D. period: Amy Pan, my best roommate, who always lent a listening ear and gave me the most understanding and support for not only my career but also my personal life. Szu-Ting Kuo and Candice Chu, my graduate companions, who always provided me comic relief and urged me to move on regardless what happened. Thanks also to many other friends who accompanied me through ups and downs: Chia-Chen Hsu, Ga-Yo Huang, Jen Hua Chuang, Yu Jou Lin, Hsiao Chien Cheng, Justine Chu, Annie Hsiao, Ya-Shan Lee, Chia-Ling Chang, Carol Chen, Ya-An Chang, Class 102, Kidland08, running club, former lab mates and many others that I am unable to acknowledge them all here. The friendships from them sustained me throughout the time I felt overwhelmed and

helped me to overcome challenges. Thank you all for the words of encouragement along the way. These are precious to me.

My deepest gratitude goes to my undergraduate advisors, Dr. Ruey-Yug Tsay and Dr. Chun-Min Lo, for being such helpful mentors and giving me enormous support since I was a freshman. Their steadfast belief in me, enables me to cross the finish line of Ph.D. study and is partly the reason the person I am today. I cannot envision the endeavor I would have to spend without their advice and encouragement. I would also like to thank Professor Je-Chin Han and his wife Mrs. Su Han devoted their time to motivate Taiwanese students at Texas A&M with various topics. Their kindness and generosity have lightened up my life in College Station.

Last of all, I truly thank my family, my parent and my brother. Though having little knowledge of my work, they trusted me in every decision. Despite 8000 miles away from Taiwan, the shape of home has become vivid in my mind throughout my time here. The fact is that all of you are irreplaceable to me. Thanks also to my cousin, Yide, who shared similar perspectives with me and always cheered me up at moments I questioned my own abilities. I am also deeply grateful for my loving grandma who insisted to pick me up and drop me off every time I travelled. When I felt frustrated, I thought of her voice and laugh. If I ever had courage and optimism instilled in me, they must come from her. Looking back the past few years, the completion of this journey could not have been possible without the help of so many people. I appreciate the time, effort, and dedication from people around me. These have all become my tender memories and embodied me a truer self. And I finally come to an understanding of the books I read before: “The

immense support from people is incalculable, thus, let's extend the gratitude to the entire universe." Thank you, the world, for letting me know the power of understanding and the strength of gentleness.

CONTRIBUTORS AND FUNDING SOURCES

Contributors

This work was supervised by a dissertation committee consisting of Professor Daniel Alge [chair], Dr. Corey Bishop [co-chair] and Professor Melissa Grunlan of the Department of Biomedical Engineering and Professor Carolyn Cannon of the Department of Microbial Pathogenesis and Immunology.

The nanoparticle data analyzed for Chapter 2 and Chapter 3 were conducted in part by undergraduate students Guillermo Palou Zuniga, Daniel Prasca-Chamorro, and David Mitchell Moore of the Department of Biomedical Engineering. The flow cytometry data in Chapter 2, Chapter 3, and Chapter 4 were facilitated by use of the BD Accuri^{TM} C6 in Professor Akhilesh Gaharwar Lab with the help from Kanwar Abhay Singh.

All work for the dissertation was completed by the student, under the advisement of Professor Daniel Alge and Dr. Corey Bishop of the Department of Biomedical Engineering.

Funding Sources

Graduate study was supported in part by the government scholarship from Ministry of Education in Taiwan and this work was made possible by the Department of Biomedical Engineering. Its contents are solely the responsibility of authors and do not necessarily represent the views of the institutions.

NOMENCLATURE

3T3	A cell line of mouse embryonic fibroblast cells
A549	A cell line of adenocarcinoma human alveolar basal epithelial cells
AAV	Adeno-associated virus
CCL-210	A cell line of human normal lung fibroblast cells
DBCO	Dibenzocyclooctyne
DLS	Dynamic Light Scattering
DMSO	Dimethyl Sulfoxide
DOTAP	1,2-dioleoyl-3-trimethylammonium-propane
DPPC	1,2-dipalmitoyl-sn-glycero-3-phosphocholine
EDC	1-ethyl-3-(3-dimethylaminopropyl) carbodiimide hydrochloride
EV	Extracellular Vesicle
aEV	azide-functionalized Extracellular Vesicle
eEV	engineering Extracellular Vesicle
EthD-1	Ethidium homodimer-1
FBS	Fetal Bovine Serum
GFP	Green Fluorescence Protein
hMSCs	human Mesenchymal Stem Cells
ILV	Intraluminal vesicles
LbL	Layer-by-Layer Deposition
LbL-eEV	Layer-by-Layer-coated eEV
miRNA	microRNA

ManNAz	N-azidoacetylmannosamine-tetraacylated (Ac4ManNAz)
MFL	Membrane Fusogenic Liposome
MVB	Multivesicle bodies
nGMFI	normalized Geometric Mean Fluorescence Intensity
NaAC	Sodium Acetate
NHS	N-Hydroxysuccinimide
NTA	Nanoparticle Tracking Analysis
OD	Optical Density
PAA	Poly(acrylic acid)
PBAE	Poly(β-amino ester)
PBS	Phosphate Buffered Saline
PEG	Polyethylene Glycol
POPC	1-Palmitoyl-2-oleoyl-sn-glycero-3-phosphocholine
POPG	1-Palmitoyl-2-oleoyl-sn-glycero-3-phosphoglycerol
PVDF	Polyvinylidene Fluoride
RNAi	RNA interference
siRNA	short interfering RNA
shRNA	short hairpin RNA
SPV	Sulfo-Phospho-Vanillin
TCO	Trans-Cyclooctene
TEM	Transmission Electron Microscope
Tz	Tetrazine

TABLE OF CONTENTS

Page

LIST OF FIGURES

Page

LIST OF TABLES

Page

1. INTRODUCTION

1.1. Overview of Extracellular Vesicles: Composition and Biogenesis Mechanisms

Extracellular vesicles (EVs) are small lipid membrane-based vesicles secreted by cells. They have been originally thought to be a collection of cellular wastes from the endocytosis and exocytosis processes. A landmark study published by Valadi *et al.* in 2007 showed that various RNA (coding and non-coding RNA) and protein messages can be transported between cells *via* EVs,[1] drawing attention to EVs as intercellular communication tools. A number of studies further proved that EVs play pivotal roles in genetic information transfer, signal transduction, and modulation of immune responses.[2-4] Since then, research focus on EVs further shift towards the development of EV- based therapeutics or drug delivery platforms.[5-8]

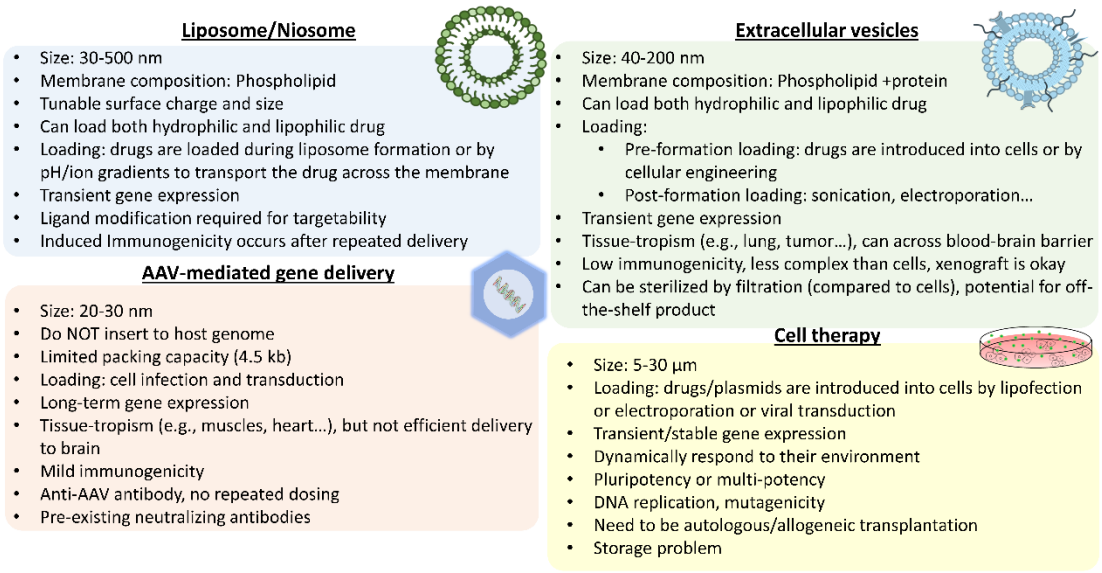

Figure 1.1 Comparison between extracellular vesicles, liposome/niosome, adeno-associated virus, and cell-based therapies.

There are several advantages of EVs over other systems (**Figure 1.1**): It has been found that these self-derived vesicles are generally low toxicity in tissues due to their biological origin. They have been identified as active components of cell's secretomes, thus implicating their therapeutic potential as a possible alternative to whole cell therapy for tissue engineering applications. Because EVs lacks the ability of *in vivo* replication, it can be exploited as cell-free therapy to avoid the safety concern from the whole cell therapy. It is also amenable for filtered sterilization to meet the FDA regulatory requirements, given the potential to be stored as an off-the-shelf product. In addition to their many advantages over cell therapy, EVs are also considered as competent drug delivery carriers. They have been found to possess unique biological functions compared to other synthetic carriers. For example, they have an extraordinary ability to interact with recipient cells and may present specific organotrophic targetability,[9] tissue penetration ability, and capability to cross blood brain barrier. Heusermann *et al.* demonstrated that exosomes entered recipient cells as single vesicles within minutes without accumulation at the cell surface, whereas cationic liposomes firstly accumulated into islands at the cell surface and subsequently endocytosed after a few hours.[10] Liang *et al.* suggested that the soft and deformable bio-mechanical features of EVs result in the capability to extravasate across leaked tumor vessels and tissues.[11] In addition, it is found that EVs can avoid uptake by the reticulo-endothelial system (RES) by exhibiting the surface protein CD47. These intrinsic properties of EVs can potentially compensate for the drawback of current drug

delivery systems and provide advantages over the synthetic nanocarriers. Through the natural processes of endogenous cellular machinery to sort the desired cargo inside EVs or a series of post-EV isolation modification process, it is feasible to manipulate the loading of cargo in EVs. This feature of EVs is especially favorable for nucleic acid and protein-based cargo loading compared to other synthetic systems, due to the sensitivity of cargo to solvent and enzymatic degradation in the manufacturing processes of synthetic carriers.

In the past few years, the potential of EVs has been heavily focused on gene therapy, which has become a revolutionary therapeutic strategy to treat numerous diseases and possibly cure in certain cases,[12] such as monogenic disorders (*e.g.,* cystic fibrosis,[13] bone marrow disorders[14]) or other chronic diseases caused by the presence of genetic mutation (e.g., cancer[15]). Transferring genes is proposed to correct, replace, supplement, or inhibit the transcription or translation of aberrant gene expression in a temporary (*e.g.,* non-viral[16]) or permanent manner (*e.g.,* viral-based,[17, 18] or CRISPR/Cas9-[19] or DNA-based[20]). Studies to date have employed various methods− viral vectors and non-viral strategies to deliver genetic materials to the cells of interest. While adeno-associated virus (AAV) has recently become the most popular viral vectors as new emerging clinical therapeutics, the high prevalence of neutralizing antibodies against AAV capsid in human population is a concern.[21, 22] Because EVs' inherent capability of carrying microRNA, they have received much attention as not only their natural characteristics, but a possible alternative for non-viral gene delivery.

While EVs have been demonstrated to be a promising tool for therapeutic treatments, how to choose and design a best EV carrier to achieve effective therapeutic effect remain elusive. Increasing knowledge of EV formation/release and their physiological relevance will help gain further insights into potential translation. Therefore, at the beginning of this chapter we summarize current knowledge of EV categories and biogenesis. Then we discuss the selections and state-of-art strategies of engineering EVs for therapeutic applications. The pros and cons of different methods and recent studies in the use of EVs as drug delivery platforms are included. Understanding factors tailoring the functionality of EVs will be the key to successful utilization for clinical applications. Of note, despite both prokaryotic and eukaryotic cells can secrete EVs, since prokaryotic bacterial EVs are likely to exist virulent factors, leading to a great immune response and infection in human body,[23] in this study we only focus on mammalian cells-derived EVs.

1.1.1. Nomenclature of Extracellular Vesicles

The term "extracellular vesicles (EVs)" is referred to the location of which are released outside of the cells. In general, the sizes of EVs are between 30-5000 nm in diameter. The structure and membrane composition of vesicles vary from different types of vesicles (**Figure 1.2**). There are several ways for classifying vesicles, which could be categorized by size, density, biogenesis, cell origin, and so on.[24] It is worth noting that EVs are highly heterogeneous that even in the same category of vesicles, a cell may release subtypes of vesicles containing various cargos and components, which rely on the cell type and the cell condition (*i.e.,* physiological, pathological status). The general accepted classification of EVs is divided into three categories, exosome, microvesicles (ectosome),

and apoptotic bodies, based on their distinct subcellular origin. Briefly, exosomes and microvesicles (ectosomes) show a partial overlapping of their size distribution. While ectosomes are released outward directly from the cell membrane, the exosomes are produced within the accumulation of intraluminal vesicles (ILVs), a group of inward budding vesicles inside the cell at late endosomal maturation, and they are released upon exocytosis from multivesicular endosomes (MVE). On the other hand, apoptotic bodies are vesicles generated during the apoptosis process of a cell. As a result of apoptosis, the vesicle population is more heterogeneous and usually with a larger size distribution compared to the other two.

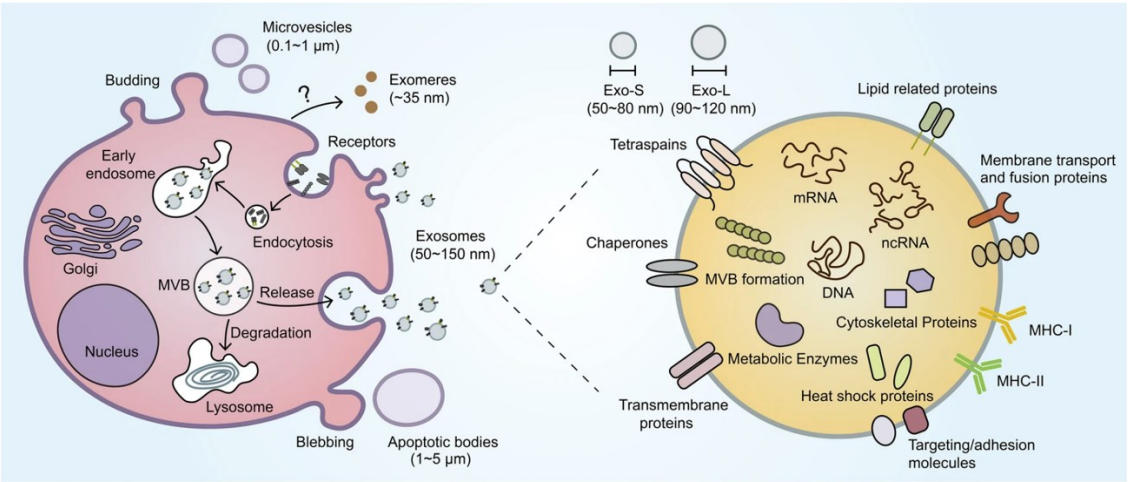

Figure 1.2 Biogenesis and composition of EVs. Reprinted with permission from © 2020 Springer Nature from Zhou *et al*.[25]

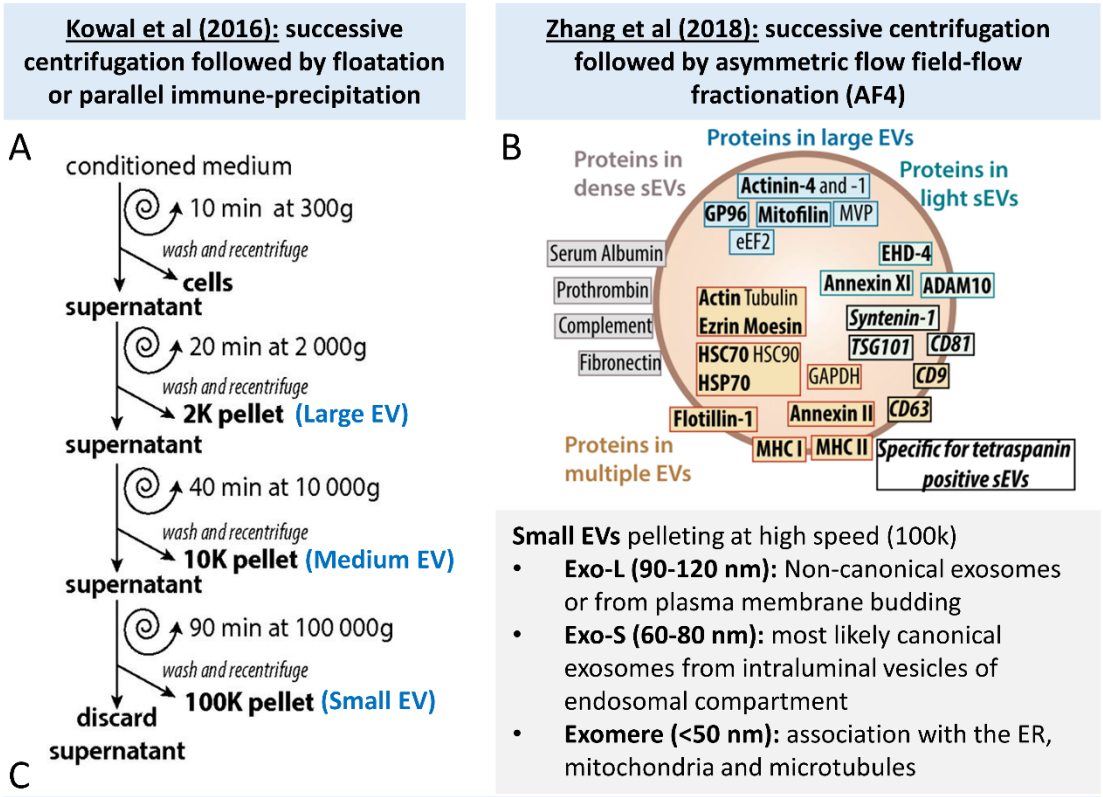

Nomenclature of Extracellular Vesicles and Nanoparticles

Name	Category	EV class	Size	Typical sedimentation	Protein Markers	Biogenesis
Classical exosome	Exosome	Small EV[a]	40 - 150 nm	100,000 - 200,000 × *g*	CD63 (CD81 CD9)	Multivesicular endosome
Non-classical exosome	Exosome	Small EV	40 - 150 nm	100,000 - 200,000 × *g*	(CD63- CD81- and CD9-negative)[c]	Multivesicular endosome
Classical microvesicle	Microvesicle	Large EV[b]	~ 150 - 1000 nm	10,000 - 20,000 × *g*	Annexin A1 (ARF6 Annexin A2?)	Plasma membrane budding
Large oncosome	Microvesicle	Large EV	1 - 10 µm	10,000 × *g*	Annexin A1 (ARF6 Annexin A2?)	Plasma membrane budding
ARMM	Microvesicle	Small EV	~ 40 - 100 nm	100,000 - 200,000 × *g*	ARRDC1 (TSG101)	Plasma membrane budding
Apoptotic body	Apoptotic EV	Large EV	1 - 5 µm	1,000 - 10,000 × *g*	Annexin V (PS exposure)	Apoptosis
Apoptotic vesicle	Apoptotic EV	Small to large EV	~ 100 - 1000 nm	10,000 - 200,000 × *g*	Annexin V (PS exposure)	Apoptosis
Autophagic extracellular vesicle	Autophagic EV	Small to large EV	40 - 1000 nm?	10,000 - 200,000 × *g*	LC3B-PE, p62	Unknown but autophagy-related
Exomere	Nanoparticle	Non-EV	~ 35 - 50 nm	100,000 - 200,000 × *g*	HSP90, HSPA13	Unknown
NV fractions	Nanoparticle	Non-EV	? (vaults: ~ 70 nm)	100,000 - 200,000 × *g*	Fibronectin, Histones, MVP, HSPA13	Unknown

EV, extracellular vesicle; ARMM, arrestin-domain-containing protein 1 (ARRDC1)-mediated microvesicle; PS, phosphatidylserine; NV, non-vesicular
[a]Small EVs are <200 nm in diameter; [b]Large EVs are >200 nm in diameter; [c]Hypothetical exosome not expressing CD63, CD81 and CD9

Figure 1.3 Nomenclature and classification of EVs.[26-28] Adapted with permission from © 2016 PNAS and ©2019 Elsevier from Kowal *et al.*[26] (A, B) and Jeppesen *et al.*[28] (C), respectively.

Due to the challenge to demonstrate the EVs' intracellular origin after isolation, the term of exosome in published literature is mostly used for the small vesicles collected from ultracentrifugation. On the other hand, large EVs generally are referred to plasma

membrane derived EVs, microvesicle. However, this may cause a lack of clear understanding on the specific functionality of each EV subtypes during data interpretation.[26] Because EVs share similar biophysical characteristics (size, density, and membrane orientation) in wide ranges, centrifugation techniques based on the size or density cannot identify and separate EV subtypes efficiently. In 2016, Kowal, J *et al.* detailed the sub-categorization of EVs by successive centrifugation followed by floatation or parallel immune-precipitation.[26] In their studies, large EVs, medium EVs, and small EVs were firstly isolated from the pellets by centrifuge speed 2k, 10k and 100k, respectively (**Figure 1.3**). A comparative analysis of the protein composition of all EVs were subsequently analyzed. Surprisingly, the classic exosome markers (*e.g.,* tetraspannin protein CD63, flotillin-1, heat-shock protein HSC70/HSP73) were not only abundant in the small EVs (100k speed) but were also detected in other EVs. 4 sub-categories of small EVs were therefore further defined by different relative abundance of proteins in distinct EV populations, and only small EVs enriched in CD63, CD9 and CD81 were identified as the canonical exosome in this study. Their investigations showed multiple markers are required for classifying the EVs' biogenesis and secretion pathways.

In addition to the difference of intracellular origins in EV subtypes, it is worth noting that there are other intracellular budding events commonly co-precipitated by ultracentrifugation, including granules, lipoproteins, or exomeres.[29] In 2018, Zhang, H *et al.* was the first to fractionate these mixtures to two exosome subpopulations (Exo-L: 90-120 nm and Exo-S: 60-80 nm) and a non-membranous nanoparticle termed "exomeres" by employing asymmetric flow field flow fractionation (AF4) (**Figure 1.3**).[27] The

presence of transmembrane proteins or glycosylphosphatidylinositol (GPI)-anchored proteins on EVs was suggested to be used as the standard marker to demonstrate the lipid-bilayer structure of EVs. The authors further conducted a comprehensive analysis of the proteomic content and lipidomic content in these subpopulations. Exo-S enriched in proteins associated with endosomes, was confirmed to be the canonical exosomes from intraluminal vesicles of endosomal compartments, while Exo-L enriched in cell-cell contact/junction proteins may represent the non-canonical exosome or plasma membrane budding microvesicles.

In addition to the above 2 proposed classifications for EV subcategories, Jeppesen DK *et al.* in 2019 further improved methodology for EV isolation by density-gradient fractionation, followed by directly immunoaffinity. Precise determination of the molecular composition of classical exosome and shedding microvesicles were shown in this study (**Figure 1.3**).[28]

These recent investigations on EVs' categories suggested that high quality characterization of the isolated samples with multiple analytical methods are required to further distinguish EV subtypes. Therefore, in the most recent MISEV2018 guidelines for EV studies, instead of using the term of "endosome-origin exosome" or "plasma membrane-derived ectosomes (microvesicles)", the ISEV board recommended the researchers use of operational terms for EV subtypes that refer to physical characteristics (*e.g.,* size or density) or biochemical composition (CD63+, CD81+) of EVs. For example, small EV is referred to size < 200 nm and isolated by ultracentrifugation at > 100000g speed.[30] While the real categories of EVs remains to be explored, we summarized the

common feature and biogenesis pathways for the classic classification of exosomes and shedding microvesicles (ectosomes) in the below sections.

1.1.2. Exosomes

Exosomes are referred to the vesicles with a size range of 30-150 nm derived from the late endosomal processes. In general, there are three stages for the formation of exosomes. (1) At initial, transmembrane proteins and plasma membrane are endocytosed to form an early endosome. (2) During endosomal maturation, the endosomal membrane undergoes inward budding, forming several intraluminal vesicles (ILVs) inside the endosome. (3) This resulting late endosome containing ILVs, also termed as multivesicle bodies (MVBs), would either fuse with lysosome for a degradation pathway or fuse with plasma membrane for releasing intraluminal vesicles as exosomes to extracellular space. During the classical processes of endosomal maturation, the release of exosomes may happen in a delayed timing. The vesicles are accumulated in late endosome and are released in sometime after endocytosis. It is reported the release of exosomes might not be necessarily dependent on exterior stimulation on the cell, instead, it is believed to be constitutively released.[31]

To go in depth the biogenesis pathway of inward budding vesicles, two distinct pathways have been identified as the process of ILV formation, which can be mainly categorized into two classes that are reviewed in Abels and Breakefield (2016) (**Figure 1.4**):[32] 1.) Endosomal Sorting Complex Required for Transport (ESCRT) dependent pathway: The formation of ILVs through this pathway requires ESCRT family proteins and ESCRT associated proteins (ALIX, TSG101, Chmp4 and SKD1) to form MVBs. The

incorporation of transmembrane proteins into ILV occurs by protein ubiquitination or protein-protein interaction (Syndecan-syntenin-ALIX). In this pathway, the ESCRT family proteins recognize these ubiquitinated proteins and are recruited to the early endosomes to drive the intraluminal membrane budding. 2.) ESCRT independent pathway: Although ESCRT pathway is generally believed to be the main initiator of exosome biogenesis, the exosomes can be produced in parallel to the ESCRT pathway by the presence of certain lipids. It has been found the sphingolipid ceramide generated by sphingomyelinases (nSMAse-2) can facilitate the membrane invagination of ILVs. The presence of phosphatidylethanolamine and MVB acidification by pH modulation are also critical factors controlling the secretion of exosomes.

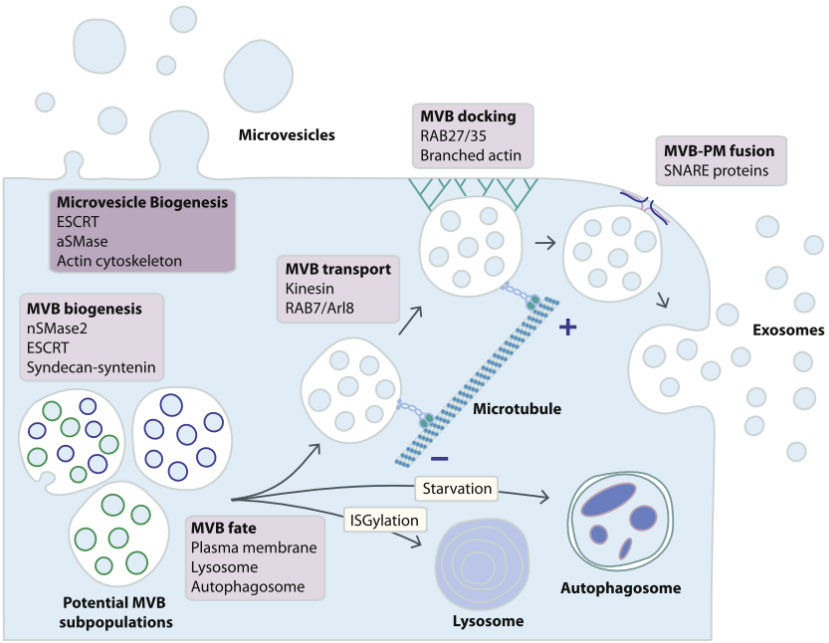

Figure 1.4 Biogenesis pathway of exosomes and microvesicles. Reprinted from an open access article from Bebelman et al.[33]

By engineering the above biogenesis pathways, it is most likely a higher number of ILV-derived exosomes can be obtained. However, the proteins/lipids involved in these pathways are not exclusive to exosome biogenesis, but may also be detected in plasma membrane-derived microvesicles.[29] In the recent publication from Mathieu *et al.,*[29] and Zhang, H *et al.,*[27] the characterization of tetraspanins CD63, CD9, and CD81 all together is proved to be necessary to identify classical exosome from intraluminal vesicles of endosomal compartment. The lipids on exosomal membrane include cholesterol (high concentration, 40-50% of exosomal lipids), sphingomyelin (SM, 2.5-fold increase compared to the plasma membrane, 10-30 % of exosomal liposome), phosphatidylserine (PS, 2-fold increase compared to the plasma membrane, 5-10% of exosomal liposome), glycosphingolipids (1.8-fold), and ceramide (role in budding).[34, 35] In contrast, the increase of these lipids come at the reduce of phosphatidylcholine lipid (PC). The types of membrane proteins usually are surface adhesion protein (integrins), transport and fusion proteins (*e.g.,* annexins, flotillin, GTPase), tetraspanins (*e.g.,* CD61, CD63, CD81, and CD82), heat shock proteins, components of late endosomal machinery (TSG101, Alix, the ganglioside GM1),[36] etc. While the microRNA and long non-coding RNAs enriched in exosomes represent the physiological and pathological states of the cells and serve as specific disease biomarkers, many of the presumed components in exosomes have been evident to be absent in the classical exosome by Jeppesen *et al.*[28] For example, double strand DNA (dsDNA) and the associated histone was previously reported in certain

exosomes.[28] However, it has been demonstrated the presence of extracellular dsDNA is more likely the co-precipitated contaminants due to the limit of isolation technique.

1.1.3. Shedding Microvesicles

In contrast to exosome, shedding microvesicles (ectosomes) are generated from outward budding of plasma membrane with a size distribution of 150-1000 nm diameter. The phenotype of MVs also reflects their parent cell as well as exosome, and the content of the vesicle cargo also includes membrane and cytosolic proteins, mRNA, and miRNAs.[37] Note that the larger the EV is, the more likely molecules or organelle in the cells would be incorporated in the vesicle during the membrane budding process. Therefore, Golgi, endoplasmic reticulum and mitochondrial or nuclear component may exist in large EVs, but less likely present in small EVs or exosome.[30] Contrary to the biogenesis of exosomes, ectosomes are generated by assembling in the cell membrane at a fast rate. The vesicles can be released within a few minutes. Further, the formation rates increases with specific cell stimulation, for example, activation of cell surface receptors.[38] Ectosomes have been predominantly characterized as cell products of endothelial cells and platelets. Their biological functions include procoagulant activity, proinvasive properties of tumors.[38] Like exosomes, microvesicles can also be generated *via* several mechanisms. For example, ESCRT family (ESCRT I/II/III) is also involved in the process of plasma membrane budding. Additionally, these microvesicles can be released by actin cytoskeleton rearrangements. The enrichment of specific lipids, for example, phosphatidylethanolamine (PE) and phosphatidylserine (PS), may also lead to the shedding of microvesicles from specific plasma membrane location.[39] Interestingly,

microvesicle is considered to be a sign of cancer invasion and metastasis, which is frequently secreted by high aggressive cancer cells.[33] While the characterization of microvesicles is less defined than the exosome, Jeppesen *et al.* has identified Annexin A1 as a specific marker of microvesicles distinct from exosomes that Annexin A1-positive vesicles were observed to bud directly from the plasma membrane and are absent from classical exosome.[28] Haraszti *et al.* also showed the protein composition differed substantially between exosomes and microvesicles using a proteome analysis.[40]

On the other hand, apoptotic vesicle is the other type of shedding ectosomes with a large size range of 500-4000 nm in diameter. Apoptotic vesicles are formed from blebbing of the plasma membrane in cells during apoptosis, releasing the apoptotic bodies, which contain fragmented DNA, organelles, proteins from parent cells.[37] The key functions of these vesicles have been found to horizontal transfer oncogenes or DNA, inducing the presentation of T cell epitopes upon uptake by phagocytic cells or representation of B cell autoantigens.[41] Hence, it has been found the uptake of apoptotic vesicles may lead to immunosuppression.[42] While it is difficult to distinguish the EVs based on their content, protein-to-lipid ratio has recent been proposed as an alternative standardization for EVs.[43] Apoptotic bodies exhibit the highest protein-to-lipid ratio, followed by microvesicles and then exosomes.[44]

1.2. Therapeutic Potential of Extracellular Vesicles: Producer Cell Source Selection

It is known that the phenotype of EVs and the content inside the vesicle reflect their parent cells and are largely dependent by the releasing cell type and the corresponding cellular stimuli. When choosing the producer cell for different therapeutic

purpose, the immune-regulation and preferential delivery from the cells are the 2 foremost properties should be concerned. Knowing the native properties of EVs associated with different cells would allow us to better utilize these knowledges for therapeutic applications. Here, we mainly discussed small EVs (mostly exosome)-based drug delivery system for therapies because shedding microvesicles and apoptotic bodies used for therapeutic applications are less reported.

1.2.1. Immuno-regulation: Suppression or Activation

It is widely accepted that EVs are likely to be minimally reactive to the immune system for prolonged circulation time, due to their biological origin. Several studies have demonstrated the safety and non-immunogenicity of EVs for administration in humans. However, EVs, especially exosomes, has been found to be able to modulate the innate and adaptive immunity.[45-47] Zitvogel *et al.* firstly showed in 1998 that exosomes secreted from APC cells not only express tumor antigens but also present functional MHCI, MHC II and T-cell costimulatory molecules (CD80 and CD86) on the exosomal surface. This unique feature have been shown to prime specific cytotoxic CD4+ and CD8+ T cells *in vivo*, resulting in inhibition of established tumor growth.[48] Generally, EVs derived from antigen presenting cells, such as B cells, macrophages and dendritic cells[49-51] are able to stimulate immune response. The expression of MHC I and MHC II, which preferentially induce Th1 type (cell-mediated) immune response would direct T cells to attack abnormal cells or infected.[52] These types of EVs could be developed as cell-free vaccines. For example, exosomes derived from dendritic cells are particularly suitable for immunotherapy of

cancer diseases. In addition, tumor-derived EVs containing tumor antigens in combination with adjuvants have also been exploited to activate immune response.[53, 54]

It is worth noting that EVs from the same origin of the cells may be exploited with opposite immune-regulation purposes. For example, immune cells can potentiate immune response but can also maintain immune homeostasis, depending on the cell source obtained and the cell condition. Veerman *et al.* detailed summarized the immune-modulation properties of immune cell-derived EVs.[55] It is suggested that EVs derived from immature immune cells exhibit the immunosuppressive capacity, which can be used in transplantation therapy for the prevention of allograft rejection. For example, EVs derived from immature dendritic cells show a reduced expression of MHC complexes, co-stimulatory molecules and ICAM molecules, result in immune-inhibitory functions and significantly prolonged survival of C57BL6 mice after transplantation.[56] EVs contain LFA-1, ICAM-1 and carbohydrate binding C-type lectin receptor have been found to interact with brain vessel endothelial cells with immune-suppressive properties.[57] Therefore, the control of the parental cells' condition/source is critical for the clinical translation of EVs to mediate the immune response.

In addition to the immune-activation and suppression capabilities of EVs, EVs have also been used as drug delivery carriers with low immunogenicity. Despite dendritic cell derived-EVs have also been developed for RNAi delivery to brain with low immunogenicity *in vivo*,[58] non-immune cells derived EVs are more commonly exploited as cargo delivery vehicles, because they do not present strongly immune-stimulation tendency. Stem cell-derived EVs (*i.e.,* hMSC derived-EV) are especially widely used as

candidates for drug delivery platform because hMSC can be easily obtained from a variety of tissue sources. They have been found to be less immunogenic than their parental cells due to a lower presence of MHC molecules on the exosome membrane.[59]

While the prior addressed examples induce immune-activation or avoid the immune surveillance by surface composition on EVs, certain type of EVs and their cargo have been found to present immunomodulatory function. EVs derived from stem cells or progenitor cells have been found to possess desirable therapeutic contexts and act as paracrine mediators for tissue regeneration. Pre-clinical studies based on hMSC EVs suggest that EVs-MSCs possess a potent immunoregulatory capability on macrophage and lymphocytes in models of cardiovascular, neurologic and renal injuries.[60] Those EVs are effective to reduce activation, oxidative stress, chemokine receptor expression and pro-inflammatory cytokines on M1 macrophage, and subsequently switch M1 to a M2 phenotype.[61] Kim *et al.* also performed comparative molecular profiling of MSC EVs and demonstrated TGF-β1, PTX3, let-7b-5p and miR-21-5p are key effectors mediating the immunomodulatory function of EVs. Another example is the reflection of M1 or M2 macrophage status on the characteristics of macrophage derived EVs. While M1 macrophage-derived EVs has been shown to promote an inflammatory immune response,[62] the M2 macrophage-derived EVs was demonstrated to promote the progression of tumor cells.[63]

1.2.2. Site-specific Selectivity

The innate capability of EV being transported to specific recipient cells is very attractive for drug delivery purpose. However, the understanding of exosome selective

trafficking and communication mechanisms remain elusive. It is uncertain whether all the EVs transport to the tissues and recipient cells with selectivity. In the following sessions, the site-specific selectivity of EVs was discussed by the tissue-scale delivery *via* different administration routes and cell-scale preferential uptake by *in vitro* mammalian culture.

1.2.2.1. Tissue Scale

A number of studies have investigated the pharmacokinetics of exogenously administered exosomes by labeling lipophilic fluorescent or radioactive dyes to exosomes for *in vivo* tracking.[64] It has been postulated that exosomes may avoid the pitfalls of synthetic nanoparticles and prolong the circulation after administration. However, many studies have observed rapid clearance of EVs by liver and spleen after intravenous administration. A resemblance of biodistribution and clearance of exosomes (derived from adenocarcinoma MCF-7, carcinoma 4T1, and prostate adenocarcinoma PC3 cells) to the PC: Cho liposome formulation was demonstrated by Smyth *et al.* with intravenous injection to a tumor bearing mouse model.[65] Both the exosomes and liposomes predominantly accumulated in the liver and spleen at 1hr post-injection, while no significant accumulation of exosomes than liposomes was observed in the tumor tissue. Takahashi *et al.* further investigated the delivery of exosomes from 5 different mouse cells including B16BL6 melanoma, C2C12 myoblast cells, NIH3T3 fibroblast, aortic endothelial cells and RAW264.7 macrophage to naïve mice model. Surprisingly, the *in vivo* imaging revealed a half-life of only 2-4 min. rapid elimination of exosomes in blood circulation. This phenomenon was also validated to be irrespective of the exosome labeling methods.[66, 67] The immunofluorescent staining further showed the exosome were

taken up by F4/80+ macrophages in the liver and spleen, which was consistent with the other observations of delayed exosome clearance in macrophage-depleted mice.[68] These findings indicate the macrophages plays a key role in the clearance of exogenously administered exosomes.

While intravenous injection of most EVs results in a higher accumulation in liver and spleen, another studies from Peinado *et al.* found the exosomes derived from highly malignant B16-F10 preferably localized in lung and bone marrow (24 hr. after intravenous injection) compared to the exosomes from other normal cell lines, indicating the tumor exosomes may alter the organotropic sites.[69] Moreover, these B16BL6 exosomes were confirmed to be taken up by the endothelial cells in the lung instead of macrophage.[68] On the other hand, although intravenous injection of exosomes had no greater accumulation in tumor than liposome, a significant greater degree of exosome accumulation in tumor than liposome was observed when delivered the formulation intratumorally.[69] The exosomes loaded with doxorubicin injected intratumorally also resulted in a greater retention and suppressed tumor growth better than the PC:Chol liposomes.[69] In addition to the EV preferential uptake by intratumorally delivery, another example of the different biodistribution was demonstrated by Wiklander *et al.* In contrast to the intravenous injection, the intraperitoneal and subcutaneous administration of HEK293 EVs resulted in higher accumulation in pancreas and gastrointestinal tract. The highest total accumulation of EVs in tissues was observed by intraperitoneal injection.[70] Munagala *et al.* demonstrated that administering bovine milk-derived EVs to *in vivo* mice model *via* oral gavage route resulted in an uniform tissue distribution within liver, lung, kidney, pancreas,

spleen, ovaries, colon and brain, whereas the EVs predominated resided in the liver *via* intravenous injection.[71] These results suggested the different administration routes would influence the EV distribution pattens. Moreover, it was also corroborated that a higher dose of EV resulted in a wider biodistribution profile in multiple organs.[72] Additionally, it has been found bone marrow derived-mesenchymal stem cell (MSC) EVs would preferentially accumulate in the pathological brain by inflammation-driven after intranasal administration, and thus were used for neurodegenerative studies in Alzheimer's and autism model mice.[73] While the innate tropism of EVs with different cell types and the biodistribution mechanisms of EVs remain to be explored, the above findings suggested EVs are likely to be more useful as a local administered formulation than the systemic administration for tissue-specific delivery purpose.

1.2.2.2. Cell Level

Despite the pharmacokinetics of EVs in organs seems to be non-selective in systemic circulation and largely depends on the reticuloendothelial (RES) system, increasing studies have proved the selective uptake of EVs by *in vivo* local administration or *in vitro* cell culture.[74] While the internalization of EVs can be influenced by the phagocytic activity of recipient cells,[75] many studies demonstrated EVs may exhibit preferential uptake in the same cell types, also called homing capability.[76-78] The targetability of EVs towards tumor cells has especially drawn a great deal of attention from researchers.[79] Toda Y *et al.* demonstrated the strong cell tropism of glioblastoma-derived exosomes (U251) to their parental cells (U251) than other cell lines.[76] EVs derived from mantle cell lymphoma (MCL) also showed a preferentially uptake by their parental

cells B lymphocytes.[77] Albero *et al.* used hollow gold nanoparticle (HGN, 40 nm) as a tool to confirm the internalization of EVs between cells.[80] By incubating the nanoparticles with certain parental cells, HGN-loaded EVs were secreted from these cells and subsequently delivered to different cell lines (MSC, monocyte, tumor (B16-F1) and metastatic (B16-F10)). In this study, the time-lapse imaging demonstrated the EVs would be preferentially uptake by the same cell line and not by other cells present in the proximity under co-culture conditions. Similar results were also obtained by Qiao *et al*. The cell specificity of exosome localization matched the cell of origin for both *in vitro* and *in vivo* model of mouse tumor-derived exosomes.[81] Although the EVs delivered by intravenous injection predominately present in the liver, Qiao *et al.* demonstrated the EVs from the same type of cancer (HT1080) colonized to the tumor site in a greater degree than the EVs from other cell types.[81] Another studies from Xu *et al.* used Design of Experiments (DOE) to investigate the factors affecting the EV uptake properties in pancreas cancer cell line (PANC-1).[82] Their results suggested that PANC-1 cells prone to internalize more EV particles with increasing time or doses, regardless of EVs' origin. However, preferential uptake of their daughter EVs became more significant after longer incubation time (12 hr. and 24 hr.) or at a higher dose ($> 3.6\times10^{10}$ per 30,000 seeding cells).[82]

It is postulated the protein compositions on exosomal membrane influence the selective cellular uptake. Rana *et al.* evaluated the *in vitro* and *in vivo* uptake profiles by delivering 4 exosome types from rat pancreatic cancer cell BSp73AS with various tetraspanin expressions (naïve EVs, transfected with Tspan 8, chimeric Tspan 9, Tspan8 plus β4).[83] EVs with distinct exosomal tetraspanin-complexes resulted in different tissue

accumulation after intravenous injection. While Tspan8 expressing EVs were present in pancreas, spleen and large vessel, the Tspan 8-β4 expressing EVs preferentially bound to peritoneal exudate cells, lung and kidney tissues. Another study also evident the attachment of EVs on dendritic cells is by the association of the adhesion molecules (CD11a, CD54 and integrin $\alpha_v\beta_3$) on dendritic cells and the tetraspanins (CD9 and CD81) on the exosomes.[84] In addition to the transmembrane protein tetraspanin, Hoshino *et al.* found that distinct integrin expressions on tumor exosomes are responsible for organotrophic targeting.[85] While exosomes expressing integrin $\alpha_6\beta_4$ and $\alpha_6\beta_1$ are associated with the binding to lung fibroblast and epithelial cells, integrin $\alpha_v\beta_5$ is correlated to liver Kupffer cell targeting.[85]

Besides the surface protein interaction, lipids and carbohydrates on the exosomal membrane are also reportedly involved in the selective cellular uptake. Toda *et al.* reported the disruption of surface protein by enzymatic treatment (trypsin and proteinase K) did not affect the uptake of glioblastoma (U251)-secreted EVs in their parental cells, indicating the selective cellular internalization was likely mediated by other components on exosomal membrane.[76] Phospholipid phosphatidylserine (PS) on exosome has been shown to be one of the key factors for circulation time owing to the recognition by macrophages through the uptake receptor-scavenger receptor class A family (SR-A).[86] In addition to PS, macrophage can also recognize the α 2,3-linked sialic acid on the exosome through the CD169 (Siglec-1) presenting on macrophage.[87] CD47, an integrin-associated protein presenting on the surface of EVs, has been found to increase the circulation time of EVs by protecting from phagocytosis.[88] Xu *et al.* suspected the exosome circulation

time is a crucial factor determining the preferential uptake of exosomes by self-tissue in *vivo*.[82] Their studies demonstrated that the exosomes (*i.e.,* from PANC-1) presenting high CD47 expression on the membrane exhibited a self-tropism to pancreas tumor, whereas the exosome with low expression of CD47 (*i.e.,* from B16-F10) was not able to locate to their parental tumor cite and undergone rapidly clearance within 10 min. circulation *in vivo*.[89] These studies demonstrated the lipids and proteins on exosomal surface are important factors affecting their cell tropism and *in vivo* biodistribution. The expression of these molecules can potentially be the selection criteria for targeted delivery purposes.

1.3. Engineering Extracellular Vesicles as Therapeutic Platforms

Engineering EVs to be nanoscale delivery platforms or therapeutic medicine has become the focus of increasing interest. The ISEV position paper in 2015 summarized the therapeutic applications of EVs into 2 categories and 4 classifications (**Figure 1.5**),[36] as below:

(1) **Unmodified EVs for immune-modulatory and regenerative therapies**, as a "next-generation cell therapy". This category is considered as "biological medicine" following the regulatory guidelines and the EVs can be regarded as the active substance in the pharmaceutical formulation. It can be further divided into 2 classifications, including: *(i) native EVs from genetically non-manipulated cells* and *(ii) native EVs from genetically modified cells without trans-gene-products.*

(2) **Modified EVs for targeted drug delivery.** This category can also be divided into 2 classifications, including: *(iii) native EVs from genetically modified cells with trans-gene-products,* which are considered as gene therapy products, and *(iv) EVs as drug*

delivery systems loaded with synthesized chemicals or defined recombinant molecules. The iv classification can be determined as a biological medicine. The EVs may be part of the active substance in the formulation, depending on whether EV themselves mediate the therapeutic effects.

There have been many articles reviewed the manufacturing approaches of these 4 types of EV-based therapeutics for clinical use.[90-92] The isolation methods and standardization have also been summarized.[93] Despite these promising results of EVs' capabilities for therapeutic applications have been demonstrated in the recent years, the low yield of the EVs derived from cells is often an obstacle for research investigation and clinical translation. Therefore, to provide a quick guidance on the EV therapeutic strategies, a brief overview of mass production and consideration of the cell culturing conditions is first discussed in 1.4.1 subsection. The approaches for engineering EV's surface composition and payload capability are subsequently discussed in 1.4.2 and 1.4.3 subsections.

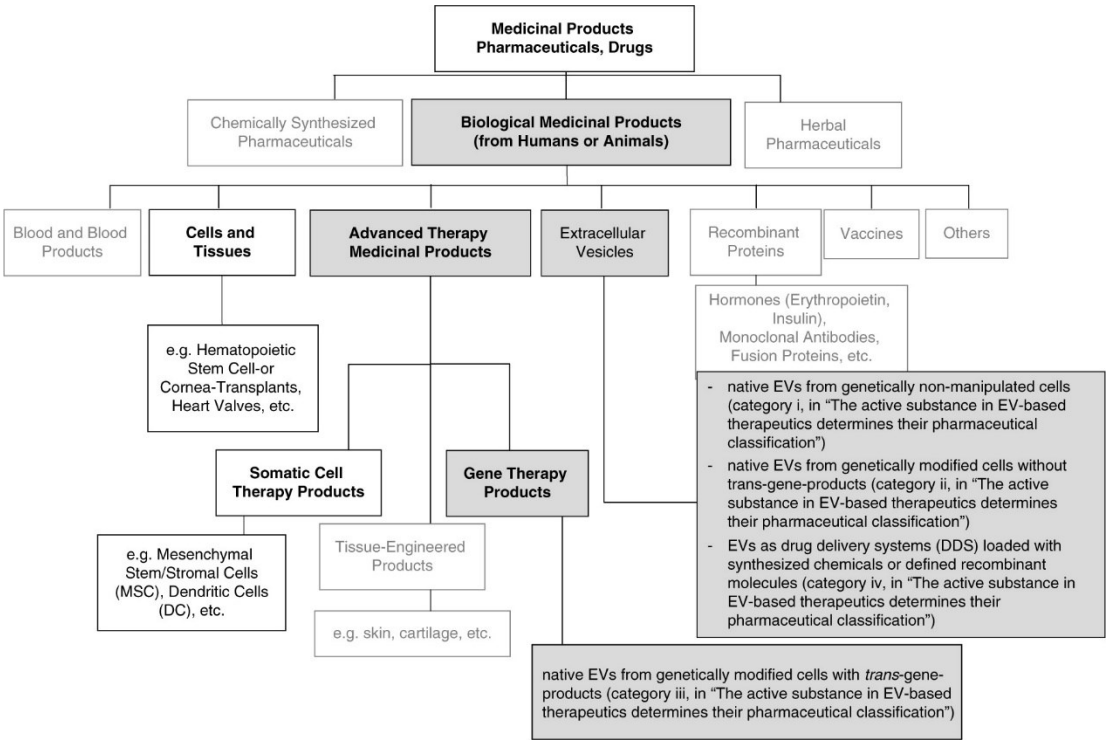

Figure 1.5 Pharmaceutical categories and classification of EV-based therapeutics. Reprinted from an open access article from Lener *et al*.[36]

1.3.1. Mass Production of Extracellular Vesicles

Despite there being several advantages of EVs, the major obstacle of mass producing the EVs limits their use within the clinic. The average yield of EVs is merely ~0.2 pg of associated protein or ~200 EVs per cell (equals to 1.74 µg total protein/2×10^9 EVs from 10^7 cells),[94-96] while typically a dose of 10^9-10^{11} EVs is required per administration to mouse (or 10^8-10^9 EV per kg human body[97]) to achieve therapeutic outcome.[98] The efficiency in EV production is tightly correlated with the parent cells, as well as the EV induction method, time and the secreting cell culture platform.[99] Studies have reported MSC as the most prolific EV producer among the mammalian cell lines that

generally a 10-fold greater amount of EVs was secreted by MSC than other cell types.[100-102] HEK293 has also been reported as an efficient EV producer among non-stem cell type cell lines. Other than mammalian cell lines, human red blood cells secreted EVs have been suggested for large-scale EV production. They can be readily available in blood bank with a yield of 5-10 $\times 10^{13}$ EVs from ~200 ml blood.[103] Bovine milk-derived EVs have also been proposed as a scalable source of EVs that 335 mg total protein of EVs can be obtained from per liter milk.[71, 104] Although these different sources of EVs can be the alternative to solve the limitation from laboratory cell culture, their cellular tropism and bioactivity *in vivo* could be a limiting factor for different therapeutic purposes, and thus the scale-up EV production based on parental cell selection could be limited.

In addition to parental cell type selection, there are several strategies on the alteration of culturing or cell conditions for enhancing exosome production. Jafari *et al.* detailed summarized the most up-to-date approaches and categorized these strategies into two main categories (**Figure 1.6**). *(1) Stimulating EVs production through different environmental stimulators or media composition*, such as glucose starvation, pH, oxidative stress, addition of different components to the culture media. *(2) Genetic manipulation of exosome biogenesis and recycling pathways*.[105] In the first category, triggering EVs release by different internal or external stimuli to the cell, often varies between different cell lines and sometimes may be considered as "accidental observations". For example, the effects of serum deprivation on different type of cells appear to be different. Sun *et al.* demonstrated serum-depleted cell culture stimulated 2.5-fold more EVs (microvesicles obtained from 16000 ×g centrifuge speed) in myeloma cell

lines.[106] In contrast, a 6 to 10-fold decrease of the exosome yield (from 100,000 ×g centrifuge speed) and no drastic change in the microvesicle yield (from 10,000 ×g centrifuge speed) from bone-marrow and adipose derived MSCs with serum-deprived culture were observed by Haraszti *et al*.[40] It is worth noting that cell stress affects the amount of EVs release but may also selectively enrich proteins or miRNA in EVs.[106] In the same study from Haraszti *et al.*, they further found that stressed exosome showed a higher uptake/cargo transfer bioactivity, which resulted in a 5- to 22- fold increase of siRNA delivery in their experiment model. Nevertheless, an opposite result of the stress-dependent bioactivities was observed in microvesicles where serum depletion impaired the bioactivity of microvesicles.[40] Extending the incubation period of culturing cells to 7 days, has also been reported to yield a 4-fold increase, compared to the original incubation time of 24-48 hours.[107] This method, however, would not be suitable for EVs which were induced *via* serum-deprived media or under hypoxic conditions because the extended incubation period would lead to secretion of EVs with different compositions (*e.g.,* undesired apoptotic-related biological cues).[108] Another strategy is delivering small molecule drugs to the parental cells to increase exosome production, such as fenoterol, norepinephrine, N-methyldopamine, mephenesin, forskolin and so on. These small molecule modulators can increase the exosome secretion from 2 to 5-fold in a dose dependent manner,[109] the threshold settings to induce the secretion effects are different in different small molecules. Wang *et al.* demonstrated the treatment of small molecule modulators would upregulate nSMase (neutral sphingomyelinase), microphthalmia-associated transcription factor (MITF), Rab27a and Rab27b, and these modulations on

exosome secretion is a cell-specific process. Their results showed the enhancement of exosome production could be related to energy production (glucose and ATP), as a result of enhanced metabolic activity.[109] In addition, they demonstrated the treatment of small molecule modulators does not alter the intrinsic functionality of hMSC EV, including anti-fibrosis, angiogenesis and macrophage polarization.[110]

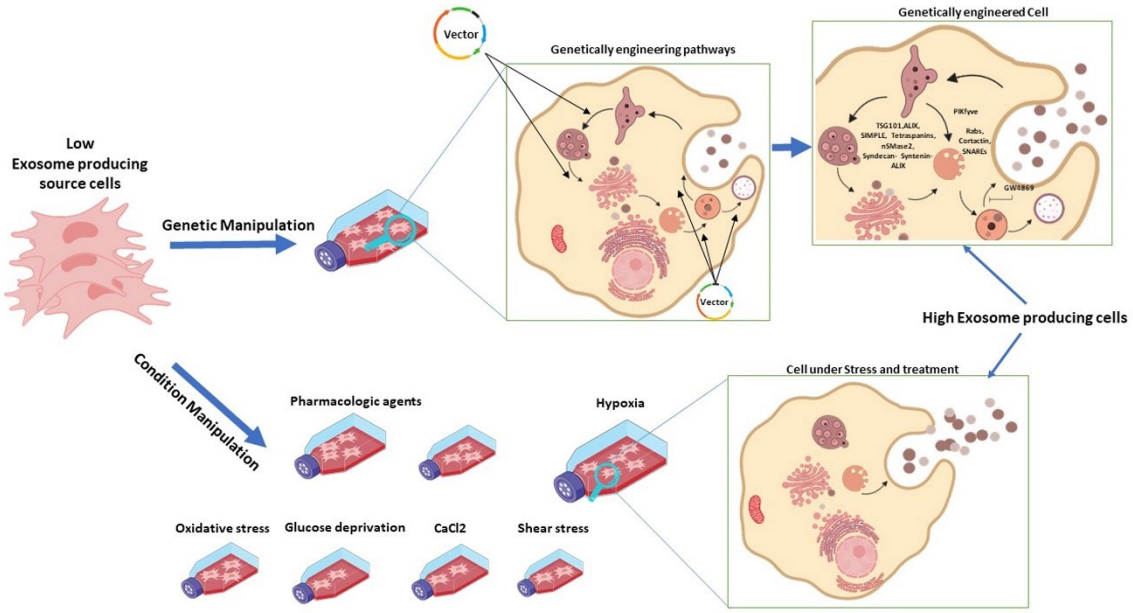

Figure 1.6 Strategies for enhancing EV production. Reprinted with permission from © 2020 Taylor & Francis Academic from Jafari *et al.*[105]

The second strategy for enhancing EV production is to manipulate the gene expression involved in exosome packaging, endocyclic trafficking, and secretion to increase the exosome production rate.[105] ESCRT-dependent pathway is commonly leveraged to induce exosome production. For example, Wang *et al.* generated a transgenic

mouse model overexpressed with the heat shock protein HSP20 in cardiomyocytes, which protects cells against stress conditions. The HSP20 protein was shown to directly interact with ESCRT factor Tsg101 and thus induced ~5-fold secretion of beneficial exosomes within the myocardium.[111] On the other hand, the overexpression of tetraspanins (*i.e.,* CD63 and CD9), a family of transmembrane proteins independent of ESCRT biogenesis machinery, has also been shown enhanced 3 to 5-fold exosome secretion.[112, 113] In addition to the initiation of exosome biogenesis pathway, factors associating with the MVB trafficking can also be regulated to facilitate the exosome secretion without altering the cargo composition. For example, the overexpression of Cortactin, an actin-binding protein controlling the number of MVB docking sites at the plasma membrane, can promote the exosome secretion to ~2-fold increase.[114]

While many strategies have been attempted to increase the EV production of laboratory culturing cell lines, large-scale cell culture is still a rate-limiting step to obtain sufficient amounts of EVs using the traditional 2D culturing flasks. Several studies have developed scalable EV generation method by changing the culture techniques. A two-compartment system initially designed for monoclonal antibody production, namely the Integra CELLine culture system, has been utilized by Mitchell *et al.* for EV scale-up purposes.[115] The compartment with a semi-permeable membrane allows a constant flow of media to pass through cell culture flask, which led to an increase of 8 to 12-fold in the EV production yield (10 μg of affiliated protein on EV per mL) compared to a traditional 75cm^2 flask. Similarly, Haraszti *et al.* reported a 20-fold increase can be obtained by culturing cells in microcarrier-based three-dimensional cultures, although it resulted in 2-

to 4-fold lower particle-to-protein ratio than conventional 2D culture.[98] Further, 7-fold increase EV yield was reported using a tangential flow filtration system for purification.[98] Adapting the methods for isolating viruses using polyethylene glycol (PEG) to efficiently purify EVs has also been developed and can provide an ~8-fold-enrichment of EVs compared to the conventional isolation method by ultracentrifuge.[116-118] Yang *et al.* developed a cellular nanoporation biochip to stimulate cells to produce large numbers of EVs with high mRNA loading through exosome biogenesis mechanisms that respond to calcium ions and heat shock.[119] This technique allows for the cells after nanoporation to produce a 50-fold more exosome release and a 10^3-fold increase in exosome mRNA payload capability. Compared to EVs produced by methods manipulating the cell conditions, the development of these culture techniques is more robust in mass-producing EVs from multiple types of source cells.

1.3.2. Surface Modification of Extracellular Vesicles

It is generally accepted that native EVs are capable of selective trafficking to specific recipient cells, however, the retention of cellular tropism from the on-bench isolated EVs remains controversial. The exogenously administered EVs may lack of targeting specificity due to the change of molecular properties during manufacturing/storage processes, and thus may have limit clinical applicability for preferential uptake. Therefore, modification of exosomal surface may still be necessary to ensure efficient targeted delivery. Salunkhe *et al.*,[120] Rayamajhi and Aryal,[121] and Armstrong, Holme and Steven,[122] have summarized the surface functionalization strategies for exosome target-specific delivery, including two main categories: (1) Cellular

engineering on parent cells and (2) chemical modification on parent cells or direct modification on EVs. The advantages and downsides of the strategy designs are discussed in the below 2 sections.

1.3.2.1. Cellular Engineering

The earliest method for surface modification of EVs is genetic engineering their parental cells to express certain membrane protein fused with target ligands. Alvarez-Erviti *et al.* designed a plasmid vector encoding membrane protein Lamp2b, which is abundant in exosome membrane, fused with a neuron-specific peptide (RVG) for brain targeting.[123] The RVG-expressing EVs were collected from plasmid-transfected dendritic cells and subsequently delivered to neuron, microglia and oligodendrocytes in brain *via* intravenous administration in mice. Tian *et al.* transfected a plasmid encoding Lamp2b fused with integrin binding peptide (iRGD) to immature mouse dendritic cells and obtained their daughter EVs for breast cancer (MDA-MB-231) targeting.[124] Platelet derived growth factor protein on exosome transmembrane domain was also used to fuse with GE11 peptide, which binds specifically to epidermal growth factor receptor (EGFR), for EGFR-positive breast cancer (HCC70) targeting by Ohno *et al.*[125] Although successful *in vitro* target-dependent uptake and *in vivo* administration were shown in these studies, a potential pitfall of peptide degradation by endosomal proteases during exosome biogenesis was reported by Hung and Leonard.[126] For those targeting peptides susceptible to acid-dependent proteolytic degradation (*i.e.,* Lamp2b), glycosylation is required to enhance the stability. However, there are potential drawbacks for this strategy. The glycosylation may affect the expression/sorting of other exosomal proteins in EVs and not every peptide

contains putative glycosylation sites for modification. Tetraspanin (*i.e.,* CD63, CD9, CD81) involved in exosome biogenesis is another set of transmembrane proteins commonly used for protein fusion with fluorophore (*i.e.,* green fluorescent protein) or antibody drugs.[127] Nevertheless, it has also been reported the antibody complex protein may lose functionality after protein fusion due to the highly transverse transmembrane protein structure.

Glycosylphosphatidylinositol (GPI)-lipid anchored protein, a type of post-translational modified proteins enriched in lipid-raft microdomain of EVs and involved in exosome biogenesis, has been leveraged as the alternative to transmembrane protein fusion for the expression of targeting moieties on EVs. Kooijmans *et al.* fused anti-EGFR nanobodies to GPI anchor peptide (CD55) on exosome membrane for tumor targeting.[128] The advantages of engineering GPI anchor over the transmembrane protein fusion are the small size of GPI anchor (~37 amino acids) and high solubility. These small peptide anchors would not interfere recombinant protein folding, and hence can be used for complex tertiary structure. However, yet still there are concerns including the uneven distribution of GPI-anchor on the lipid domain and the involvement of undesired RNA sorting in lipid-raft containing EVs.

Engineering fusion protein that specifically bind to phosphatidylserine (PS), which constitutes 5-10% of lipids on exosomal membrane, is another strategy for decoration of EV surface.[129-131] Kooijmans *et al.* transfected a vector encoding PS-binding domain of lactadherin (C1C2) fused with EGFR nanobody, into EV producer cells (red blood cells and Neuro2A cells). The soluble C1C2-EGFR protein was released from the cells and then

bound to PS-positive EVs for tumor targeting.[132] This approach offers the advantage of decorating EVs without the need/possibility to modify the molecular composition or cargo sorting process of native EVs from the producer cells and can be applied for multiple cell sources.

To summarize the above strategies of EV surface decoration by cellular engineering the EV producer cells, it is worth noting that the protein fusion design can be challenging and time-consuming to establish a stable gene-expressing cell line. Moreover, the expression of engineered proteins on the surface of EVs may not result in a high decoration density as expected. More efficient approaches (*i.e.,* chemical conjugation or metabolic engineering) may be preferred for tailoring exosomal surface.

1.3.2.2. Chemical Modification

To circumvent the need to genetically modify EV producer cells, chemical modification of EV surface has also been used in many studies. Strategies of *covalent* modification of EV surface and *non-covalent* modification are discussed in the following paragraphs.

Functional moieties can be directly added to the exosomal surface by chemical covalent modification between certain functional groups on exosome and target molecules. EDC/NHS covalent coupling of amine-/carboxylic- containing biomolecules to the carboxylic-/amine- terminated protein or phospholipid on EV surface is one of the most common functionalization strategies. Azide-alkyne cycloaddition click chemistry is another powerful tool that has been increasingly exploited in living cell system. The click chemistry reaction is more desirable for EV functionalization because of their high

specificity and less cytotoxicity. Smyth *et al.* functionalized alkyne groups on exosomal surface by EDC/NHS reaction with 4-pentynoic acid. Following alkyne functionalization of exosome, azide-fluor 545 was conjugated by copper-catalyzed azide alkyne cycloaddition.[133] Approximately 1.5 alkyne groups modification was achieved for every 150 kDa exosomal protein (2.06 μM alkyne on 40 μg exosome in 200 μl) in their results. Tian *et al.* further conjugated functional ligands (cyclo(RGDyK) peptide) for ischemic brain targeting using copper-free azide alkyne cyclo-addition.[134] Reactive dibenzylcyclooctyne (DBCO) groups were first incorporated to amine groups on exosomes by DBCO-sulfo-NHS. The DBCO-conjugated exosomes were subsequently reacted with the azide-containing peptides, resulting in a conjugation efficiency of 523 nM peptides on 1 mg/ml exosomes.

Besides EDC/NHS coupling reaction on exosome, the metabolic engineering of glycoprotein[135, 136] and choline-containing phospholipids[137, 138] in the EV producer cells have also been leveraged to enable azide functionalization on exosome surface for click chemistry conjugation. This approach utilizes the natural biosynthetic pathways of glycosylation (*i.e.,* sialic acid) or Cho-phospholipid by supplementing cell culture media with azide-containing metabolic precursors/analogs. The metabolic precursors/analogs are taken up by cells and can be incorporated into the glycoproteins or phosphatidylcholine on cell surface. Because exosomes are generated by the inward budding of late endosomes from cytoplasmic membrane, it is expected to contain metabolically labelled sites with the azide groups. To bypass the biosynthetic pathways of EV producer cells, direct incorporation of azide-presenting membrane fusogenic liposomes (*e.g.,* DSPE, DMPE,

DSPE-PEG) to parent cell membrane is another approach to obtain azide-functionalized EVs.[139]

Direct membrane fusion of target biomolecules or clickable moieties into EV membrane by non-covalent reaction (*e.g.,* hydrophobic interaction) has also been applied for exosomal surface modification. Di *et al.* incorporated maleimide-terminated DSPE-PEG (DSPE-PEG-Mal) into exosomal membrane by 4ºC incubation for 10 min., as a result of spontaneous hydrophobic insertion of DSPE.[140] The maleimide-functionalized EVs were further conjugated with thiolated magnetic particles or gold nanoparticles. Sonication, extrusion and repetitive freeze-thaw cycles of liposome with EVs have also been proposed to be a reagent-free strategy for exosomal membrane fusion and functionalization.[141, 142] In addition to lipid-based hydrophobic interaction, surface functionalization of EVs with cationic moieties *via* electrostatic interaction has also been reported in several studies.[143] For example, Nakase *et al.* incorporated GALA peptide, a pH-sensitive fusogenic peptide, to exosomal membrane by mixing cationic lipids (lipofectamine LTX) and the peptides with EVs for 20 min. incubation at room temperature. Enhancement of the cytosolic release of exosomal content from the GALA functionalized EVs were observed in this study.[144]

Despite the above non-covalent functionalization approaches seems to be simple and facile, the efficacy may be largely dependent on the chemical structure of lipid moieties, mixing ratio of the EVs mixture, and other technical handling factors. The fusion efficiency, lamellarity/membrane orientation, and purity of membrane fused vesicles are required to be carefully examined for the validation of membrane functionalization.

1.3.3. Packing of Cargo into Extracellular Vesicles

There have been several methods developed to load cargo into EVs (**Figure 1.7**).[5, 92, 145-147] The engineered EVs loaded with therapeutic cargo can be obtained by (1) **Pre-formation (endogenous) loading:** The loading of therapeutic drugs is based on cellular uptake of drugs into EV producer cells (simple incubation or lipotransfection) or the endogenous machinery of the cells (genetic engineering), and then cargo-loaded EVs are released by natural EV producing processes from the cells. (2) **Post-formation (exogenous) loading:** The cargo can be loaded into EVs *via* different techniques (*e.g.,* incubation, sonication, electroporation, etc) after EV isolation from the cells. Therapeutic drugs are directly incorporated into exosome vesicle.

Cargo including small molecule drugs (*e.g.,* chemotherapeutics or inorganic nano-compounds), small nucleic acids (*e.g.,* siRNA, microRNA, size ~23 nucleotides), large nucleic acids (*e.g.,* dsDNA/plasmid (>500 nucleotides), mRNA (>100 nucleotides), CRISPR-Cas9 plasmid), and protein (CRISPR-Cas9 protein, antibodies) have been investigated using both loading strategies. The loading techniques are introduced in the following sections.

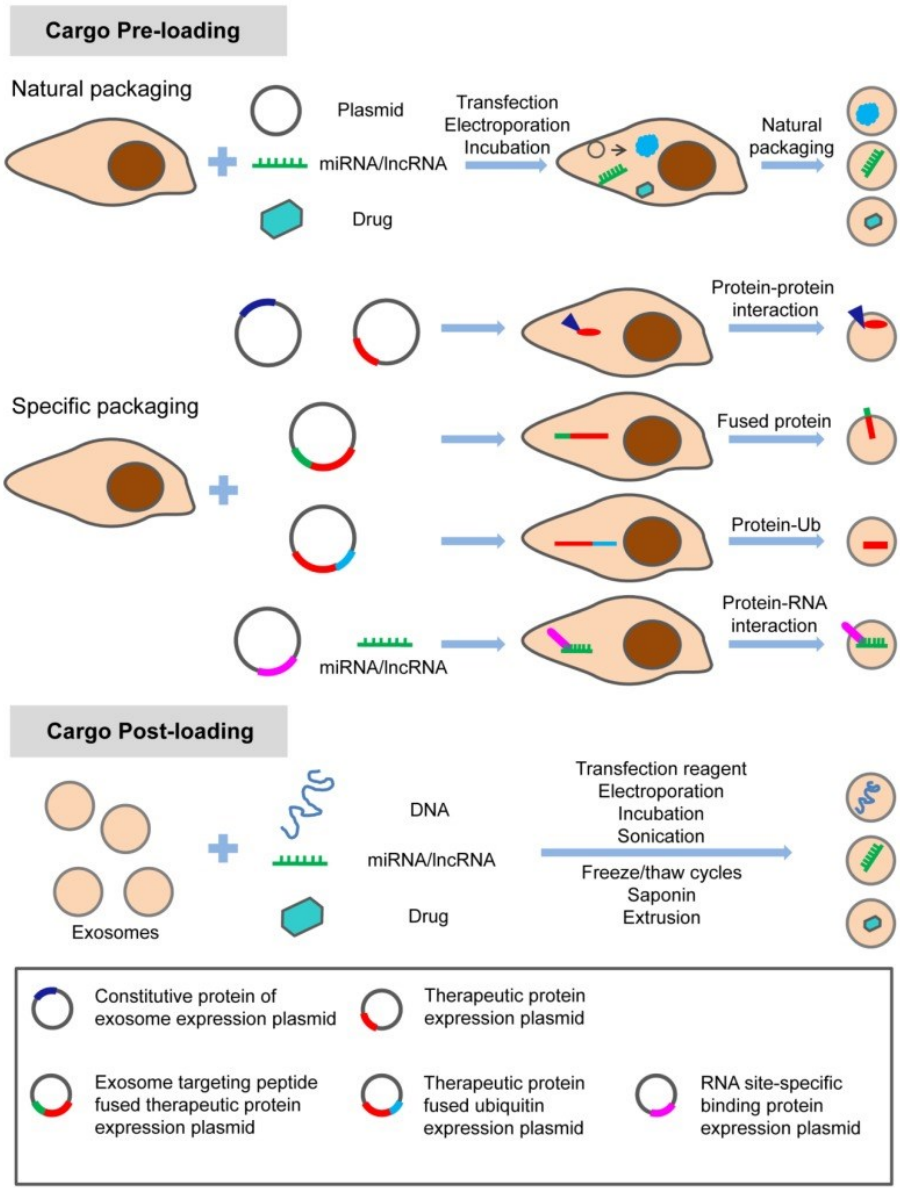

Figure 1.7 Methods of cargo loading into EVs. Reprinted from an open access article from Liu and Su.[148]

1.3.3.1. Pre-formation (endogenous) Loading

Incubation of therapeutic drugs with EV producer cells is the earliest and the most common method to package cargo into EVs. The incubation method can be employed for

various drugs with different properties, such as small molecule drugs, nucleic acid materials (*i.e.,* small/large nucleic acids). For example, Pascucci *et al.* generated Paclitaxel (PTX)-loaded MSC EV by exposing the cells (murine stromal cell line SR4987) with high concentration of fluorescein-labelled PTX.[149] Despite the cells were arrested in a G2/M cell cycle, the cells were able to remain viable and release PTX-loaded EVs. Of note, this method requires the use of parental cells resistant to the loading drug (*i.e.,* high p-gp drug-resistant gene expression) and it may give a poor yield of PTX packaging efficiency in different cell lines. The delivery efficiency of cargo *via* (passive) incubation into the cells is largely dependent on the hydrophobic/electrostatic interaction with the cell membrane, and therefore, it seems to be used more often for hydrophobic drugs. Due to the anionic nature of nucleic acids, genetic cargo must be pre-incubated with transfection materials (*e.g.,* lipofectamine, polyethylenimine (PEI)) to form nanocomplex by electrostatic condensation. The nanocomplex is then incubated/transfected to the cells to obtain nucleic acid-loaded EVs from the transient expression of cells. For instance, transforming growth factor β1 (TGF-β) siRNA-loaded EVs was obtained from siRNA-lipo-transfected mouse fibroblast (L2929) for tumor suppression.[150]

Unlike chemical drugs or nucleic acids, proteins cannot passively penetrate cellular membrane.[151] Protein-loaded EVs can be obtained by the overexpression of certain genes in the cells *via* plasmid transfection. However, same as the passive incubation method, packaging efficiency of the cargo varies from cells and it's difficult to control. Huang *et al.* designed and generated EVs with osteo-inductive abilities by constitutively expressing BMP2 protein in parental hMSC cells. Surprisingly, despite the

BMP2 signaling cascade was potentiated, their results demonstrated the corresponding EVs do not contain BMP2 protein as a constituent cargo in EVs.[152] These findings indicate that systemic bioinformatic studies on the mechanism of EVs' cargo sorting are required to understand the impact of overexpressing genes on the functionalities of these engineered EVs. Therefore, to manipulate selective protein loading, combining the biogenesis pathways of EVs may result in a higher yield of packaging efficiency. A commercialized exosome protein loading technology XPACK was developed by System Bioscience company (USA). This technology is based on the finding from Shen *et al.* that certain plasma membrane anchor (*e.g.,* the N-terminal acylation tag MGCINSKRKD-) can target oligomeric cytoplasmic protein (*e.g.,* TyA) to sites of vesicle budding and EVs.[153] Therefore, targeting proteins can be designed to anchor on the inner side of the exosomal membrane. The downside of this approach is the subcellular localization of delivered proteins may be limited. Yim *et al.* developed another approach for selective protein loading *via* optically reversible protein-protein interaction (EXPLORs). This method allows for delivering soluble proteins into the cytosol *via* controlled, reversible protein-protein interactions (PPIs) by blue light illumination.[151, 154] The protein-protein interaction is a dimerization module between Arabidopsis CIB1 (or a truncated version CIBN), a basic helix-loop-helix (bHLH) protein and cryptochrome 2 (CRY2).[154, 155] This module is reversible by light on-off with minutes and triggers protein translocation in sub-second time scale.

1.3.3.2. Post-formation (exogenous) Loading

Passive incubation can also be employed to the direct loading of drugs into EVs. The loading efficiency is depending upon the concentration gradient and hydrophobicity of the drugs.[156] Sun *et al.* successfully loaded curcumin into exosomes by simple incubation on ice for 30 min, a 5-fold higher amount of curcumin was detected in the exosome after purification compared to the curcumin original concentration.[157] While hydrophobic drugs can simply enter the exosomal membrane, active loading methods such as saponin, freeze-thaw cycles, sonication and extrusion may be required for other types of therapeutic drugs to enhance the loading efficiency.[158] Haney *et al.* compared the loading efficiency of different techniques by loading protein catalase into EVs.[158] Their results demonstrated the loading efficiency *via* sonication and extrusion were similar level and were greater than freeze/thaw cycles and simple incubation method. They also showed the highest integrity of EVs was remained by extrusion method, whereas the EVs post-sonication showed low vesicle integrity. Similar loading efficiency was obtained from Kim *et al.* by loading PTX into EVs. Sonication method resulted in a significantly higher loading efficiency than electroporation and incubation method.[159] On the other hand, Fuhrmann *et al.* demonstrated that hypotonic dialysis loading and saponin treatment yielded to a 10-fold higher loading amount compared to extrusion, electroporation and incubation method.[160]

To load hydrophilic drug (*e.g.,* doxorubicin) or charged biomolecules (*e.g.,* nucleic acids) into EVs, electroporation is the most used technique among the active loading methods. When a short duration and high voltage of an electric field are applied to EVs,

reversible pores within membrane can form which allows for exogenous molecules to enter the vesicle. Although electroporation has been widely used for nucleic acids loading, the loading efficiency was found to be size-dependent. While high loading efficiency was shown in small nucleic acids (*e.g.,* siRNA, 20-25 bp size), the loading efficiency drastically dropped in double strand DNA with the size larger than 750 bp.[161] Moreover, extensive aggregation of nucleic acids and vesicles was observed after electroporation by Kooijmans *et al*. It is suspicious that the electroporation-induced aggregation caused an over-estimation of the loading efficiency into EVs.[162] Sonication was proposed to be a potential alternative by Lamichhane *et al*.[163] The aggregation of nucleic acids was reduced using sonication compared to electroporation. However, the nucleic acid cargo was found to be susceptible to degradation after 30 sec. of sonication. The incorporation of nucleic acids into vesicles was also found to decrease for times greater than 30 sec. Interestingly, it was shown in the literature that the intracellular cargo delivery was not impacted, but instead, was enhanced by the sonication method. However, compared to electroporation that only generates transient membrane pores *via* a short duration of electric field, a complete assessment of permanent membrane structure change and degradation by sonication is yet needed. Additionally, hydrophobically modified siRNA (hsiRNA) is suggested to enhance the loading efficiency into exosomes.[164] By conjugating a cholesterol moiety to the 3' end of the passenger strand of siRNA, a loading amounts of ~1000 siRNA copies per EVs was achieved by co-incubation of hsiRNA with exosomes.

It is worth noting that the protein/surface ligands on exosomal membrane may be disrupted during the loading process for all the above loading methods, resulting in a

different route of uptake than the natural EVs. More efforts are needed to optimize the loading parameters to ensure the retention of EVs' integrity and bioactivity while achieving high loading capacity.

1.4. Challenges and Future Perspectives

Great potential of EVs in cell-free therapy and drug delivery have been revealed over the past years. However, significant challenges for the development of EV-based formulation remains to be overcome, including: (1) standard isolation and characterization procedure, (2) large-scale production, (3) identification of the molecule compositions within EVs from different cell sources (safety concern), (4) efficient drug loading, and (5) quality control to ensure the batch consistency and stability for long-term storage. Further studies on these topics are still needed.

1.5. Research Aims

Nano-sized extracellular vesicles (EVs), which are shed or secreted by most cell types, have been identified as a drug carrier and can be exploited as tumoricidal tumor-targeting vehicles.[165] However, several challenges remain before EVs' utility can be realized within the clinic, including mass production and efficient drug loading. To resolve scale-up issues, we propose to explore an innovative technique to engineer cell-derived EVs to incorporate synthetic lipid-based materials yet retain native biological properties of exosomes, such as cell specificity. In addition, a drug delivery system that can co-deliver two or more therapeutic agents simultaneously is urgently necessitated for cancer combinatorial therapy. We therefore propose to develop an EV-based, targetable delivery platform for diverse therapeutics, in the absence of off-target toxicity. In addition to the

potential as gene-modulating drug delivery system, EVs are gaining increased attention for their function in immune-modulation. Therefore, we propose to develop surface modified EVs with reactive moieties for click chemistry reaction (*e.g.,* azide groups, tetrazine groups). The surface functionalized EVs will be covalently tethered to implantable microporous annealed particle (MAP) hydrogel in the future.

The aims of this study involve exosome composition engineering (Aim1 & Aim2), tumor-targeting tumoricidal therapy (Aim2 & Aim3) and tissue engineering (Aim 4). Our long-term goal is to execute the following specific aims to develop combinatorial therapeutics modalities for cancer therapy and tissue regenerative/immune-modulatory applications:

Aim 1: Engineer and quantitatively characterize unmodified and engineered EVs (eEVs) without therapeutic agents

a. To induce and characterized the EVs from different parental cells

b. To engineer modified EVs by incorporating various lipids

Aim 2: Quantify the payload capability and functionality of eEVs

a. To quantify the drug encapsulation and loading efficiency of eEVs

b. To evaluate the cytotoxicity and intracellular delivery efficiency

Aim 3: Quantify in vitro safety and efficacy of siRNA/chemotherapeutics combinatorial treatment

a. To engineer an EV-based co-delivery platform *via* lipid-hybridization and polymer layer-by-layer (LbL) deposition and characterize the vesicles and payload capability

b. To evaluate the intracellular delivery and RNAi knockdown/cancer killing efficacy of LbL-eEV

Aim 4: Develop a clickable exosome to improve the therapeutic effect of MAP hydrogels for tissue regeneration

a. To characterize azide-and tetrazine- functionalized human mesenchymal stem cells (hMSC)

b. To quantify the azide- and tetrazine- functionalization on EVs derived from hMSC

Completion of aims 1-3 will yield biocompatible, targetable combinatorial therapeutic modalities that can effectively eradicate tumor cells. These aims will yield drug delivery platforms that can incorporate multiple therapeutics in one formulation and retain bioactivity. Completion of aim 4 will yield clickable EVs that can be conjugated to hydrogels *via* bio-orthogonal click chemistry. The incorporation of exosome into scaffolds could be applied to various tissue engineering strategies and facilitate tissue regeneration.

2. ENGINEERED EXTRACELLULAR VESICLES WITH SYNTHETIC LIPIDS VIA MEMBRANE FUSION TO ESTABLISH EFFICIENT GENE DELIVERY*

2.1. Introduction

The delivery of RNA molecules (*i.e.,* short interfering RNA (siRNA), microRNA (miRNA), short hairpin RNA (shRNA)) to silence aberrant expression of genes in a cell is a potentially powerful therapeutic strategy for a variety of diseases and cancer in recent decades. Inducing RNA interference (RNAi)[166] by the delivery of exogenous small RNA molecules as a therapeutic holds great promise for anti-cancer applications,[167] as the RNAi process can inactivate specific oncogenes or inhibit cell migration or cell growth.[168] Despite the great therapeutic opportunities of siRNA, due to the inherent characteristics of siRNA, effective delivery of siRNA into target cells is the key challenge remaining to be resolved by the RNAi scientific community. Owing to the molecular weight (~13-14 kDa) and highly negatively-charged phosphate backbone of siRNA, naked siRNA cannot efficiently traverse the cell membrane.[169] In addition, siRNA is vulnerable to enzymatic degradation by prevalent RNases within the *ex vivo* and *in vivo* environment. Although chemical modifications help RNA stability, superior small RNA molecule delivery carriers must be engineered.

Extracellular vesicles (EVs), such as exosomes and microvesicles, have been acknowledged for their potential use as a therapeutic for the past 17 years.[170-172] EVs are

* This chapter is based on the article ©2020 Elsevier. Reprinted with permission from Jhan Y-Y, Prasca-Chamorro D, Zuniga GP, *et al*. Engineered extracellular vesicles with synthetic lipids *via* membrane fusion to establish efficient gene delivery. International journal of pharmaceutics 2020; 573: 118802.

naturally secreted by most cell types. Typically, exosomes, which is a sub-population of EVs, are in the range of 30 – 150 nm in diameter.[173, 174] These vesicles have been uncovered to function as intercellular communicators that shuttle a variety of cargo, particularly miRNAs, to local cells or distant tissues.[175] They are able to direct their cargo to specific recipient cells, which holds great promise for exploiting EVs as targeting, drug and gene delivery vehicles. Since EVs are phospholipid structures and exhibit surface marker/protein ligands on their membranes, they can potentially overcome biological barriers and reduce off-target effects within the body.[176, 177] Increasingly more studies have indicated EVs present fewer safety issues compared to cell therapy strategies or other conventional drug delivery systems.[171] Furthermore, EVs' functionality can be tailored by manipulating their cell sources, or endogenous tailoring through genetic or metabolic engineering, or by exogenous tailoring methods involving packing payloads post-isolation of the vesicles.[122, 156] These versatile capabilities of EVs lend credence to their potential as cell-free, active targeting vehicles for a variety of RNA therapeutics.

Excitingly, Alnylam recently received the first U.S. FDA approval for a sugar (GalNAc)-based RNAi formulation, which opens the door for 510(k) clearances. However, despite intense EV studies within a wide range of RNAi therapeutic applications ,[5, 178] most of the EV-related clinical trials have begun in the last 5 years, thus most clinical trials are in phase I/II,[179] One of the major hurdles is the lack of cost-effective methods to obtain sufficient quantities of EVs with consistent biochemical characteristics for clinical application.[180, 181] There is difficulty in scaling up EVs from a manufacturing standpoint; the yields for EV isolation and purification from *in vitro* cell culture are extremely low

and often impractical. Moreover, the abilities to develop a stable, effective, and more scalable extracellular vesicle-based formulation which can be loaded with exogenous cargo remains elusive. A potential solution to help clinically translate siRNA delivery therapeutics could be integrating synthetic/exogenous lipids into already-isolated EVs to help control the physicochemical properties and the mass production. However, by doing so, the EVs' targeting functionality may decrease as the density of the endogenous protein decreases. We hope to balance these two trade-offs, while ensuring both are sufficient for a given application. In this study, we report an engineering approach to mass produce lipid-doped extracellular vesicles post-EV isolation by generating synthetic lipid-hybridized EVs. The physicochemical properties and functionalities of our hybridized EVs have been thoroughly characterized and are described herein.

2.2. Materials and Methods

2.2.1. Materials

1,2-dioleoyl-3-trimethylammonium-propane (chloride salt) (DOTAP) (# 890890C-25mg, Avanti Polar Lipids, Inc.); 1-Palmitoyl-2-oleoyl-sn-glycero-3-phosphocholine (POPC) (# COATSOME® MC-6081, NOF America Corporation Ltd.); 1,2-dipalmitoyl-sn-glycero-3-phosphocholine (DPPC) (# 850355C, Avanti Polar Lipids, Inc.); 1-Palmitoyl-2-oleoyl-sn-glycero-3-phosphoglycerol, sodium salt (POPG-Na) (#COATSOME® MG-6081LS, NOF America Corporation Ltd.); 0.4 cm electroporation cuvette (#1652088, Biorad); 400 mesh Formvar/carbon-coated copper grids (#FCF400-CU-50, Electron Microscopy Sciences); 6X DNA loading Dye (#R0611, Thermo Fisher Scientific); anti-CD63-eFluor 660 antibodies (#50 112 4280, Thermo Fisher Scientific);

CellTiter 96® Aqueous Cell Proliferation assay (Promega G5421); cholesterol (#ICN10138201, MP Biomedicals); chloroform (molecular biology grade, Thermo Fisher Scientific); anhydrous D-trehalose (#AC309870250, ACROS); bovine serum albumin (BP1600-100, Thermo Fisher Scientific); Deep Red Plasma Membrane Stain Cell Mask (Life Technologies, #C10046); Dulbecco's Modified Eagle's Media (DMEM, #10-014-CV, Corning); Dulbecco's Modified Eagle's High Glucose Media (#10-013-CV, Corning); dynamic light scattering (Zetasizer) cuvette (ZEN0040); fetal bovine serum (FBS) (#10437028, Gibco); GeneRuler 100 bp DNA ladder (#SM0241, Thermo Fisher Scientific); Glass coverslips (Thermofisher, #1254581); Hoechst33258 (Invitrogen, #H3569); glutaraldehyde (#16019, EMS); isopropanol (#AC412790010, ACROS); Lipofectamine RNAiMax (Invitrogen); Micro bicinchoninic acid (Micro BCA) protein assay kit (#23235, Thermo Fisher Scientific); methyl cellulose (#M6385, Sigma); non-essential amino acids (MEM-NEAA, # 11140050, Gibco); O-Phosphoric acid (#A242500, Thermo Fisher Scientific); Opti-MEM I Reduced Serum Media (#31985062, Thermo Fisher Scientific); OptiPrep™ Density Gradient Medium (#D1556, Sigma); oxalic acid (#423152500, ACROS); paraformaldehyde (#28906, Thermo); penicillin (Invitrogen); phosphate buffered saline (PBS) (#10010023, Gibco); phosphotungstic acid (#P4006, Sigma); potassium chloride (#BP366500, Thermo Fisher Scientific); potassium phosphate dibasic (#BP363500, Thermo Fisher Scientific); TRIzol reagent (Invitrogen); SYBR Safe DNA gel stain (#S33102, Invitrogen); trypsin-EDTA, 0.05% (wt/vol; Gibco); uranyl acetate (#NC0788109, Thermo Fisher Scientific); vanillin 99% (#AAA11169-22, Alfa Aesar).

2.2.2. Methods

2.2.2.1. Extracellular Vesicle Induction and Isolation

3T3 and A549 cells were grown with complete media until ~100% confluent. The media was removed from the culturing flasks and the flasks were washed with phosphate-buffered saline (PBS) twice to remove any remaining media. After which, the cells were continued to be cultured in FBS-depleted media for 48 hrs. to promote the secretion of EVs. The conditioned media was collected and the EVs were isolated by serial centrifugation at 4°C,[182, 183] using a TX150 rotor and ST8 centrifuge. The media was centrifuged at 300 ×g for 10 min., 2,000 ×g for 20 min., and 10,000 ×g for 30 min. The first, second, and last centrifugations were to remove intact cells, dead cells, and cell debris, respectively. Note that the pellet was discarded after each centrifugation. The supernatant media was then transferred to ultracentrifuge tubes and centrifuged at 125,000 ×g (Beckman Coulter centrifuge with TLA-55 rotor) for 70 min. at 4°C. The pellet was resuspended in PBS, then filtered using a low protein binding polyvinylidene fluoride (PVDF) 0.22 μm filter. The isolated EVs were stored at a concentration of 10^{10} particles/ml at -20°C. To remove unwanted non-vesicular particles, OptiPrep™ density gradient solutions (Sigma, #D1556) were used to separate particles by their density (exosome: 1.1-1.19 g/ml) according to literature.[182] In our small-scale preparation, no significant difference of protein: lipid ratios between the samples using ultracentrifugation and OptiPrep™ density gradient centrifugation were observed, however.

2.2.2.2. Engineered Extracellular Vesicles *via* Extrusion

The eEVs were fused using a serial extrusion technique (**Scheme S1**). The lipid solutions were dissolved in chloroform (10 mM) according to literature.[141] The organic solvent was evaporated in a vacuum chamber to yield a thin lipid film on the bottom of a glass vial. The lipid film was then hydrated by adding a PBS buffer. Prior to membrane extrusion, the lipid solutions were heated at a temperature above their phase transition temperature and vortexed until they were visually homogeneous. The phase transition temperature of each individual lipid is shown in **Figure S1**. The EVs were subsequently warmed to 37°C. The lipid: EV solutions were mixed at varying volumetric ratios (9:1, 4:1, 1:1); the lipid solution was at a concentration of 5 mM and the EV concentration was 1.5×10^{10} particles/ml (or 50 μg/ml of protein according to a Micro BCA assay. The mixtures were vortexed and sonicated for 2 min. using a 120Watt, 20 kHz sonicator (Fisher Scientific FB120) at 20% max amplitude to fully solvate the solution. Subsequently, the mixtures were serially extruded through pore sizes of 400 nm, 200 nm, and then 100 nm. For each extrusion procedure, the mixtures were push forward and backward manually more than 25 times according to the manufacturer's instruction (T&T Scientific) (**Scheme S1**).

2.2.2.3. Physicochemical Quantification of EVs from Cells and eEVs

2.2.2.3.1. Membrane Protein Quantification Assay

The total quantity of protein within EVs was quantified *via* a Micro BCA Protein Assay Kit, according to the manufacturer's instructions. Briefly, a set of protein standards were prepared within the linear working range of 2-40 μg/ml. EV samples with different

concentration were mixed with working solution in a 96 well microplate and incubated at 37°C for 2 hr. Absorbance in each well was measured using a plate reader (Cytation 5, BioTek Instruments, Inc.) at 562 nm.

2.2.2.3.2. Flow cytometry – Characterization of EV surface marker and purity

EVs obtained after differential centrifugation and filtration were then analyzed by flow cytometry for the presence of exosome marker CD63.[184, 185] Initially, EVs were diluted to the concentration of 5000 ng of affiliated protein or a total 10^{10} particles in 50 µl of PBS solution. The solutions were subsequently mixed with 0.125 µg (1.25 µl) of anti-CD63-eFluor 660 antibodies to a final volume of 100 µl of PBS with 0.2% bovine serum albumin (BSA) blocking solution. The mixture was incubated at room temperature for 30 min. in the dark before conducting flow cytometry analysis. Flow cytometry was accomplished using a BD Accuri™ C6 Cytometer at a flow rate of 11 µl/min. Auto-fluorescence was quantified using the samples in the absence of the anti-CD63-conjugated eFluor 660 antibodies. POPC, which has no CD63 surface marker expression, was used to identify the background fluorescence *via* flow cytometry for gating purposes. To characterize the percentage of CD63 expressing vesicles or the percentage of EVs within our solution, the percentage of eFluor 660 fluorescence was quantified using the FL4-H channel.

2.2.2.3.3. Nanoparticle Tracking Analysis – Size, Concentration, and Production Yield

The size and concentration of exosomes were characterized by nanoparticle tracking analysis (NTA) (Malvern NanoSight LM10, Amesbury, United Kingdom). An appropriate working concentration in the measurable range of 10^8 particles/ml

was used to determine the original concentration of EVs. The EV samples with serial diluted concentrations (in PBS) were injected in the NTA sample chamber using sterile syringes. Data for each sample were collected for 60 s at room temperature and analyzed using NanoSight NTA 3.2 software. Three individual measurements of each condition were performed immediately after the sample was injected into the chamber. The error bars shown are standard deviations of the mean size and the original concentration was calculated using a dilution factor. A dilution factor was necessary to be within the measurable concentration range for NTA (10^{7-9} particles/ml). The production yield of EVs was further normalized to the cell number per flask (or dish) at ~100% confluency, counted by hemocytometer. Likewisely, an appropriate working concentration of eEVs in the NTA measurable range of 10^8 particles/ml was prepared to determine the size and concentration of eEVs. The concentration of eEVs were normalized to the concentration of native EVs to quantify the production yield, in terms of the fold increase of eEVs.

2.2.2.3.4. Transmission Electron Microscopy – Morphology

A pellet of EVs or eEVs (~10^8 particles) was resuspended in 50 µl of PBS and stained on Formvar/carbon-coated copper grid for microscopy imaging purposes following the protocol in previous literature.[186] Details of the steps for sample staining are depicted in *Supporting Information*. A drop of 5 – 10 µl of EV suspension was put on clean Parafilm. The sample grids were then allowed to vacuum dry overnight and observed *via* TEM (JEOL 1200EX) under 100 kV of energy and 100,000× to 150,000× magnification.

2.2.2.3.5. Zeta Potential Measurements

To obtain information about the stability of the vesicles in terms of particle aggregation and flocculation, the zeta potentials of the vesicles were evaluated measured in PBS and water. The zeta potential of vesicles was measured using a Zetasizer (NanoZS) from Malvern Instruments with a detection angle of 173° and laser wavelength of 633 nm (cuvette: ZEN0040). 10 μg/ml (affiliated protein concentration) of EV and 10^9-10^{10} particles/ml of eEVs were used for the measurements.

2.2.2.4. Quantifying Native EV Fraction within eEVs for Validating Membrane Incorporation

2.2.2.4.1. Membrane Composition Quantification Assay

To validate the membrane incorporation of lipids to extracellular vesicles, we conducted membrane composition analysis to quantitatively evaluate the efficiency of membrane fusion. Osteikoetxea *et al.* demonstrated that the protein to lipid ratios characteristic could be a consistent parameter to characterize extracellular vesicles populations.[44] Therefore, we quantify the EV fraction within eEVs by quantifying the protein (which is EV-derived) and the lipid content (which is both EV- and synthetic lipid-derived) within. The protein quantification method (Micro BCA) was described previously in "*Membrane protein quantification assay*". A sulfo-phospho-vanillin (SPV) assay was used following previous protocol.[44] Details of the steps for lipid quantification are depicted in *Supporting Information*. Total protein to total lipid ratios were further calculated to determine the fusion efficiency of exosomal membrane. To confirm the lipid molecules

presenting in the samples did not interfere with the total protein determination in terms of causing false-positive protein results, we tested the pure lipid solution for their assay interference with the protein determination, followed by quantification of the total protein to lipid ratios for pure lipid solution.

2.2.2.4.2. Flow Cytometry-based eEV/EV Ratio Quantification Assay

To quantify the native EV portion within the eEVs, anti-CD63 conjugated eFluor 660 antibody was used as a labeling marker for EVs. Same procedure for sample preparation was conducted as described in previous section "*2.2.3.2 Flow cytometry – Characterization of EV surface marker and purity."* The amount of eFluor 660 fluorescence was quantified using the geometric mean of FL4-A of the vesicle population, which is commensurate with the amount of CD63 per exosome. The fraction of EV incorporation with synthetic lipids were calculated using the normalized geometric mean values, according to the following equation (note that the EV fraction in eEVs = 1-Synthetic lipid fraction):

$$\text{EV fraction in eEVs} = (GM_{eEV}/GM_{background})/(GM_{EV}/GM_{background}) \quad (2.1)$$

Auto-fluorescence or background fluorescence was quantified using samples in the absence of the anti-CD63-eFluor 660 antibody. POPC was used as a stained negative control to compare with native EVs. Isotype igG1 was also pre-tested to get rid of the nonspecific binding concern of antibodies. Note that the above equation will result in values ranging from 0 to 1, where 0 is 100% synthetic lipids and 1 is 100% native EV.

2.2.2.5. EV and eEV siRNA loading

2.2.2.5.1. siRNA loading method

siRNA was loaded within EVs and eEVs *via* electroporation using a modified protocol as was previously described.[187] Briefly, electroporation mixture was prepared in a concentration of 100 μg/ml EV (3×10^{10} particles/ml) or $10^{10} – 10^{11}$ particles/ml of eEV containing 1 ng/μl siRNA. Note the mass of EVs is represented by the affiliated protein amount as quantified by the Micro BCA assay. Opti-MEM or a hypotonic electroporation buffer (1.15 mM K_2HPO_4; pH 7.2; 25 mM KCl, 21% OptiPrep according to the protocol [123, 187] were used as the sample solution. Hypotonic buffer was proposed to drive a faster water uptake across vesicle membrane by an imposed osmotic gradient, which facilitates the uptake of genes, resulting in an increase of the transfection efficiency.[188-190] Sample volumes of 100 μl were used for electroporation. The siRNA/vesicle mixtures were then transferred to 0.4 cm electroporation cuvettes (#1652088, Biorad) and electroporated using a Bio-Rad Gene Pulser II system, using the following conditions: 400 V, a capacitance of 125 μF, and an exponential pulse induction process. 2 pulses were applied to increase the nucleic acid incorporation or entrapment within the EVs and eEVs, as described previously.[161] After electroporation, samples were kept on ice for 1 hr. to allow for membrane recovery prior to further experiments.

2.2.2.5.2. Loaded siRNA content quantification

To quantify the amount of siRNA loaded within EVs/eEVs post-electroporation, the samples were ultracentrifuged at 125000 ×g for 70 min. twice to remove free siRNA in solution. The supernatant was discarded after ultracentrifugation and fresh PBS was

replenished to each sample as an ultracentrifuge-wash cycle to completely remove loosely bound, free siRNA from EVs/eEVs. As a first step in evaluating the capability of exogenous cargo loading, the actual siRNA amount loaded into the vesicles was quantified. To isolate siRNA from vesicles, a modified TRIzol RNA isolation protocol was used according to previously published literature.[191] Details for the TRIzol RNA isolation are depicted in *Supporting Information*. After siRNA isolation, Quant-iT RiboGreen RNA fluorescent dye (preferentially fluoresces in the presence of RNA (when the nucleic acid is <500 bp)) was used for the quantification of siRNA, following the manufacturer's instruction. siRNA at varying concentrations were prepared and measured to generate an siRNA calibration curve. We quantified the amount endogenous RNA within the exosomes, which merely measured at 0.8 ± 0.3 ng of nucleic acid from 10^9 (1E9) exosomes. Compared to our exogenous loading amounts of siRNA (100 ng), it is only ~1% of the total amount.

As a control between different lipid-doped systems, a concentration of ~E10 particles per formulation was carried out under the same vesicle densities for accurate comparison of electroporation efficiency. The loading efficiency (left y-axis) is determined by numbers of siRNA in vesicles normalized by numbers of vesicles, which represents as siRNA copies per vesicle. The encapsulation efficiency (right y-axis) is determined by mass of siRNA in vesicles normalized by mass of the feeding siRNA.

2.2.2.6. Mitigation of cytotoxicity and aggregation

2.2.2.6.1. Cell viability assay

The relative metabolic activity of the samples was evaluated using the CellTiter 96® Aqueous Cell Proliferation assay (Promega) (MTS assay) to assess the viability or cytotoxicity levels. Prior to MTS treatment, siRNA-loaded eEVs were incubated with cultured A549 cells at 60 – 70% confluency for 2 hr. After 2 hr. incubation, cells were washed to remove excess eEVs and replaced with fresh media for further cell incubation. The MTS assays were conducted after 24 hr. of siRNA treatment, following the manufacturer's instruction. Recent animal studies of EVs reported that a dose of 10^9 – 10^{11} EVs (with 1-500 μg siRNA) per 10^5 –10^6 tumor cells (initial cell number) is typically required to achieve therapeutic effects when it is administered every day or every other day.[98, 187, 192, 193] In regard to our cell viability assay and aggregation studies, we delivered a single dose of 10^9 –10^{10} eEVs with 100-400 ng siRNA per 10^4 cells.

2.2.2.6.2. Aggregation determined by microscopic image analyses and spectroscopy assays

In addition to NTA and DLS measurements for particle number and size quantification, the degree of aggregation was quantified by light a microscopy imaging method[194] using Cytation 5 for electroporation-induced aggregates. Particle diameter and number were quantified by Cytation 5's imaging analysis software. To distinguish between background and particles, the bright field intensity was set at 5000 a.u. and the particle size range from 0.5 to 100 μm were set as thresholds. 5 spots per well were imaged and were analyzed. Additionally, spectroscopic assays were employed according to

previous studies[195-197] to determine the turbidity (*i.e.,* the absorbance) of the solution. Absorbance spectra were quantified between 230 nm and 998 nm using a spectrometer (Cytation 5). The reading was recorded immediately after loading samples into a 96 well UV transparent plate. The maximum optical density (OD) in the spectrum at 230 nm was used to compare between samples.

2.2.2.6.3. Mitigation of aggregation and cytotoxicity via electroporation parameters

To assess the electroporation media effects on electroporation-induced aggregation, Opti-MEM, Opti-MEM+EDTA, 50 mM trehalose, and hypotonic electroporation buffer were prepared. In regard to the condition of Opti-MEM+EDTA, 5 mM EDTA was added to the electroporated mixture immediately after electroporation following the protocol from Lamichhane, Raiker and Jay, who reported similar effects can obtain with EDTA addition either before or after electroporation.[161] 50 mM trehalose, shown by Hood, Scott and Wickline as a membrane stabilizer to ameliorate the electroporation induced-aggregation,[198] was prepared accordingly. Commonly used hypotonic electroporation buffer[187, 199] was also prepared as mentioned in "2.2.5.1 siRNA loading" section.

2.2.2.7. Quantification of RNAi knockdown and eEV targetability

2.2.2.7.1. Quantification of siRNA knockdown in A549 cells

To evaluate the knockdown efficiency of EV-mediated siRNA delivery within the constitutively expressing-GFP-A549 cells over time, GFP fluorescence was measured and quantified using a plate reader (Cytation 5) every day for 12 days.[200] To ensure the decrease of green fluorescence intensity is due to the RNA interference of GFP-siRNA in

the cells and not caused by the cytotoxicity of the delivery system, each sample type or condition was delivered with scrambled siRNA as a control. The knockdown efficiency was calculated using the below equation:

$$\text{Knockdown\%} = 100 \times \left(1 - \frac{(F_{si} - F_{bg})}{F_{osi}} \times \frac{(F_{osc})}{(F_{sc} - F_{bg})}\right) \quad (2.2)$$

where F_{si} is the fluorescence of the well using GFP-siRNA, F_{sc} is the fluorescence of the well using corresponding scrambled siRNA, F_{bg} is the fluorescence background of the media without cells, F_{osi} is the initial fluorescence of the well just prior to delivery for the GFP-siRNA formulations and F_{osc} is the initial fluorescence of the well prior to delivery of the corresponding scrambled siRNA control group. Commercial Lipofectamine® RNAiMax formulation was used as a positive control to compare the knockdown efficiency between samples. The formulation was prepared according to the manufacturer's instruction. Briefly, 0.3 µl of Lipofectamine® RNAiMax was used to deliver 1 pmol of siRNA. The siRNA-Lipofectamine® RNAiMax complexes were mixed in Opti-MEM® media and incubated at room temperature for 10 min. before delivery to the cells. For the *in vitro* siRNA delivery and knockdown assessment, each sample mixture was delivered to the cells for 2 hr. After 2 hr., the sample solutions were replaced by the typical culturing media (with serum) for continual measurements. Area under the curve (knockdown efficiency vs time) was calculated to determine the difference in duration using GraphPad Prism 7 software.

2.2.2.7.2. Uptake experiments in A549 and CCL-210 cells

2.5×10^4 cells were seeded on glass coverslips 24 hours prior to imaging and quantification. Deep Red Plasma Membrane Stain Cell Mask was used to label EVs/eEVs

following the protocol modified from previous literature.[201] Briefly, EVs/eEVs were incubated with CellMask (1:10000 dilution) in PBS for 5 min. at 37^{0}C and then wash-centrifuge three times to remove free Deep Red dyes. Deep Red dye labeled-EVs/eEVs were subsequently added to the cells and incubated for 2 hours at 37^{0}C. All cells were then fixed with 4% paraformaldehyde and counterstained with 5 μg/ml of Hoechst 33258 for nuclei visualization. Cell samples were imaged using a confocal microscope (Olympus FV1000). All the images were analyzed with Image J software. To further quantify the uptake efficiency in the cells, cells were washed with PBS, trypsinized and assayed using a BD Accuri^{TM} C6 Cytometer at a 14 μl/min of flow rate. 10000 events were collected per sample with triplicates. The signal of Deep Red fluorescence was quantified using the geometric mean of FL4-A of the cell population, which is commensurate with the amount of EV/eEV uptake per cell. To eliminate any cell line-specific difference in the signal background, the following equation was used for calculation:

$$\text{Uptake efficiency in cells} = \frac{\frac{GM_{\text{EV or eEV in A549 or CCL210}}}{GM_{\text{untreated cells (A549 or CCL210)}}}}{\frac{GM_{\text{eEV in A549}}}{GM_{\text{untreated A549}}}} \quad (2.3)$$

Untreated A549 and CCL-210 cells were measured as a negative control. The uptake of POPC-EV in the absence of Deep Red dye staining in A549 and CCL-210 was also examined to confirm no auto-fluorescence interference from the vesicles. It is important to note that the excessive lipophilic dye staining with exosomes may cause non-specific binding to the cell membranes, resulting in false-positive signals or the change of exosome uptake pathways (Dominkuš *et al.*,[202] and Simonsen JB[203]). Our (dye only) control which was similarly centrifuged serially and assayed *via* flow cytometry indicated

the background fluorescence was only 1.4 ± 0.3% and 4.2 ± 0.9% of the A549 and CCL210 cells' samples, respectively.

2.2.2.8. Statistics

Data are presented as the mean ± the standard deviation (SD). All experiments were conducted with triplicates (Exception are indicated specifically as below). Statistical data analyses were performed using GraphPad Prism 7 software. The α value was set at 0.05, where *, **, ***, **** represent *p*-values <0.05, <0.01, <0.001, and <0.0001 respectively. The following statistical tests were conducted for each figure: **Unpaired, two-tailed Student's t-test:** Figure 2.1B; Figure 2.2A/B; Figure S10; Figure S15A and B; Figure S17. **One-way ANOVA, followed by Dunnett's multiple comparison test (post-hoc):** Figure 2.2C (compared to EV); Figure 2.2E (compared to EV in water and PBS, respectively); Figure 2.3A (compared to EV); Figure 2.3D (compared to EV; n=2 for negative control group); Figure 2.4 (compared to EV); Figure 2.6A (compared to Opti-MEM group); Figure S14 (compared to untreated cells); Figure 2.7B and D (compared to EV). **One-way ANOVA, followed by Tukey's multiple comparison test (post-hoc):** Figure 2.2D; Figure S4; Figure 2.3A (to compare each lipid-doped eEVs at varying ratio, no statistical difference in the results); Figure 2.5A (technical replicates of n=3); Figure 2.6B; Figure S7; Figure S12C; Figure S17A and B; Figure 2.7C; Figure 2.8B.

2.3. Results and Discussion

Lipid hybridized EVs, called engineered extracellular vesicles (eEVs), were prepared by sonication and extrusion method, as summarized in **Scheme S1**. To manufacture eEVs, EVs were first collected and characterized. In this work, we obtained

batches of EVs from A549 and 3T3 cells using a gold standard protocol,[204] involving serial centrifugation and ultracentrifugation to isolate EVs, specifically exosomes, from culturing media. However, it is reported that EVs isolated from ultracentrifugation often produces exosomes containing impurities of microvesicles or impurities of protein aggregates adsorbed on the isolated vesicles.[199] Due to the possibility of co-presence of microvesicles and exosomes within our population of vesicles, we named our system "extracellular vesicles" (EVs) to avoid any confusion or argument.

2.3.1. Physicochemical Quantification of EVs from Cells

The isolated EV populations were initially characterized by transmission electron microscope (TEM), nanoparticle tracking analysis (NTA), total protein content and flow cytometry. Representative size distribution profiles of EVs revealed by NTA are shown in **Figure 2.1A**. Average particle diameters of 124.3 ± 14.7 nm and 90.1 ± 18.6 nm were obtained for EVs derived from 3T3 (3T3 EVs) and A549 cells (A549 EVs), respectively. The EVs from both cell types had uniform and narrow size distributions. No larger particles above 500 nm were observed. TEM morphology (inlet image of **Figure 2.1A** and **Figure S1**) demonstrated spherical shape of the vesicles. In terms of the production yield, we obtained 3T3 EVs on the order of $(1.97 \pm 0.37) \times 10^9$ particles from 10^7 cells, namely, 197 ± 37 EVs per cell; whereas a higher amount of EVs were released per cell from A549 cells, on the order of $(4.80 \pm 0.23) \times 10^9$ particles from 10^7 cells (480 ± 23 EVs per cell), as shown in **Figure 2.1B** (left y-axis). On the other hand, representative protein amounts of EVs quantified by Micro BCA assay are shown in **Figure 2.1B** (right y-axis). Amounts of 0.20 ± 0.08 μg protein and 0.08 ± 0.05 μg protein within 10^8 EV particles were

quantified in 3T3 EVs and A549 EVs, respectively. Our characterizations of EVs are similar to the production yields of U937 (human monocytic cells)- and HEK293T (human embryonic kidney cells)-derived exosomes reported from previous studies.[94, 192] As a model system for gene delivery, the yields of EV production from parental sources and the selectivity to the cells of interest need to be considered. Our data demonstrated A549 cells had a 2.4-fold higher (***p <0.001) production yield of EVs compared to the EV yields of 3T3 cells. We chose A549 cell as the source of EVs to generate batches of eEVs because of their relatively higher production yield and potential targetability of tumor derived-extracellular vesicles to tumor cells.[83, 205] Although human mesenchymal stem cells (hMSCs)-derived EVs are well-known as an efficient mass producer of EVs[102] (~2100 ± 300 released hMSC EVs/cell, ~5-folds higher than A549 cells, based on our data), due to the limited expansion of hMSC culture[206] and favorable doubling time of A549 cells (>50 hours for hMSCs[207] whereas 22 hours for A549), we opted to use A549 cells, for the purpose of demonstrating the development of scalable eEVs. Isolated A549 EVs were then analyzed by flow cytometry for the presence of specific markers. As shown in **Figure 2.1C**, fluorochrome-labeled anti-CD63 binding EVs and nonfluorescent isotype control showed discernible populations in the gate FL1 versus FL4 (anti-CD63-eFluor 660). Results showed CD63 is highly enriched in the isolated EV samples. 87.4 % of the isolated samples were positive for the exosomal marker CD63 (**Figure 2.1D**). Therefore, we expected the majority of our EVs to be exosomes (CD63+), as opposed to microvesicles where CD63 was typically not detected (CD63-).[208]

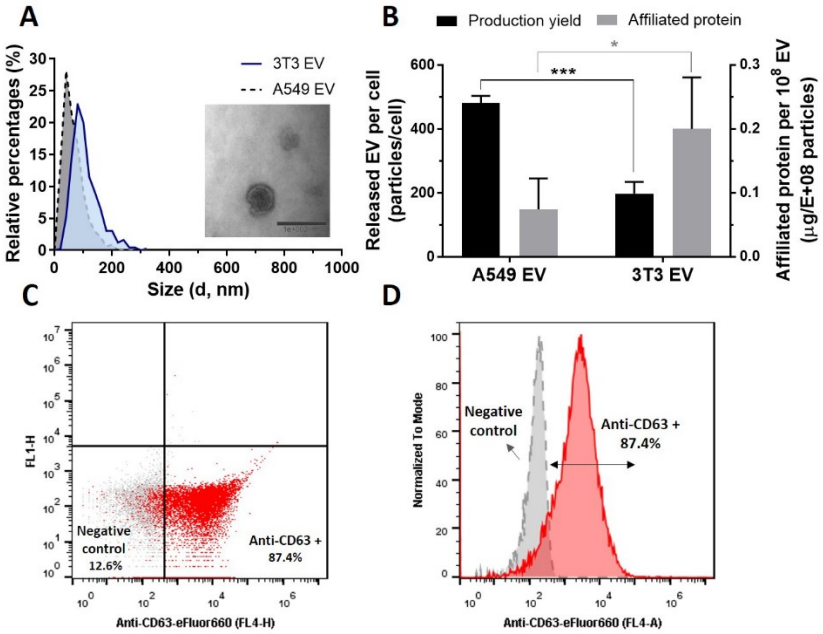

Figure 2.1 Characterization of extracellular vesicles (EVs) after ultracentrifugation. (A) reports the relative size (diameter) distribution profiles for A549 (dashed line, gray peak) and 3T3 cell (solid line, blue peak) -derived EVs. A transmission electron microscope (TEM) image inlaid within (A) showed the spherical structure of EVs (3T3 EV; scale bar: 200 nm). (B)'s left y-axis reports the production yield of EVs secreted by A549 and 3T3 cells. Affiliated protein per EV (Micro BCA assay) is reported on the right y-axis of (B). (C, D) Flow cytometric analysis of EVs stained with fluorescent labelled antibodies targeting CD63. (C) reports a scatter plot of A549 cell-derived EV (red dots on bottom right of (C)) and the negative isotype control (gray dots, bottom left box of (C)). (D) reports a histogram of $CD63^+$ A549 EVs stained with anti-CD63-eFluor 660 (solid line, red peak) and negative isotype control (dashed line, gray peak). (* and *** represent p-values <0.05 and <0.001, respectively). Reprinted with permission from © 2020 Elsevier from Jhan *et al*.[209]

2.3.2. Physicochemical Quantification of eEVs from Cells

To generate eEVs, the isolated EVs were then fused with pre-hydrated lipids using a sonication and serial extrusion procedure. We investigated whether different charges of lipids could be incorporated to native/naïve cell derived EVs. A library of lipids (DOTAP, POPC, DPPC and POPG) were therefore prepared for membrane hybridization. The

structures of these lipids are as shown in **Figure S2**. After producing lipid-doped eEVs, we characterized the morphology, size, mass production and zeta potential of eEVs. **Figure 2.2A** and **B** show the size distribution profiles of pre-hydrated POPC liposomes alone and POPC-doped eEVs, respectively: 138.8 ± 9.1 nm and 126.3 ± 4.0 nm (***p<0.001; statistically significant). The inlaid TEM images of **Figure 2.2A** and **2.2B** depict the morphology of pre-hydrated POPC liposomes alone and intact structure of POPC-doped eEVs. While heterogeneous size of pre-hydrated liposomes was shown in **Figure 2.2A**, a lamellar structure and uniform size of vesicles approximately 100 nm were demonstrated in **Figure 2.2B** for eEVs. The TEM morphology confirmed the vesicle structure was not impaired by the sonication-extrusion method, indicating the extrusion apparatus is a suitable method for fabricating lipid-hybridized eEVs. We further characterized a variety of lipid-doped eEVs at varying extruded ratios (from 1:1 to 9:1 of lipid to EV mixing ratio) by performing the same sonication-extrusion processes, as shown in **Figure 2.2C**. As expected, the average diameters of eEVs measured by NTA indicated that eEV formulations are much smaller than 200 nm size, thus these formulations would likely be able to take advantage of the enhanced permeability and retention effect.[2] Among each individual lipid-doped eEVs, no statistical difference on the particle size for eEVs at varying extruded ratio was observed.

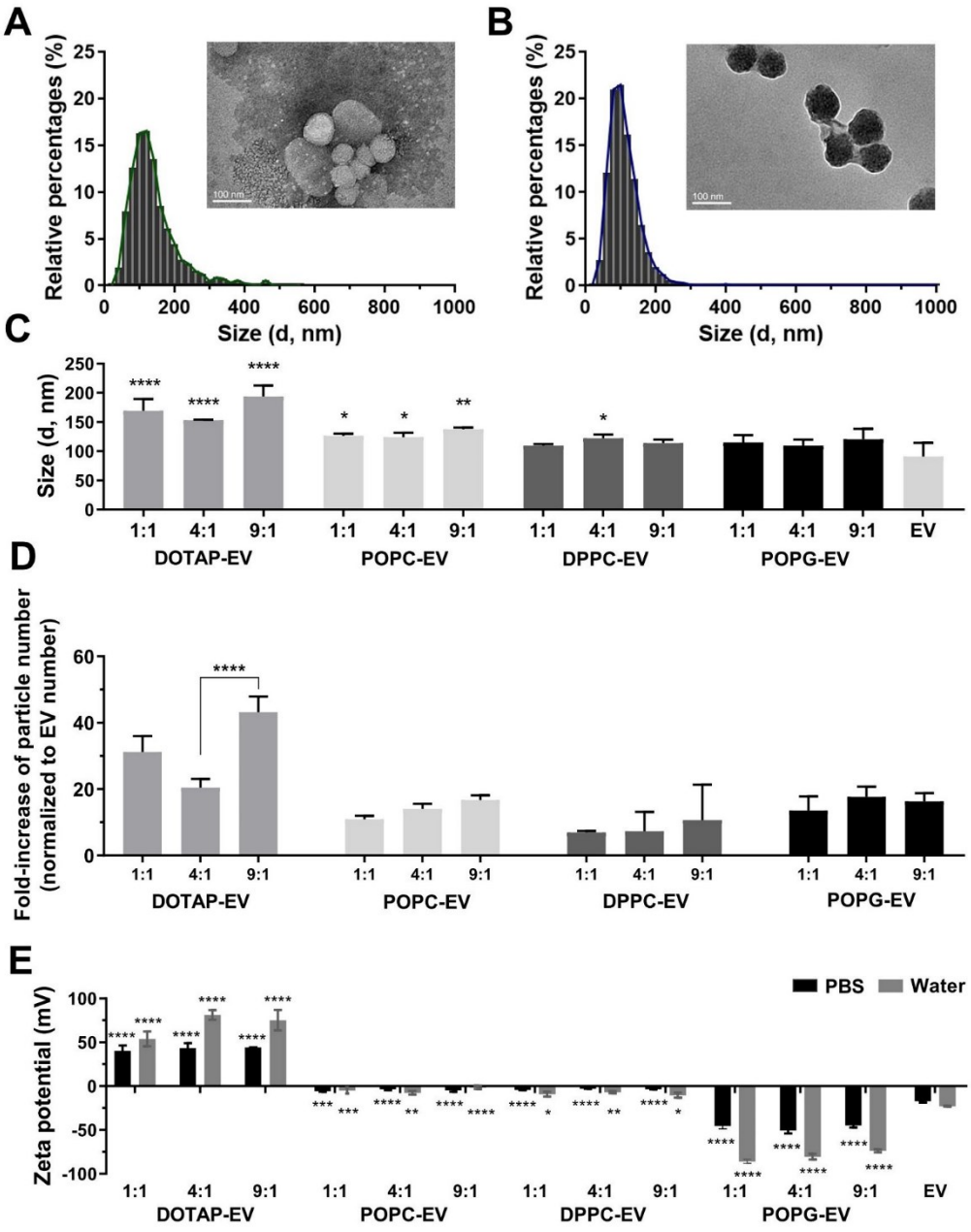

Figure 2.2 Morphology, size, quantification of mass production and zeta potential measurement of engineered extracellular vesicles (eEVs). The size distribution profiles and morphology of vesicles for hydrated lipids POPC (A) and engineered EVs: POPC-EV (B) were measured by NTA and TEM. Scale bar represents 100 nm. The mean diameters (C) of different lipid-doped eEVs were determined by NTA measurement. Fold increase in particle number (D) was quantified by normalizing the concentration of eEVs after extrusion processes to the concentration of original native EV concentration before extrusion processes. Zeta potential values measured in water and PBS are reported in (E). (*, **, ***, ****, represent p-values <0.05, <0.01, <0.001, and <0.0001, respectively). Reprinted with permission from © 2020 Elsevier from Jhan *et al*.[209]

Several studies have endeavored to develop scalable techniques at the stages of EV generation and purification, such as: using a two compartment culture (Integra CELLine);[115] a microcarrier-based 3D culture;[98] a hollow-fiber culture system;[210] and a tangential flow filtration system for purification.[98] Among these studies, a 7-fold to 40-fold increase in the production yield of EVs was achieved. In this study, instead of scaling up the production of EVs from the cells, we attempted to mass produce the vesicles after EV isolation. By evaluating the quantity of eEVs using NTA measurements, we observed a constantly higher production yields over various conditions (*i.e.,* different lipid-doped eEVs and varying lipid:EV ratios) obtained by our sonication-extrusion technique compared to native EV production yields, as shown in **Figure 2.2D**. On average, there was a 6-fold (for DPPC-EV 1:1 samples) to 43-fold (for DOTAP-EV 9:1 samples) increase on the overall amount of particle number upon the sonication-extrusion processes (**Figure 2.2D**). While DOTAP-EV showed an average of 20-fold further increase of particle yields, POPC-EV, DPPC-EV and POPG-EV showed similar 10-fold increase values. Initial particle number of different lipid types in same molar concentration were also quantified in **Figure S3**. No statistical difference of particle number was shown among different types of lipids. These results indicated that the increase of particle number after sonication-extrusion technique most likely depends on the physical-chemical properties of lipids (*i.e.,* charge), instead of the initial particle numbers of lipids. Overall, the production yields of eEVs generated post-EV isolation were about ~8-fold higher than

the number of EVs obtained from hMSCs using typical cell generation method, according to the results of hMSC EV from previous literature.[98, 102]

While others have integrated other synthetic materials (*i.e., via* freeze-thaw methods and PEG-induction methods) to already-isolated-EVs, such as liposomes and have proposed such systems as potential drug delivery carriers,[211] our system highlights the ability to mass produce the number of vesicles, as opposed to multi-lamellar/hybridized EVs.[141, 212] Furthermore, our data of different lipid-doped eEVs demonstrate that the mass production can be tuned by the incorporation of EVs with cationic, anionic, and zwitterionic lipid chains.

To evaluate the difference of lipid: EV mixture before and after the sonication-extrusion processes, zeta potentials of the vesicles were measured, as shown in **Figure S4**. The data showed the sonication-extrusion processes significantly alters the zeta potential of the samples in comparison to the samples of physical mixture (*$**p<0.01$ and $***p<0.001$ for POPC-EV 4:1, 1:1 and 9:1 group, respectively*). The zeta potentials of the eEVs at varying extruded ratio were also statistically different (*$****p<0.0001$*) compared to the native exosomal membrane (**Figure S4**). We further characterized the zeta potentials of EV and eEVs measured in PBS and water, as shown in **Figure 2.2E**. It is known that phospholipids, such as cholesterol, phosphoglycerides, ceramides and saturated fatty acids, are rich within EV membranes.[95] The presence of saturated phospholipids and the anionic surface charge help contributed to the high stability of EVs.[95] Therefore, relatively negative zeta potentials of EVs were obtained with -22.9 ± 0.6 and -17.3 ± 1.4 mV in water and PBS, respectively. Compared to the zeta potentials

of samples measured in pure water, zeta potentials in PBS were closer to neutral (0 mV). These results can be attributed to the charge shielding effects by salt ions present. These data are similar to the zeta potential of EVs generated from the neuroblastoma cell lines reported previously,[213] which ranged from -14.8 ± 1.6 to -12.0 ± 0.2 mV in a PBS solution. On the other hand, the zeta potentials of eEVs were found to correspond to the charge of extruded lipids. DOTAP-EV, POPC-EV and DPPC-EV, and POPG-EV showed positive, neutral, and negative charge, respectively (**Figure 2.2E**), indicating the zeta potentials of eEVs can be tuned by hybridizing EVs with different charge types of synthetic lipids. Taken together, our data demonstrate the sonication-extrusion processes significantly alters the zeta potential of eEVs, suggesting that there were substantial alterations of the lipid content within the eEVs.

2.3.3. Quantifying Native EV Fraction within eEVs for Validating Membrane Incorporation

In the current study, we first chose lipid (SPV) and protein (Micro BCA) assays that are widely used in the EV field to determine membrane incorporation within the vesicles. Before determining the protein to lipid ratios in EVs/eEVs, preliminary tests of individual lipid species were measured as references, which showed good linearity of absorbance in the range of 0-2 μg/μl lipid concentration using SPV assay (**Figure S5**). In parallel to the lipid quantification, pure lipid solutions were also tested for their assay interference with the protein determination **(Figure S6**). No substantial interference on the protein Micro BCA assay by lipids was observed, as the data did not result in strong colorimetric reactions. We then evaluated the protein quantities between the physical

mixtures of EV: lipid and the eEVs following sonication-extrusion processes. **Figure S7** evidences a statistically significant change (****p <0.0001) of protein quantities in the lipid-EV mixture before (physical mixture in the absence of sonication-extrusion processes) and after sonication-extrusion processes (lipid-doped eEVs). To further determine the fusion efficiency of exosomal membrane in eEVs, we quantified the protein to lipid ratio, which has been proven to be a good quality control parameter of EVs previously.[44] **Figure 2.3A** presents the calculated protein to lipid ratios of EVs/eEVs. The protein to lipid ratios of eEVs (0.069 ± 0.004 to 0.594 ± 0.055) significantly (****p<0.0001) dropped compared to the protein to lipid ratio of EVs (3.529 ± 1.015). These results demonstrate the exogenous synthetic lipids were doped within EVs. With the addition of lipids to EVs, the overall percentage of lipids within the membrane increases, results in the dropping of the protein to lipid ratios within eEVs. In comparison to the pure lipid solutions (**Figure S6**), our results showed a 5-fold (DPPC-EV 4:1/DPPC lipid=0.29/0.057) to 42-fold (DOTAP-EV 4:1/DOTAP lipid=0.59/0.014) of protein to lipid ratio change within eEVs upon the membrane extrusion procedure. Note that the protein to lipid ratio only slightly changed at varying extruded ratio, as no statistical difference was observed (**Figure 2.3A**). Similar trend of the protein to lipid ratio within eEVs was obtained while using the EVs from different cell sources (3T3 EV and A549 EV) (**Figure S8)**, indicating this technique for membrane incorporation can be applied to EVs derived from different parental cells.

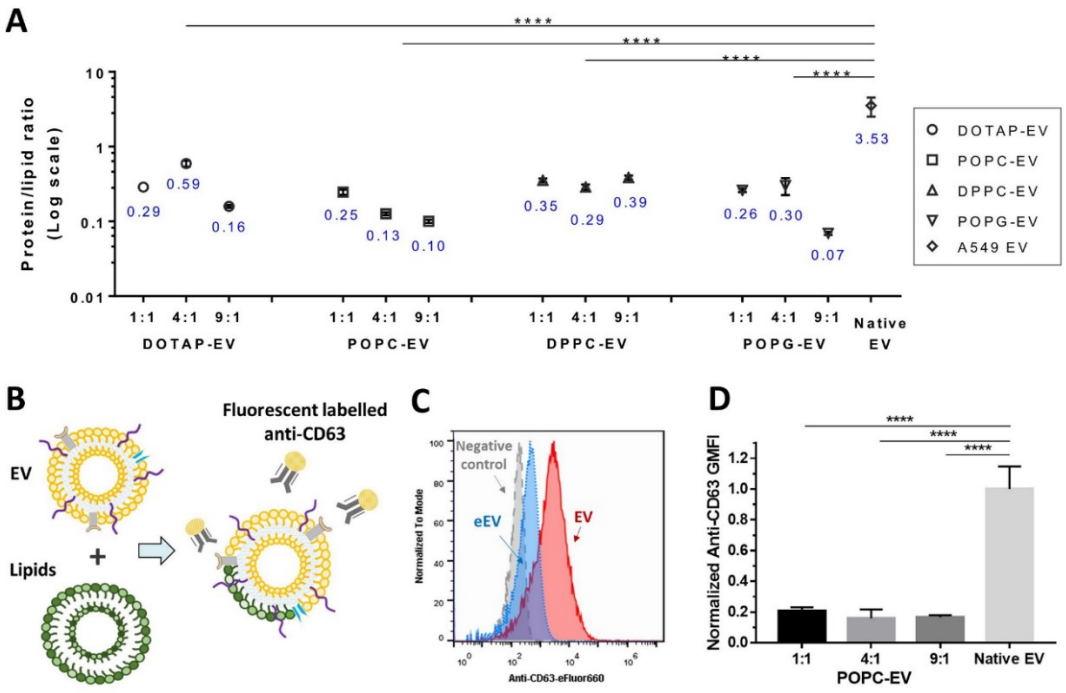

Figure 2.3 Assessment of membrane incorporation of engineered extracellular vesicles (eEVs) *via* protein: lipid ratio quantification and FACS analysis. The protein: lipid ratios within the membrane of different lipid-doped eEVs were quantified in (A). An illustration of membrane incorporation validation within eEV entities using anti-CD63 detection *via* flow cytometry is shown in (B). Flow cytometry histograms (C) of: A549 EVs stained with anti-CD63-eFluor 660 (solid line, red peak); eEV stained with anti-CD63-eFluor 660 (dotted line, blue peak); and a stained isotype (dashed line, gray peak), functioning as a negative control. The normalized anti-CD63 geometric mean fluorescence intensities (GMFIs) are shown in (D) and quantify the fusion ratio of synthetic lipids doped within EVs, thereby forming eEVs (0-1 represents 0%- 100% native EV). (**** represents p-values <0.0001). Reprinted with permission from © 2020 Elsevier from Jhan *et al*.[209]

To further confirm the membrane fusion of exogenous synthetic lipids within the EVs, as opposed to synthetic lipids and EVs being physically mixed, flow cytometry was used to detect the fluorescence of each entity (**Figure 2.3B**). The histogram plot of anti-CD63 fluorescence is shown in **Figure 2.3C.** Normalized geometric means of fluorescence confirmed the percentage of membrane incorporation in POPC-EV (1:1, 4:1, 9:1) samples as a fraction ratio of 0.16 to 0.21 (**Figure 2.3D**), meaning the eEVs having

16 − 21% native EV membranes within them. Similarly, no statistical difference was observed at varying extruded ratio for eEVs. The results of our flow cytometry-based assays and the membrane protein/lipid assays corroborate each other, in that both illustrate our sonication-extrusion process fused a fraction of each of the synthetic lipids within the EVs. The histogram plot of anti-CD63 fluorescence in flow cytometry demonstrated individual eEVs present higher CD63+ levels compared to the isotype control of liposome-POPC) as background fluorescence and lower levels compared to native/naïve EVs, suggesting the successful fusion of exosomes with lipids. These data demonstrate our method of generating EVs can increase the yield of particles post-EV isolation while retaining native protein (*i.e.,* CD63) within each entity.

It is interesting that we did not observe statistical differences of eEVs at varying extruded ratios in both protein/lipid assays and flow cytometry experiments, indicating we were likely at a point of saturation, in terms of the amount of synthetic lipid that could be incorporated into the membrane. These results are different from the lipid-hybridized EVs triggered by PEG-induced fusion reported from literature,[212] who showed that 9% to 56% of lipids could be incorporated by varying EV:lipid ratios. This discrepancy between the two methods could likely be attributed to the difference of lamellarity and localization of lipids within the EVs. While 30 − 40% of multi-lamellar vesicles tend to form using PEG-induced lipid:EV fusion,[212] additional studies for lipid-doped eEVs using sonication-extrusion processes would need to be conducted to suggest a percentage, which we plan to do in the near future.

2.3.4. EV and eEV siRNA Loading

The capability of EVs for efficient drug loading without drastic physicochemical modification of the native vesicles is one of the major and practical obstacles in the clinic. After generation of lipid-fused eEVs, we attempted to encapsulate exogenous siRNA into the vesicles. As a first step in evaluating the efficacy, we assessed the changes of physicochemical properties following electroporation. **Figure S9A** reveals intact and round shaped morphology of eEVs post-siRNA loading *via* electroporation. Occasionally, we found the vesicles appeared fused or aggregated after electroporation (**Figure S9B**). No obvious alternations on the vesicle size of the samples after electroporation were observed by NTA measurement at the concentration of ~10^8 particles per ml (**Figure S10A**). However, there was a statistically significant change (*p<0.05) on the z-average diameters of the vesicles post-electroporation, as measured by DLS at concentration of ~10^{11} particles per ml (**Figure S10B**). **Figure S10C** demonstrates the zeta potentials of eEVs after electroporation significantly decreased (**p<0.01) from -4.9 ± 3.5 mV to -28.0 ± 3.5 mV. Possible reasons for the differences between the results from the two instruments could be that DLS is biased towards large particles or aggregation occurs at higher concentration of the samples required for DLS measurement (~10^{11} particles/ml) compared to the sample concentrations required for NTA measurements (~10^8 particles/ml).

We furthered assessed the actual siRNA amount loaded into the vesicles. Prior to siRNA purification and quantification procedures, free unbound siRNAs in the sample mixture were removed by centrifugation and wash. By repeating these steps, our data

showed only 1.2 ± 0.2% of free siRNA retained in the pellet after centrifugation, validating the efficacy of removing free unbound siRNA. To evaluate siRNA loading efficiency *via* electroporation, we first demonstrated the buffer used for electroporation (hypotonic buffer vs isotonic Opti-MEM) does not substantially affect siRNA loading efficiency (**Figure S11**; no statistical difference) but does affect the retention of siRNA within the vesicles (**Figure S12**). The gel images and semi-quantified results in **Figure S12** demonstrated the siRNA was confined in the sample well with the electroporation condition using Opti-MEM media, resulting in a lower siRNA migration amounts than the samples using hypotonic electroporation buffer. In other word, using Opti-MEM media, siRNA was retained and bound within the vesicles. Based on these findings, Opti-MEM was used for all further evaluations.

Subsequently, we quantified the loading efficiency (**Figure 2.4, left y-axis**) and encapsulation efficiency (**Figure 2.4, right y-axis**) of each lipid-doped eEV system. We demonstrated exogenous siRNA can be loaded into eEVs and the loading efficiency is dependent on the hybridized lipid types. The loading efficiency results showed we were able to obtain 23 – 327 copies of siRNA per vesicle. Particularly, DOTAP-EVs showed highest loading efficiency, which was at least 8-fold higher than other lipid-extruded eEV systems. Moreover, the loading efficiency of cationic lipid-doped eEVs is comparable to the loading efficiency of unmodified, native EVs (**Figure 2.4**; no statistical difference). Taken together, zwitterionic eEVs (POPC-EV and DPPC-EV) and anionic eEVs (POPG-EV) exhibit generally comparable loading profiles (no significant difference between each other).

Consistent with the previous findings by the Wood's research group,[123, 187] we obtained similar electroporation efficiencies (~15 – 20% of siRNA could be encapsulated in EVs/eEVs by electroporation). Overall, in our results, electroporation seems to be a robust method for cargo loading within our eEVs, albeit aggregation issues could be a concern for cell studies. To explore the potential electroporation-caused aggregation of vesicles, we will now further discuss the sub-micron aggregates and their effects on cells.

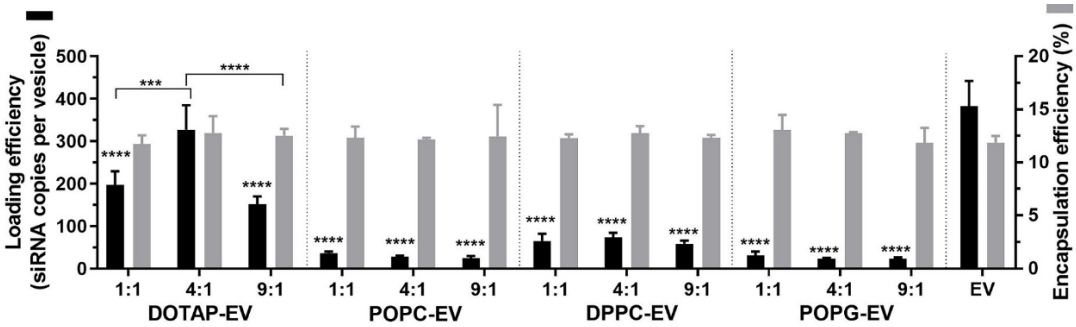

Figure 2.4 Exogenous loading of siRNA *via* electroporation system. Left y-axis reports siRNA loading efficiency (black) and right y-axis reports encapsulation efficiency (gray). (*** and **** represent p-values <0.001 and <0.0001, respectively). Reprinted with permission from © 2020 Elsevier from Jhan *et al*.[209]

2.3.5. Mitigation of eEV Aggregation and its Effects on Cytotoxicity

In the present study, we established a more stable (in comparison to what was initially commercially procured), and higher GFP-expressing tumor cell model (A549) for *in vitro* cell studies. The detailed methods and results are depicted in ***Supporting Information*** (**Figure S13**). This GFP model allows us to easily visualize and quantify the delivery of anti-GFP siRNA, and the resulting knockdown of the GFP using fluorescence

microscopy, fluorescence plate readers, and flow cytometry. In this section, we first conducted the cell viability (MTS) assay to evaluate if there is any cytotoxicity issue with siRNA loaded EV/eEV (10^{10}-10^{11} vesicles/ml) post-electroporation (**Figure S13**). Unexpectedly, independent of the lipid-doped eEV used, the viability was lower than 70%. Although in the previous section DOTAP-EVs were associated with higher siRNA loading efficiency, here it resulted in the highest toxicity, ranging from 18.2 ± 3.8% to 56.5 ± 3.9% at varying lipid:EV ratio (**Figure S14**). The cytotoxicity of DOTAP-EV could potentially be attributed to the charge of lipids, which has been shown to be toxic to the cells at high concentrations, although it is commonly used as a transfection agent.[214] In addition to the charge effects from the lipids, we hypothesized these cytotoxic results could likely be attributed to particle aggregation and sedimentation of the eEV-siRNA delivery system, as was seen in the brightfield images (**Figure S14**), note the precipitation of eEV within the bright field image of the engineered DOTAP-EV and DPPC-EV formulation. It is currently believed that the electric pulses from electroporation may cause undesirable metal ions to release from the electrodes and subsequently affect the lipid oxidation and the solubility of a variety of biomolecules.[215] In order to investigate whether the toxicity was due to the electroporation process or not, **Figure S15** quantifies the cytotoxicity of eEVs with siRNA mixture in the absence of electroporation, that the viability remained high (~80 – 125%) and was relatively independent of particle concentration. In other words, there were no obvious signs of toxicity observed in A549 cells while increasing the eEV concentrations from (0.13 – 1.08) $\times 10^{11}$ and (0.95 – 15.72) $\times 10^{11}$ particle/ml for the engineered DOTAP-EV and POPG-EV formulations, respectively. However, there

was a significant reduction of cell viability for both eEV-siRNA mixture assessed post-electroporation: DOTAP-EV (post-electroporation) decreased 7-fold to only 18% viability (***p<0.001) and POPG-EV (post-electroporation) decreased 2-fold to 51% viability (**p<0.01). These results validated that the electroporation processes may cause undesirable consequences, such as aggregation, resulting in high cytotoxicity. Therefore, it highlighted the need for investigating ***the aggregation effects post-electroporation*** as well as ***optimization of the electroporation processes*** to avoid any adverse effects on the cells, which are discussed below in two sub-sections.

2.3.5.1. Aggregation Evaluation by Spectroscopic Assays and Microscopy Image Analysis.

To quantitatively determine the degree of aggregation post-electroporation, we used spectrometry and microscopy techniques. **Figure S16A** shows the UV-Visible spectra of siRNA, EV, and various lipid-doped eEVs. In all cases, the samples were electroporated either with ("+siRNA") or without siRNA ("vesicle only"). The Opti-MEM and pre-electroporated eEVs conditions were measured as baselines and their spectra appear to overlap substantially. Because there was not a signature absorbance peak in the spectra (**Figure S16A**), we used the maximum absorbance at 230 nm to quantify the aggregation as a turbidity measurement,[194, 216] as shown in **Figure 2.5A**. On the other hand, a few representative images for siRNA, EV w/o siRNA ("vesicle only"), and DOTAP-EV w/o siRNA ("vesicle only") are shown in **Figure S16B** which were used for the microscopy image analysis. The results from both experiments showed the electroporation-induced aggregation occurred in not only membrane vesicles but also

naked nucleic acids (siRNA). These finding were in line with previous observation from Stapulionis[215] and Kooijmans *et al*.[162] Notably, the quantitative results of turbidity (OD: 230 nm) (**Figure 2.5A**) and semi-quantified image data (**Figure S17**) showed a decrease of the tendency of aggregation when the electroporation is carried out in the presence of both siRNA and vesicles, compared to electroporating vesicles/siRNA alone. Moreover, the data suggest that in most cases, the degree of aggregate formation decreased for all lipid-doped eEVs, compared to native EVs post-electroporation. A larger library of lipids would need to be assessed in order to elucidate the entire parameters affecting the aggregation, however.

We also validated the aggregation of siRNA loaded EVs/eEVs, in terms of the turbidity (OD: 230 nm), number, and the size of aggregates. We found the results vary in a concentration-dependent manner for all EV/eEV formulations. Our data demonstrated the degree of aggregation (**Figures 2.5B**, **C**, and **D**'s y-axis are OD: 230nm, aggregate concentration, and size, respectively) significantly increased 9- to 17-fold at the concentrations used for DLS and cell studies ($>10^{10}$ particles/ml), in comparison to the sample concentration used for NTA measurement (10^8 particles/ml). These findings point out the electroporation-caused aggregation may be far more significant than previously believed. Given that NTA is commonly used for particle analysis in the scientific community at a concentration of approximately hundred-fold lower than the dose applied for cell studies, the aggregation effects are likely underestimated. We provided evidence that strong aggregation of samples occurs after electroporation, which may result in far more severe impacts for *in vitro* and *in vivo* studies than NTA appears to be suggesting.

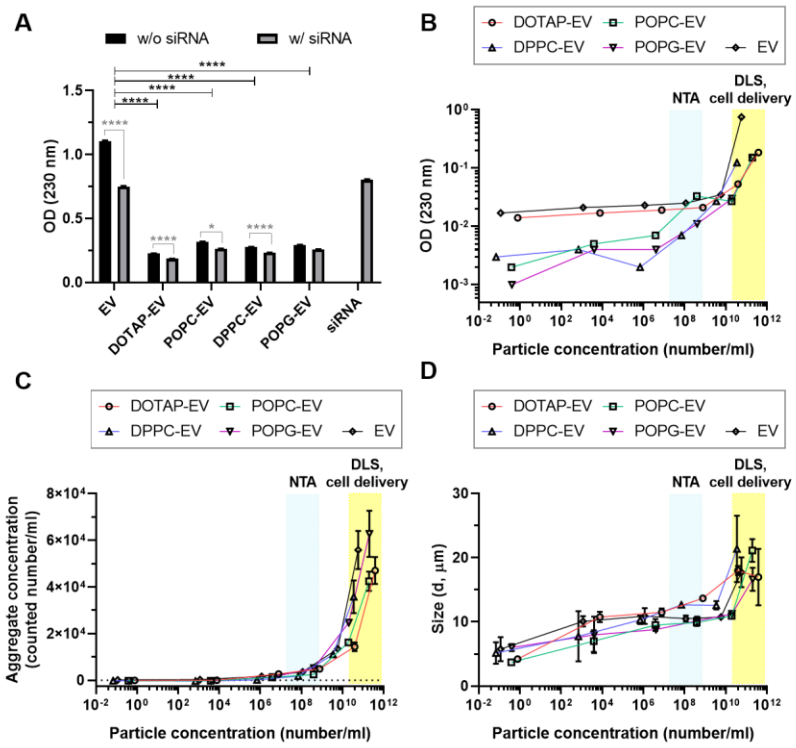

Figure 2.5 Characterization of aggregation post-electroporation by spectroscopic assays and microscopy image analysis. (A) shows the turbidity (OD: 230 nm) for EV, eEVs and siRNA conditions in the absence of siRNA (w/o siRNA, meaning only vesicles in the solution) or in the presence of siRNA (vesicle +siRNA) during electroporation. The absorbance values in y-axis have the background values (Opti-MEM media/pre-electroporated samples) subtracted. (B) is a log-log plot of turbidity (OD: 230 nm) versus vesicle concentration after electroporation. (C, D) are semi-log plots of aggregate counts per ml and aggregate size (diameter) versus vesicle concentration after electroporation. Data were determined by microscopy image analysis. (B, C, D) The blue regions are the concentrations suitable for NTA quantification, whereas the yellow regions are the concentrations suitable for cell delivery and DLS quantification. Reprinted with permission from © 2020 Elsevier from Jhan *et al*.[209]

2.3.5.2. Optimization of the Electroporation Processes for Efficient Cargo Loading and Alleviation of the Electroporation-caused Aggregation and Cytotoxicity

Because we have validated substantial aggregation of EV/eEV and siRNA was formed following electroporation, we endeavored to mitigate the toxicity by tuning the

electroporation conditions. Several studies have reported a numbers of electroporation parameters could greatly influence the loading efficiency and aggregation results, such as applied voltage,[161, 215] pulse type,[161] pulse number,[161] and electroporation media.[162, 198] Here, we focused our efforts on the parameter specific to the electroporation buffer.

We evaluated the aggregation effects of various electroporation media (Opti-MEM+EDTA, 50 mM trehalose, and hypotonic electroporation buffer) after electroporation. We demonstrated the aggregation can be remarkedly decreased by adding EDTA to electroporation buffer (**Figure 2.6A**), as suggested in previous literature.[162, 215] However, unfortunately, the microscope imaging results confirmed the submicron aggregates were not removed and yet still existed in substantial amounts by microscopy image analysis (**Figure S18**). More strikingly, the effects of 50 mM trehalose on the aggregation level appeared to be different for different lipid-type eEVs. While the aggregation level of DPPC-EV, POPG-EV and native EV tended to decrease in 50 mM trehalose following electroporation, unexpectedly, the aggregation of DOTAP-EV and POPC-EV were likely to increase (**Figure 2.6A**). These results are opposite to the hypothesis from Hood, Scott, and Wickline, who reported that a 50 mM trehalose solution may minimize aggregate formation following electroporation,[198] suggesting different concentration of trehalose solution may be needed for different lipid-doped eEV system to optimize the aggregation effects. Moreover, despite hypotonic electroporation buffers are being commonly used in several studies for electroporation, we demonstrated the aggregation of eEVs in hypotonic electroporation buffers following electroporation was at least 1.5-fold higher than the eEVs in Opti-MEM (**Figure 2.6A**). This discrepancy of

results compared to previous literature could be attributed to the differences of employed assays for aggregation evaluation. While most studies used NTA measurement as a mean to determine the size and numbers of aggregates, the sub-visible aggregates may be underestimated, as discussed in the previous section. Regarding metabolic activity of EV/eEV while varying the electroporation buffers (**Figure 2.6B**), the 50 mM trehalose formulation was affiliated with the highest viability, except for POPG-EV (no statistical difference). In all cases, the formulations using Opti-MEM were significantly more toxic than the other buffers, which was 2-fold more toxic than using Opti-MEM+EDTA and 50 mM trehalose. Taken together, it is interesting to note that our results demonstrated the degree of aggregation of electroporated mixture may not be a direct linear relationship corresponding to cytotoxicity. Here, we also demonstrated the trend of cell viability with the variation of aggregation by combining the data from various media. **Figure S19** highlighted the correlation of aggregation for eEV appeared to be biphasic in response to cell viability, while the most toxic regime showed in the range of 0.2 – 0.4 measured absorbance (OD: 230 nm). Importantly, it should be noted that elucidating whether aggregation and cytotoxicity are correlative, or causative would be challenging, as aggregation is a secondary variable dependent on other factors. In other words, we cannot hold all other variables constant while varying aggregation to assess its effects on cytotoxicity alone. It is important to note that the cytotoxicity profiles of eEVs on non-cancerous cells were also examined in this study. No toxicity was observed on healthy cells using the optimized electroporation buffer (**Figure S20**). Given that the promise of electroporation continues to be hampered by a lack of appropriate and optimized

conditions, we believe investigating these parameters could be helpful for future consideration of EV-based gene therapies and enhance the potential clinical translation of EVs.

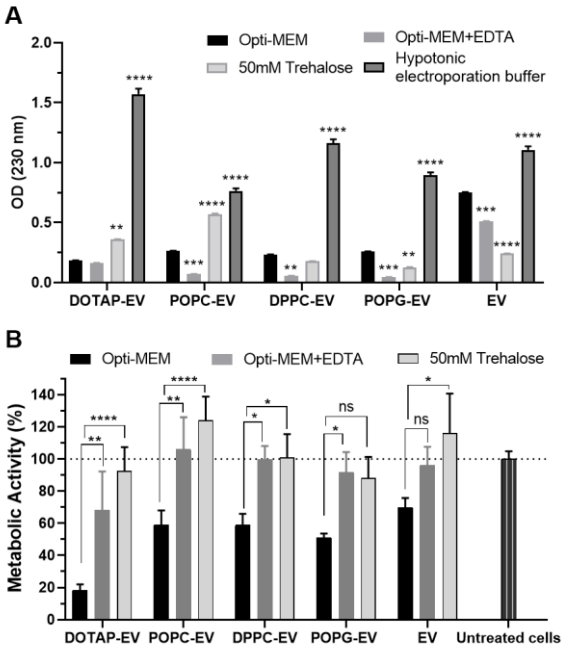

Figure 2.6 Effects of electroporation media. Effects of buffers on the formation of aggregates (A) and cell viability (B). Note: The cell viability assay was not conducted for eEVs in hypotonic electroporation buffer due to the excessively high level of aggregation. Reprinted with permission from © 2020 Elsevier from Jhan *et al*.[209]

2.3.6. Quantification of RNAi Knockdown and eEV Targetability

We opted to assess the siRNA silencing effects of EVs and eEVs electroporated in both Opti-MEM media with EDTA addition and 50 mM trehalose with the formulations which were affiliated with a cell viability greater than 80% (**Figure 2.6B**). **Figure 2.7A**

qualitatively demonstrated the decrease in the total GFP expression in the cells. To quantify the GFP expression in cells, fluorescence intensity was monitored over time using a plate reader assay. **Figure 2.7B-D** quantified the overall knockdown efficiency by analyzing the area under the curve for knockdown over time. Using 100 µl Opti-MEM, 10^{11} particles/ml, and 1 ng/µl siRNA in Opti-MEM, a 10 – 46% of knockdown efficiency was able to achieve by the eEV formulations, whereas the native EV-delivered siRNA failed to knockdown the GFP expression in an effective manner (**Figure S21A)**. An early and rapid decrease of knockdown efficiency was observed in native EV treated group at day 2, while the knockdown efficiency dropped after day 4 in eEVs. Overall, zwitterionic POPC-EV showed a highest knockdown with 41.1 ± 9.8% at 4 days post-transfection, which was comparable to commercial Lipofectamine RNAiMax of 43.3 ± 0.3% (**Figure S21B and C**). A summary of the overall knockdown efficiency in **Figure 2.7B** showed the knockdown efficiency of POPC-EV over time was statistically greater than the knockdown efficiency of EV (****p<0.0001). Next, the experiments were repeated using anionic POPG-EV to deliver the siRNAs to the cells with different dosage. Despite only 21% of knockdown was achieved by POPG-EV with initial dosage, **Figure S22A** showed that high dose of eEVs can more effectively down regulate the expression of GFP. A 2.4-fold of increase in inhibition of GFP expression was observed for 4-fold amount of dose of POPG-EV compared to initial dose. No statistical difference was observed between the area under curve of POPG-EV with the amounts of 4-fold dose and commercial Lipofectamine RNAiMax **(Figure 2.7C)**. The knockdown results among different lipid-doped eEVs implied the minimum effective dosage required varied with the properties of

hybridized lipids. Further evaluation on the dosage effect would be worthwhile in future studies.

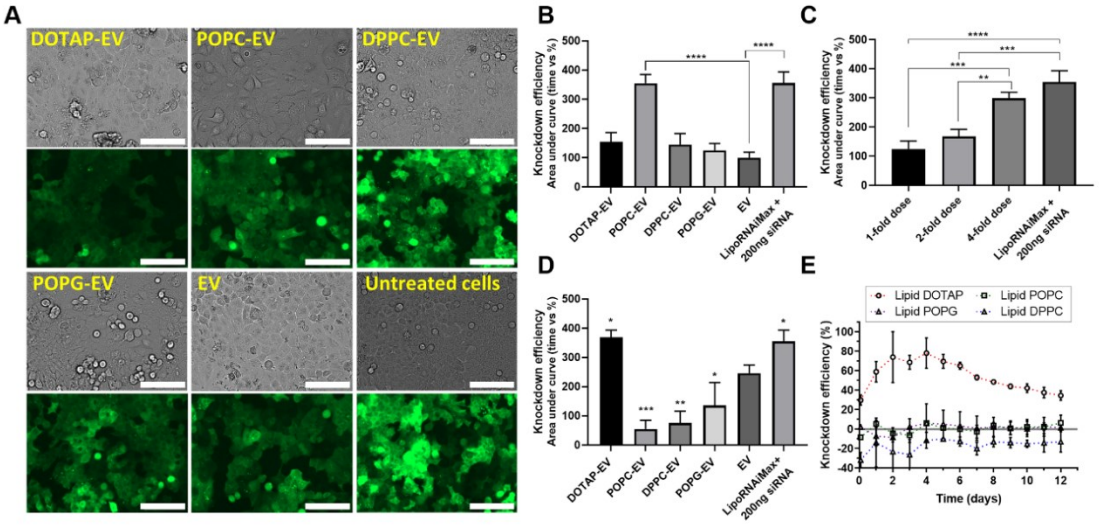

Figure 2.7 RNA interference knockdown of eEVs in lung tumor cells (A549). (A) shows fluorescence images of delivered anti-GFP siRNA with eEVs to A549 cells at 3 days post-transfection. scale bar: 100 µm. (B, C, and D) show the statistical analysis of overall knockdown efficiency of eEVs. (B) shows the effects of EV and eEVs in Opti-MEM+EDTA. (C) shows the effects of delivered dosages. POPG-EV in 100 µl Opti-MEM: 1-fold, 2-fold, and 4-fold are (10^{11} particles/ml, 1 ng/µl siRNA), ($2x10^{11}$ particles/ml, 2 ng/µl siRNA) and ($4x10^{11}$ particles/ml, 4 ng/µl siRNA), respectively. (D) shows the effects of EV and in 50 mM trehalose. (E) shows the knockdown curves over time of lipid-siRNA complexes following electroporation. Same molecule concentration (2.5 µl of 2.5 mM) of lipids as the final amounts used for eEV-siRNA delivery was prepared. Reprinted with permission from © 2020 Elsevier from Jhan *et al*.[209]

On the other hand, for the knockdown results of EVs and eEVs electroporated in 50 mM trehalose (**Figure S22B**), the extent of knockdown of EV increased to 22 − 34 % knockdown compared to the knockdown results (<10%) electroporated in Opti-MEM. These results could potentially be attributed to the decrease of aggregation for EV in

trehalose. However, like the aggregation data shown in **Figure 2.6E** and **F**, the effects of the electroporation buffer on knockdown also differed between different lipid-doped eEVs. A significant increase of knockdown efficiency to 49.0 % ± 7.3% was observed in the cells treated with cationic DOTAP-EV in 50 mM trehalose at 4 days post-transfection, while POPC-EV failed to reach 10% knockdown of the GFP expression (**Figure S22B**). The overall knockdown efficiency of eEVs in Trehalose (**Figure 2.7D**) shows only the knockdown efficiency of DOTAP-EV over time was comparable to the knockdown efficiency of commercial Lipofectamine RNAiMax (no statistical difference) and greater than the knockdown efficiency of EV (*p<0.05) in this case.

While discussing the functionality and efficacy of eEVs using different electroporated media, it should be noted that the findings of electroporation-induced aggregation pointed out a complication regarding the determination of knockdown efficiency; aggregated and precipitated particles may be uptake differently by the cells and may not be easily removed by washing. Therefore, it can be mistakenly considered as being transfected into the cells.[215] Further, to the extent of our knowledge, the scientific community has not conducted experiments to determine whether such aggregates inhibit or enhance the EV-mediated siRNA delivery into the cells.[162] Aggregation is known, however, in previous studies to cause enhanced uptake in at least certain cases.[217] Interestingly, by assessing the knockdown effects of lipid-siRNA complexes, which were the same lipids we used in our studies for doping purposes, we found RNAi only occurred when lipids POPC, POPG and DPPC were fused into EV vesicle membrane. As shown in **Figure 2.7E**, siRNA complexes with lipid POPC, POPG and DPPC was not able to down-

regulate GFP expression. These results suggest the lipoplexes which may form would not have contributed to the knockdown observed for POPC, POPG, and DPPC lipid-doped eEVs.

To further investigate if lipid-doped eEVs can direct targeting to different cell lines, we quantified the cellular uptake of native EVs and eEVs in lung adenocarcinoma (A549) and lung normal fibroblast (CCL-210). Prior to the uptake studies, Deep Red membrane dye was used to stain the exosomal membrane of EVs/eEVs, followed by incubation with the cells. The confocal images of cellular uptake (**Figure 2.8A**) revealed the internalization and localization of vesicles (red) in the cytoplasmic area. To further quantify the uptake efficiency between cell lines, flow cytometry assay was conducted and demonstrated in **Figure 2.8B**. We observed significant differences in EV uptake between the two cell lines, with the most efficient cell line, lung adenocarcinoma (A549), demonstrating a 15.8-fold higher uptake amount compared to the normal lung fibroblast (CCL-210). Remarkably, A549 cells also showed an increased propensity to take up eEVs that a 14.2-fold higher eEV uptake efficiency by A549 cells than that by CCL-210 cells was observed. Moreover, A549 cells exhibited a higher percentage of uptake population than CCL-210 cells. Approximately 84.2 % of A549 cells were uptake with eEVs, whereas only 47.8% of CCL-210 cells were uptake with eEVs (**Figure 2.8C**). Taken together, we observed a universal increase in uptake efficiency for the lung cancer cells versus normal lung fibroblast. These results supported the conclusion that the lipid-doped eEVs retained the targetability of EVs, despite the degree of selectivity on the cell lines could be declined by the decrease of EV portion in the engineered vesicle membrane. In this study, how

precisely the engineered lipid-doped eEVs entered the cells and how knockdown is achieved are yet needed to be investigated. We opted to test the cellular internalization of eEVs using zwitterionic POPC-EV because of the high knockdown efficiency (**Figure 2.7B**) and because little to no gene delivery effect was found from POPC lipid-siRNA complexes in our previous evaluation (**Figure 2.7E**) that the cellular internalization would less likely be affected by any free lipid components. Nevertheless, more research should be done in near future in terms of the uptake mechanisms (*i.e.,* clathrin- and caveolae-mediated endocytosis, macropinocytosis) to elucidate the critical factors determining EVs/eEVs uptake and targeting at molecular structure levels.

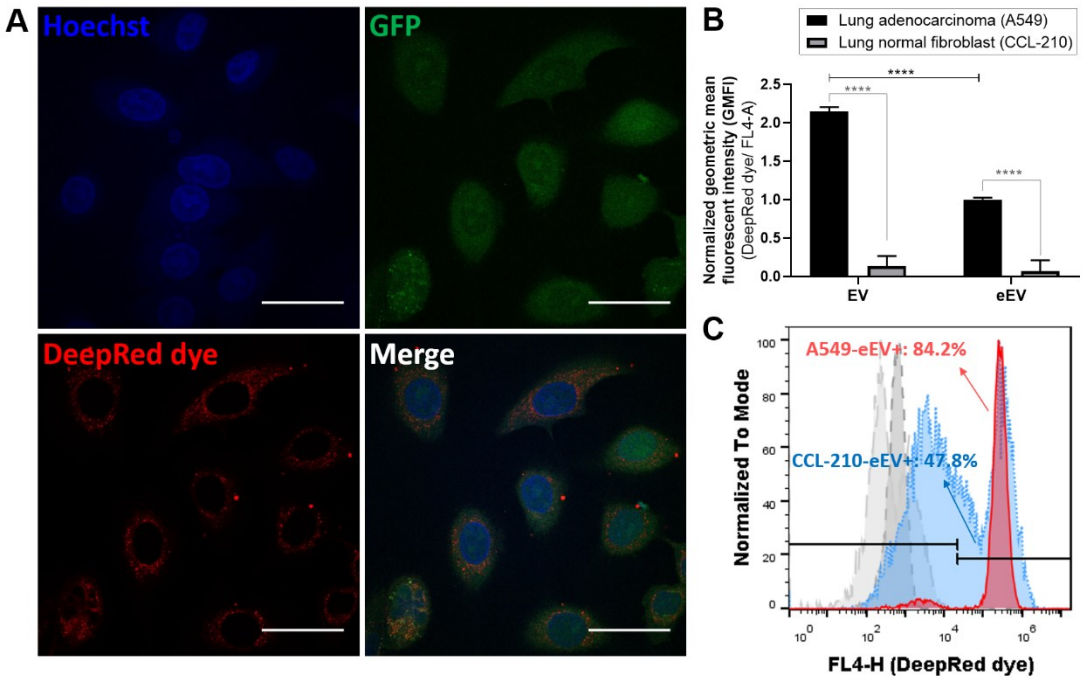

Figure 2.8 Visualization and quantification of eEV uptake to lung adenocarcinoma (A549) and lung normal fibroblast (CCL-210). Reprinted with permission from © 2020 Elsevier from Jhan *et al*.[209]

Figure 2.8 (Continued) (A) Confocal microscopy images of eEV (POPC-EV) incubated with A549 cells for 2 hours. Red indicates the DeepRed®dye for eEV membrane staining; Blue indicates Hoechst 33342 nuclei staining; Green represents the GFP expression in cell cytoplasm of A549 cells; Scale bar: 30 μm; (B) Normalized geometric mean fluorescence intensities (GMFI) from flow cytometry analysis to compare the cellular uptake efficiency of eEVs in A549 and CCL-210. 10^{11} particles of POPC-EV was used as representative of eEVs; same amounts of EVs (10^{11} particles) were delivered to the cells to compare the uptake efficiency. (C) Flow cytometry histograms (FL4-H) of eEVs uptake by A549 and CCL-210 cells; Grey dashed peak: Untreated A549 cells; Grey long-dashed peak: Untreated CCL-210; Blue dotted peak: eEV uptake in CCL-210; Red solid peak: eEV uptake in A549.

2.4. Conclusions

Despite there being increasingly more research advances in EV-mediated gene delivery, a key problem for EVs in clinical applications is the lack of methods for obtaining large-scale amounts of EV for practical use.[180] Although MSCs are commonly used for this reason, MSCs are not the most desirable cell types in all applications. In this study, we sought to: establish a simple synthetic lipid fusion technique which can be potentially applied to any lipid of interest; to quantify the level of native protein remaining; and to quantify the levels of gene knockdown, with acceptable levels of toxicity. We were successful in accomplishing these objectives using sonication and extrusion techniques to engineer EVs after isolation. We were able to achieve an 8-fold higher in the vesicle number over the common EV mass production method, while retaining 16 – 21% of native EV protein.

It is currently unknown what the balance is regarding how low the protein amount on the eEVs can be, while retaining targeting functionality. We currently have plans to investigate the sufficient levels of native protein remaining on eEVs to retain targeting functionality. Additionally, EVs derived from the cells may contain endogenous

microRNA messages, which depends on the cell status and could be a concern of causing additional cell reactions. Therefore, to efficiently engineer EVs as a drug delivery platform by "voiding" the endogenous materials in the vesicles, while retaining the membrane structure and the capability of exogenous cargo loading, is our next step for EV-based drug delivery research.

Furthermore, we found during our studies that electroporation causes an increase in the aggregation and toxicity but that such effects can be ameliorated to a degree by varying the electroporation media. We have evaluated the effects and the correlation of different electroporation buffer with aggregation. By optimizing the aggregation of eEVs, we have demonstrated the resulting lipid-doped eEVs are able to induce effective gene silencing as well as actively target to the cancer cells.

Other future studies will include the degree of lamellarity within our eEVs, as well as layer-by-layer applications which could potentially incorporate complexed or conjugated small molecules for anti-cancer applications. Additionally, the continued development of exogenous cargo loading methods, such as incorporating hydrophobic, cholesterol modified-siRNA (hsiRNA)[164, 218] into lipid-doped eEV system or using sonication method,[163] to maximize siRNA loading efficiency, in preparation for in vivo gene silencing effects for demonstrating clinical utility. Given that we have demonstrated the proof-of-principle, we will also be taking more of a high throughput approach in the future which could potentially be used to optimize targeting and gene delivery for any cell type of interest. To the extent of our knowledge, this is the first study investigating a

variety of different lipids for EV fusion intended for mass production and knockdown of a gene of interest.

3. POLYMER-COATED EXTRACELLULAR VESICLES FOR SELECTIVE CO-DELIVERY OF CHEMOTHERAPEUTICS AND SIRNA TO CANCER CELLS

3.1. Introduction

Combining chemotherapy with RNA interference (RNAi)-based therapy has attracted interest for overcoming multidrug resistance (MDR) in cancer.[219] The concept of utilizing small-interfering RNA (siRNA) provides a strategy for selectively down-regulating the abnormal genes that confer resistance, such as anti-apoptotic genes (*i.e.,* Bcl-2 and Survivin) and drug-efflux pumps (*i.e.,* P-glycoprotein).[220] Because the use of RNAi technology can be highly selective to tumor-specific genes, it is considered to be one of the most promising strategies for cancer therapy. In the recent past, the U.S. FDA has joined other regulatory bodies (*i.e.,* EMA and Chinese FDA) for approving such RNAi-based therapy including but not limited to cancer applications (*e.g.,* Alnylam's patisiran), demonstrating the clinical feasibility. Several studies have demonstrated that an increased cell sensitivity to chemotherapeutic agents and higher tumor killing efficiency can be achieved by combinatorial treatment of doxorubicin (DOX) and siRNA (*e.g.,* Bcl-2,[221] P-gp,[222] PLK1[223]), confirming that a combinatorial drug-siRNA therapy can improve efficacy. Moreover, research has found that synchronous delivery of siRNA and chemotherapeutics from a single nanocarrier is more effective at treating cancer when compared to delivery *via* two separate nanocarriers.[224] This finding suggests that the co-delivery of drugs to the same cell plays a critical role in the therapeutic efficacy.[225, 226]

Nevertheless, it is difficult to encapsulate siRNA and chemotherapeutics in a single nanocarrier due to their different physicochemical properties. While siRNA exhibits high

molecular weight (~13-14 kDa) and highly negative-charged phosphate backbone, chemotherapeutic agents, such as DOX and paclitaxel, are relatively hydrophobic small molecules. Due to the anionic nature of siRNA, the most common strategy of the carrier design is complexation of siRNA with positively charged macromolecules, such as lipids, degradable (*i.e.,* poly(β-amino ester)s (PBAE), poly(amido amine) dendrimers) and non-degradable polymers (*i.e.,* polyethyleneimine (PEI)), and inorganic nanoparticles (*i.e.,* mesoporous silica nanoparticles).[227] To date, a number of modifications to these particles have been proposed to improve the delivery efficiency, including conjugation of cell targeting ligands,[228-230] combination of different hydrophilic/hydrophobic segments,[231] incorporation of pH-responsive moieties,[232-234] and bio-reducible linkages.[235] For most of these materials, the hydrophilic or hydrophobic chemotherapeutic agent is conjugated or loaded in the core *via* self-assembly, while the anionic siRNA is complexed with cationic macromolecules *via* electrostatic condensation, which leads to a core-shell structure delivery system. While significant improvements in therapeutic efficacy have been shown in some of these studies, there is still a need to develop combinatorial delivery systems with targeting capabilities.

Nano-sized extracellular vesicles (EVs) (*i.e.,* exosomes), which are shed or secreted by most cell types, are an emerging class of nanomaterials for drug delivery.[180, 236, 237] Due to their natural role in facilitating intercellular communication, EVs possess a high payload capability to deliver signaling molecules, such as protein, mRNAs, and microRNAs. They also exhibit many biological advantages over other nanomaterials, such as low immunogenicity, high stability in circulation, excellent biological barrier

permeability, and intrinsic capabilities for selective tissue-homing and endosomal escape or fusion.[238] While most of the synthetic nanocarriers must be modified with specific ligands to enhance tumor targeting, EVs derived from different host cells have extraordinary ability to selectively target cancer cells, which circumvents the need for surface modification for active targeting. For example, Alhasan *et al.* reported that exosomes isolated from PC-3 prostate cancers cells showed 4-fold preferential delivery into PC-3 cells compared to C166-GFP endothelial cells.[239] Kim *et al.* demonstrated that Raw264.7 derived exosomes were taken approximately 30-fold higher than polystyrenenanoparticles and liposomes (95 M% of phosphatidyl choline and 5% of dioleoyl-N-(monomethoxypolyethylene glycol succinyl)phosphatidylethanolamine) by 3LL-M27 lung carcinoma cells.[159] Our recent studies have also demonstrated lung adenocarcinoma cell (A549)-derived EVs have a 15-fold higher uptake efficiency by their parental tumor cells compared to normal lung fibroblasts (CCL-210).[209] Although the exact mechanism that regulates the EVs' selective trafficking remains to be elucidated, by investigating the biodistribution and proteome of cancer-derived EVs, Qiao *et al.* recently proved cancer-derived EVs have the ability to selectively colonize to tumor site and can be used for targeted cancer therapies.[81] On the basis of these findings, in the current study, we attempted to engineer cell-derived EVs as a tumor cell-selective co-delivery platform to address the aforementioned co-delivery challenges.

The objective of this work was to develop an EV-based platform that can selectively deliver both small molecule anti-cancer drugs (DOX) and siRNA to cancer cells. Specifically, in contrast to prior co-delivery systems, instead of relying on

electrostatic condensation on the surface of nanomaterials, we aimed to encapsulate siRNA in the core of engineered EVs (eEVs) to decrease the siRNA exposure to nucleases. We then used layer-by-layer (LbL) assembly to form a polyelectrolyte multilayer on the eEV surface, which was leveraged for polymer-drug encapsulation.[240] We specifically used the polycation poly(L-lysine) (PLL) as the first layer to coat the weakly anionic extracellular vesicle surface. Next, the polyanion poly(acrylic acid) (PAA) was added to enable DOX loading. Finally, a cationic poly(β-amino ester) (PBAE) was added to facilitate siRNA delivery. After optimizing the fabrication parameters to produce a stable LbL-coated eEV delivery platform (LbL-eEVs), we examined the capability of LbL-eEVs to preferentially deliver DOX and siRNA to cancer cells using cytotoxicity studies, gene silencing assays, flow cytometry, and confocal microscopy. Finally, the synchronous delivery of siRNA and DOX to A549 cancers was evaluated.

3.2. Materials and Methods

3.2.1. Materials

1-Palmitoyl-2-oleoyl-sn-glycero-3-phosphocholine (POPC) (NOF America Corporation Ltd.); 1-Palmitoyl-2-oleoyl-sn-glycero-3-phosphoglycerol, sodium salt (POPG-Na) (NOF America Corporation Ltd.); 0.4 cm electroporation cuvette (Biorad); CellTiter 96® aqueous cell proliferation assay (Promega); chloroform (Thermo Fisher Scientific); Cy3 Label IT® siRNA Tracker Intracellular Localization Kits; anhydrous D-trehalose (ACROS); bovine serum albumin (Thermo Fisher Scientific); CellMask™ Deep Red plasma membrane stain (Invitrogen); Dulbecco's modified Eagle's high glucose media (DMEM-HG, Corning); dynamic light scattering cuvette (Zetasizer); ethidium

homodimer (Invitrogen); fetal bovine serum (FBS) (Gibco); GlutaMax (Thermo Fisher Scientific); Hoechst 33258 (Invitrogen); Lipofectamine RNAiMax (Invitrogen); micro bicinchoninic acid (Micro BCA) protein assay kit (Thermo Fisher Scientific); modified Eagle's media (EMEM, Lonza); non-essential amino acids (MEM-NEAA, Gibco); Opti-MEM I Reduced Serum Media (Thermo Fisher Scientific); poly (acrylic acid) (Mw: 1800 g/mol, Sigma); poly(L-lysine) (Mw: 30000-70000 g/mol, MP Biomedical); paraformaldehyde (Thermo Fisher Scientific); penicillin-streptomycin (Invitrogen); phosphate buffered saline (PBS) (Gibco); potassium chloride (Thermo Fisher Scientific); potassium phosphate dibasic (Thermo Fisher Scientific); Quant-iT RiboGreen RNA assay kit (Thermo Fisher Scientific); Triton X-100 (Invitrogen); TRIzol reagent (Invitrogen).

3.2.2. Cell Culture

GFP expressing A549 lung adenocarcinoma cells were purchased from Cell Biolab, Inc. (#AKR-209) and further sorted by flow cytometry to obtain a higher percentage of GFP expressing A549 cell population as reported in our previous studies.[209] A549 lung cancer cells (P5-P15) were cultured in DMEM high glucose (4.5 g/ml glucose) media supplemented with 10% v/v fetal bovine serum (FBS), 1% v/v 0.1 mM non-essential amino acids (MEM-NEAA), and 1% v/v 100 µg/ml penicillin-streptomycin. CCL-210 cells were cultured in modified Eagle's media (EMEM, Lonza) supplemented with 10% v/v FBS, 1% v/v GlutaMax, and 1% v/v 100 µg/ml penicillin-streptomycin. Both cell types were grown in an incubator using cell culture conditions of 37°C and 5% CO_2.

3.2.3. Engineered Extracellular Vesicle (eEV) preparation

The eEVs were generated according to our previous studies.[209] Briefly, EVs were first isolated from A549 conditioned media by serial centrifugation. The particle numbers and affiliated protein amounts of EVs were quantified for the use of further experiments. Next, eEVs were fabricated by lipid fusion using sonication and serial extrusion techniques using the method reported in our prior publication without modification.[209] Two types of lipids were used initially for membrane fusion in this study: zwitterionic POPC (1-Palmitoyl-2-oleoyl-sn-glycero-3-phosphocholine) and anionic POPG (1-Palmitoyl-2-oleoyl-sn-glycero-3-phosphoglycerol). The lipid:EV solutions were mixed at 1:1 volumetric ratio (5 mM lipid solution with 1.5×10^{10} particles/ml EVs, equals to 50 μg/ml protein affiliated with EV membrane).

3.2.4. Layer-by-layer Polyelectrolyte-eEV (LbL-eEVs) Preparation

The LbL-eEVs were designed to have three polyelectrolyte layers, which were poly L-lysine (PLL, Mw: 30,000 ~ 70,000 g/mol), poly(acrylic acid) (PAA, Mw: 1800 g/mol), and poly(β-amino ester)s (PBAE, Mw: 4001 g/mol). Exogenous siRNA was loaded into the eEVs *via* electroporation prior to the LbL deposition procedure. The LbL architecture was achieved by sequential deposition of oppositely charged polyelectrolytes. PLL was chosen because it is a widely used biocompatible and biodegradable cationic polypeptide.[241] PAA is a highly anionic polyelectrolyte that has also been widely used for LbL assembly in the past.[242] Additionally, small molecule drug doxorubicin (DOX) has been shown to complex with PAA *via* electrostatic interactions.[243, 244] Cationic PBAE was chosen as a final layer because of its high gene transfection efficiency and because it has

been reported to improve intracellular delivery in previous research.[245, 246] The specific PBAE used for LbL coating was BR647, which is a bio-reducible and hydrophobic PBAE with a disulfide bond along the polymer backbone and was synthesized according to a previous protocol.[247] The hydrolysis of the ester group on the BR647 polymer and the degradation of the disulfide bonds can be triggered by the reducing environment of the cytoplasm, promoting cargo release. Overall, the LbL process is shown in **Scheme S1**. Briefly, ~5×10^{11} particles/ml of eEVs were mixed with a final concentration of 200 μg/ml PLL in 150 mM sodium acetate (NaAc, pH=5) and incubated in 37 ºC for 1 hr. The mixture was then ultracentrifuged at 125000 ×g for 30 min. to pellet polyelectrolyte-coated eEVs. The supernatant was replaced with 150 mM NaAc for washing, and the ultracentrifugation/wash procedure was repeated twice to remove excess polyelectrolytes. Subsequent layers were deposited by the same procedure with 30 min. of incubation, followed by the same washing procedure. 2nd layer: PAA (0.5 mg/ml in 150 mM NaAc), drug loading: DOX (0.3 or 0.6 mg/ml in 150 mM NaAc) and 3rd layer: PBAE-BR647 (2.5 mg/ml in 25 mM NaAc) were added sequentially for LbL deposition. To reduce acidity, 25 mM NaAc was used instead of 150 mM NaAc for the final PBAE coating. The final layer of PBAE-BR647 was not washed according to the protocol of Bishop, Tzeng and Green.[200]

3.2.5. Physicochemical Quantification of Layer-by-layer Assembled eEV Complex

3.2.5.1. Nanoparticle Tracking Analysis

The size and concentration of samples were characterized by nanoparticle tracking analysis (NTA) (NanoSight LM10, Amesbury, United Kingdom) using the same apparatus described in previous protocol.[209]

3.2.5.2. Zeta Potential Measurement

The zeta potential of vesicles (10^9-10^{10} particles/ml) was measured in water using the same apparatus (Zetasizer NanoZS) described in previous protocol.[209]

3.2.6. siRNA Loading in eEVs, siRNA Retention and DOX Quantification in LbL eEVs

3.2.6.1. siRNA Loading Method

Herein, anti-GFP siRNA was loaded within zwitterionic POPC-doped eEVs *via* electroporation (Bio-Rad Gene Pulser II system) using a protocol previously reported. Briefly, an electroporation mixture was prepared in a concentration of ~7.5×10^{11} particles/ml of eEVs containing 1 ng/µl siRNA. Opti-MEM, 50 mM trehalose or a hypotonic electroporation buffer (1.15 mM K_2HPO_4; pH 7.2; 25 mM KCl, 21% OptiPrep)[123, 187] were used as sample buffer. For siRNA-loaded LbL-eEV samples, polymer deposition processes were conducted after the electroporation procedure.

3.2.6.2. Loaded siRNA Content Quantification

To quantify the amount of siRNA within the LbL-eEVs post-assembly, the actual siRNA amount retained in the vesicles was isolated using a modified TRIzol RNA isolation protocol that was previously published.[191] Purified siRNA was subsequently

quantified by a Quant-iT RiboGreen RNA assay kit following the manufacturer's instruction.

3.2.6.3. Loaded DOX Content Quantification

Small molecule DOX was loaded to LbL-eEV after PAA complexation during LbL assembly. DOX loaded LbL-eEVs were pelleted down by centrifugation and resuspended in DMSO/PBS (3:7 volume ratio) solution. The amount of incorporated DOX in the LbL-eEVs was determined by measuring the fluorescent absorbance (excitation: 485 nm/emission: 590 nm) of DOX using a Cytation 5 spectrophotometer. A linear calibration curve with DOX concentrations in the range of 0-12.5 μg/ml were used to obtain the unknown DOX loading amount.

3.2.7. Cellular Uptake Studies by Confocal Microscopy and Flow Cytometry

The same procedures for cell seeding, sample staining, and imaging were used as in our prior work.[209] The CellMask™ DeepRed plasma membrane stain was used to label the membrane of LbL-eEVs following a protocol modified from the previous literature.[201] Confocal microscopy imaging (Olympus FV1000) was performed to visualize uptake, and cells were co-stained with Hoechst 33258 for nuclei visualization. To further quantify the uptake efficiency of vesicles in the cells, the Deep Red fluorescence was detected by flow cytometry (BD Accuri™ C6 Cytometer). Uptake efficiency was calculated using the geometric mean of FL4-A channel), and the following equation was used for calculation:

$$\text{Uptake efficiency} = \frac{\frac{GM_{\text{LbL-eEV in A549 or CCL210}}}{GM_{\text{untreated cells (A549 or CCL210)}}}}{\frac{GM_{\text{eEV in A549}}}{GM_{\text{untreated A549}}}} \quad (3.1)$$

Cells were also treated with LbL-eEVs loaded with DOX/Cy3-siRNA following the procedure described above to visualize to quantify the uptake efficiency following intracellular delivery. The FL2-A channel was used for the detection of DOX and siRNA. Cy3-labeled siRNA was prepared by Label IT siRNA Tracker Intracellular Localization kit (Mirus) according to the manufacturer's instruction and diluted to a concentration of 100 nucleotides/dye prior to loading into eEVs. The cells were incubated with 3×10^{12} particles/ml of LbL-eEVs containing Cy3-siRNA. The Lipofectamine reagent mixed with 500 ng/ml (50 ng in 100 µl) Cy3-siRNA was used as a positive control group. On the other hand, cells were treated with free unencapsulated DOX at a concentration of 0.488 µg/ml, which was equivalent to the amount of DOX within the eEV/LbL-eEVs, as a positive control group for DOX delivery. The metabolic activity of the cells was not affected at this DOX concentration within 2 hr of incubation. DOX loaded poly(lactic acid-co-glycolic acid) nanoparticles (PLGA NP) were prepared as a comparison group using oil-in-water nanoprecipitation followed by solvent evaporation according to the protocol from Betancourt *et al*.[248] PLGA (50/50, 50kDa) with ester end groups was used for this nanoparticle synthesis. The PLGA NPs had a Z-average diameter of 127.4±2.9 nm and a DOX loading efficiency of 6.3%.

3.2.8. *In vitro* Evaluation: Anti-cancer Efficacy

3.2.8.1. siRNA Knockdown Efficiency

To evaluate the knockdown efficiency of LbL-EV mediated siRNA delivery within GFP-expressing A549 cells, GFP fluorescence was measured and quantified daily for 12 days using a plate reader (Cytation 5), as previously described.[200, 209] The knockdown

efficiency of siRNA-GFP was calculated by normalizing each sample type/condition to each individual negative control treated with scrambled siRNA. Commercial Lipofectamine® RNAiMax was used as a positive control to compare the knockdown efficiency between samples. The area under the curve (knockdown efficiency vs time) was calculated using GraphPad Prism 7 software to determine the overall knockdown efficiency of each condition. In this study, we delivered a single dose of 10^{10} –10^{11} LbL-eEVs with 100-400 ng siRNA per 10^4 cells in 100 µl.

3.2.8.2. DOX Cancer Killing Efficiency

The effects of DOX-loaded vesicles on A549/CCL210 cells were evaluated using the CellTiter 96® Aqueous Cell Proliferation assay (Promega) (MTS assay) to assess relative metabolic activity of the cells. Prior to MTS treatment, DOX-loaded vesicles were incubated with cultured A549/CCL210 cells at 60 – 70% confluency for 3 days at varying doses. The MTS assays were conducted after incubation for 3 days, following the manufacturer's instructions. Untreated A549 or CCL210 cells were used as positive control groups (assuming 100% metabolic activity) for normalization. Free DOX (unencapsulated) and DOX-loaded PLGA NPs were prepared as comparison groups. To obtain dose-response curves, metabolic activity was plotted versus the amount of DOX administered, which was determined based on spectrophotometric analysis of eEV/LbL-eEV/PLGA NPs. The sigmoidal dose-response curves were fitted with Hill's equation using GraphPad software,

$$Y = \text{Min} + \frac{(\text{Max-Min})}{(1+(\text{IC50}/\text{X})^{\text{Hill Slope}})} \tag{3.2}$$

where Max is the Y value at the top plateau and Min is the Y value at the bottom plateau. IC50 (inhibitory concentration, 50%) is the X value when the response is halfway between Min and Max.

3.2.9. Co-delivery of siRNA and DOX

This experiment followed the same procedure as was used for siRNA and DOX delivery. Briefly, 2.5 $\times 10^4$ GFP-expressing A549 cells were seeded onto 24-well plates for flow cytometry analysis 24 hr. before the experiment, followed by incubation with various formulations for 2 hr. at 37ºC. After 2 hr., the samples were replaced by fresh media for continual measurements. After 3 days incubation, the cells were trypsinized and collected for analysis. Of note, a concentration of 1.5 $\times 10^{12}$ particles/ml was chosen for these co-delivery experiments based on the knockdown results. At this concentration, with only 2 hr. of DOX delivery followed by 3 days of incubation, the cells were expected to maintain 60-80% of their metabolic activity at the time of flow cytometry analysis. The cells were stained with ethidium homodimer (EthD-1) prior to flow cytometry for dead cell quantification, and detection was performed on the FL3-A channel. While there is some potential for overlap from DOX, this channel is not optimal for DOX detection. Control groups of Triton-treated A549 and untreated A549 were used to set the quadratic gates.

3.2.10. Statistics

Data are presented as the mean ± the standard deviation (SD). All experiments were conducted with triplicates. Statistical data analyses were performed using GraphPad Prism 7 software. The statistical significance of differences between groups was

determined using one-way ANOVAs with Tukey post-hoc tests. The α value was set at 0.05, and *, **, ***, and **** indicate *p*-values <0.05, <0.01, <0.001, and <0.0001, respectively.

3.3. Results and Discussion

3.3.1. Fabrication and Optimization of Multi-layered Engineered Extracellular Vesicles (LbL-eEVs)

Our multi-layered engineered extracellular vesicle (LbL-eEV) platform consists of two main components: (1) engineered lipid-hybridized extracellular vesicles (eEVs) as the carrier of siRNA and (2) tri-layered shell assembly of polyelectrolytes as the carrier of chemotherapeutics (DOX). EVs were collected from A549 cells and hybridized with either zwitterionic or anionic phospholipids to create eEVs. The lipid-hybridized eEVs were generated *via* sonication and extrusion according to the protocol in our prior work.[209] Multi-layered polyelectrolyte shells were then assembled on the surface of the eEVs to produce LbL-eEVs. An overview of the multilayer fabrication process is illustrated in **Scheme S1**. We selected PLL, PAA and PBAE as cationic and anionic counterparts to form a tri-layered shell sequentially surrounding the core eEVs. The polycation PLL was applied as the first layer because the extracellular vesicle surface was weakly anionic. PAA was applied next and enabled incorporation of the small molecule drug DOX, which contains an amino group with a pK of 8.6 and, thus, will bind strongly to the carboxylate groups on PAA. PBAE, which is a superior biocompatible and bio-reducible polymer compared to non-degradable polymer PEI,[247] was chosen to facilitate cytoplasmic targeting of siRNA release.

To produce stable LbL-eEVs, we first studied the LbL deposition procedures on native and lipid-hybridized eEVs, specifically zwitterionic POPC-doped eEVs and anionic POPG-doped eEVs. **Figure S1** shows the change in zeta potential and particle concentration of the eEV mixtures following PLL deposition. A successful reversal of charge was only observed with the zwitterionic POPC-doped eEVs. The increase in zeta potential leveled off at 5 μg/ml and 50 μg/ml PLL concentration for native EVs and anionic POPG-doped eEVs, respectively, and charge reversal was not achieved (**Figure S1A**). In addition, the particle concentration after PLL coating (**Figure S1B**) was found to decrease 22-fold and 172-fold for native EVs and anionic POPG-doped eEVs, respectively, whereas zwitterionic POPC-doped eEVs did not exhibit such drastic decreases in particle number following cationic PLL deposition. Therefore, we proceeded with zwitterionic POPC-doped eEVs for subsequent experiments.

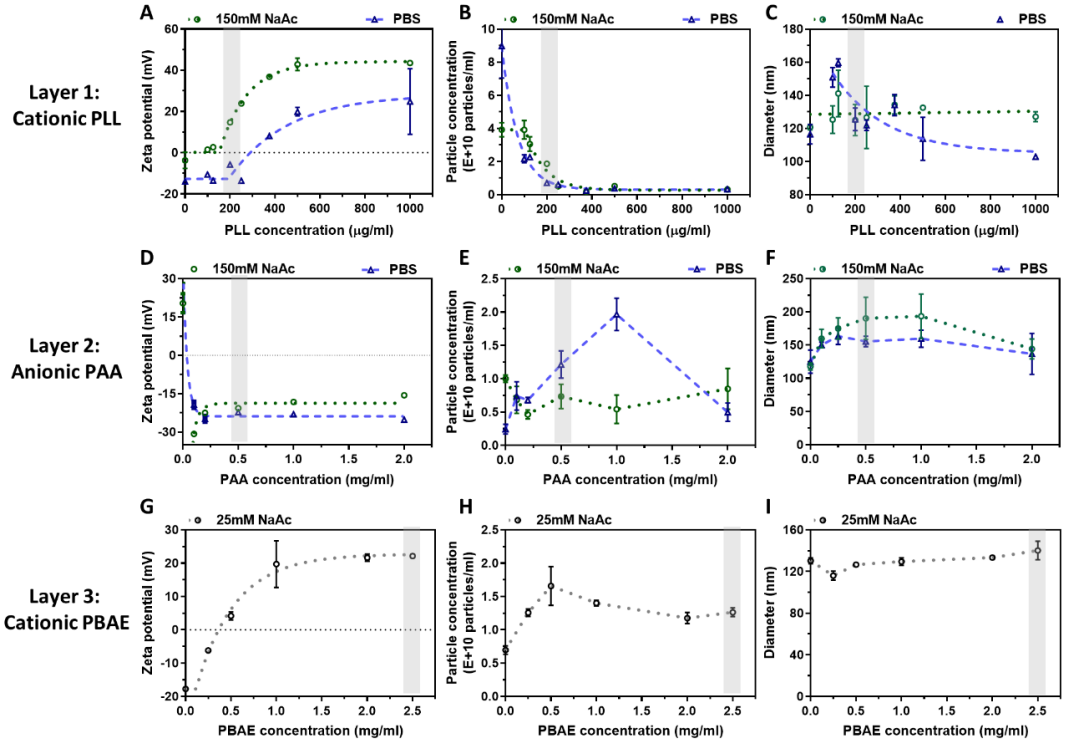

Figure 3.1 Characterization of zeta potential, particle concentration and diameter for each sequential layer of LbL-eEVs. Data after addition of the first layer: PLL (A-C), second layer: PAA (D-F), and final layer: PBAE (G-I) at varying polyelectrolyte concentration is shown.

Next, to optimize the polyelectrolyte assembly on core eEV materials, solutions for polyelectrolyte deposition and the effects of polyelectrolyte concentration were investigated. The zeta potential, particle concentration and diameter were investigated after each coating step, as shown in **Figure 3.1**. First, we compared the influence of phosphate buffer saline (PBS, pH 7.4) and 150 mM sodium acetate (NaAc, pH 5) on polyelectrolyte deposition. By simply decreasing the pH during polyelectrolyte incubation, a lower threshold for inversion of surface charge was obtained **(Figure 3.1A)**. Therefore, 150 mM NaAc was selected for the first and second layer of polyelectrolyte

coating. It is worth noting that 25 mM NaAc was used instead of 150 mM NaAc in the final layer (PBAE) to reduce acidity for later use in cellular studies, according to the prior studies.[200] Second, we examined the influence of polyelectrolyte concentration on polymer-EV complexes. In all cases, the zeta potentials **(Figure 3.1 A, D** and **G)** of coated eEV substances changed in an exponential growth/decay kinetics, followed by a plateau, indicating a saturation of the charge density. Notably, while a layer of polyelectrolyte is built up on the surface, the particle concentration (**Figure 3.1B, E** and **H**) of polymer-EV complexes decreased, as a result of charge overcompensation. However, we did not observe a statistically significant effect on particle diameter (**Figure 3.1C, F** and **I**) at varying polyelectrolyte concentrations. Our results demonstrated a balance between charge reversal and particle colloidal stability in terms of the optimal concentration of polyelectrolyte is crucial for the success of LbL deposition. These results are consistent with previous studies from Sui et al.[249] and Seyrek et al.[250] Based on the point of charge inversion and particle concentration, we selected concentrations of 0.2 mg/ml, 0.5 mg/ml and 2.5 mg/ml for PLL, PAA and PBAE, respectively, for subsequent experiments. The structures of LbL-eEVs are shown in the transmission electron microscopy (TEM) images (**Figure S2**). The exposure of tetraspanin surface proteins after application of the LbL coating to the eEVs was confirmed by performing anti-CD63 labeling and on-bead flow cytometry (**Figure S3**).

3.3.2. siRNA Loading in the eEV Core and Small Molecule Drug Loading in Polyelectrolyte Shells

Benchtop electroporation systems have been widely used to encapsulate small nucleic acids such as siRNAs into EVs.[251] In order to develop a co-delivery platform for siRNA and small molecule drugs in this study, siRNA was loaded into eEVs *via* electroporation prior to polyelectrolyte shell assembly. The characterization results from stepwise coating of eEVs with and without siRNA are summarized in **Figure 3.2**. **Figure 3.2A** shows the change in surface charge as each polyelectrolyte layer is deposited. While siRNA-loaded eEVs exhibited a greater negative charge of -27.3±0.8 mV compared to eEVs without siRNA (-15.7 ± 22.1 mV), strong electrostatic interactions between charged PLL and siRNA-loaded eEVs still led to successful PLL deposition and reversed the surface charge to a zeta potential of 33.3±1.6 mV. **Figure 3.2B** shows that the hydrodynamic particle diameter slightly increased with each addition of charged polymer during the assembly process. Interestingly, the particle size of siRNA-encapsulated LbL-eEVs did not always increase with sequential deposition of polyelectrolytes. After the first layer PLL deposition, the addition of PAA decreased the overall size of vesicles. This may be due to strong ionic interactions between PAA and the PLL-siRNA-eEV complex, resulting in the formation of a dense polyelectrolyte coating. Another explanation for the varied size of PAA-eEV-siRNA is the alteration of the composition within the polymer-eEV complex following PAA assembly, as a result of the decreased diameter.[252]

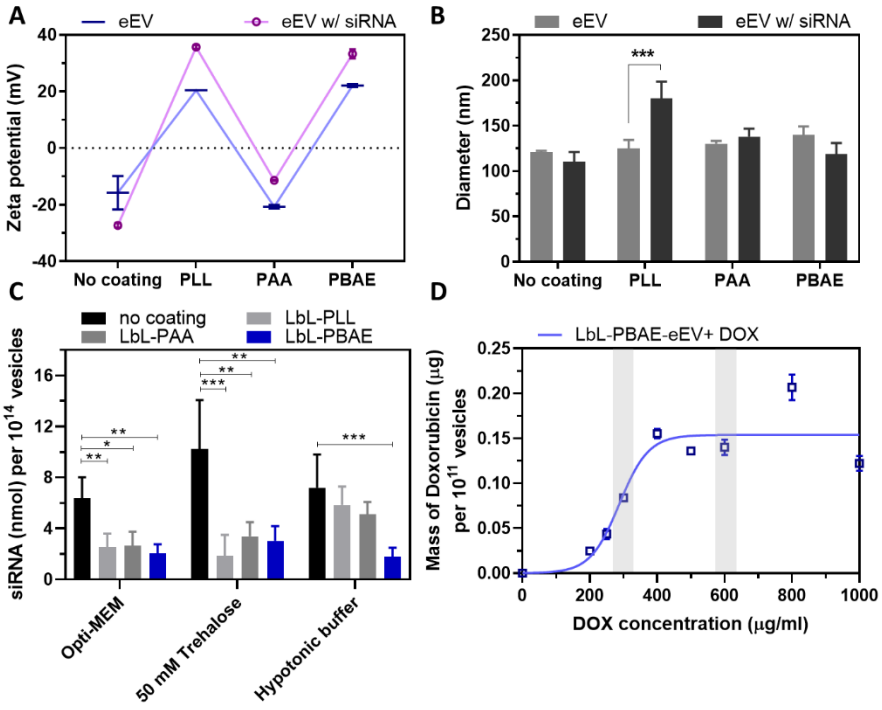

Figure 3.2 Physicochemical characterization of the optimized LbL-eEVs after addition of each polyelectrolyte layer on the eEV core. (A-B) show the changes in zeta potential (A) and diameter (B) of LbL-eEVs. First layer: 200μg/ml cationic poly (L-lysine) (PLL) in 150mM NaAc. Second layer: 0.5mg/ml anionic poly (acrylic acids) (PAA) in 150mM NaAc. Final layer: 2.5mg/ml cationic bio-reducible poly (β-amino ester)s (PBAE) (BR647) in 25mM NaAc. ***p <0.001; (C-D) show the amount of drug loaded after LbL assembly. (C) Exogenous loading of siRNA into eEVs in various electroporation media. *p<0.05, **p<0.01, ***p<0.001; (D) The amount of DOX loaded within tri-layered polyelectrolyte shells of LbL-PBAE-eEVs using different drug concentrations. A logistic non-linear regression model was used for curve fitting. The loading amount of DOX per 10^{11} vesicles was quantified by spectrophotometric method. A linear function of DOX standard concentrations versus fluorescence (Excitation:485nm/Emission:590nm) was used as the calibration curve.

To characterize the cargo loading capacity and the influence of LbL assembly on cargo retention, siRNA loading within the eEVs was quantified after each step of the LbL process. Three commonly used electroporation buffers were also tested for siRNA loading, including Opti-MEM, 50mM Trehalose and hypotonic electroporation buffer. **Figure 3.2C** shows the percent of loaded siRNA remaining following each coating step.

In our previous studies, we demonstrated siRNA encapsulation into lipid-hybridized eEVs with a loading efficiency of 0.6 nmol siRNA within 10^{13} particles of zwitterionic POPC-doped eEVs. The quantity of siRNA loaded in the present work is comparable to our prior work. Interestingly, while loading with hypotonic buffer improved siRNA retention during the earlier steps of LbL coating, only ~30% of the loaded siRNA could be retained by the final step, regardless the buffer used. The decrease in the amount of loaded siRNA after LbL coating can potentially be attributed to the disassociation of affiliated siRNA surrounding eEVs, since a challenge of bulk electroporation systems is that a portion of siRNAs may not be entirely encapsulated into the vesicles post-electroporation and may not be fully removed after the wash-purification procedure.[162] The effects of siRNA loading in various buffers on gene silencing efficacy are in section 3.4.1.

On the other hand, the small molecule drug DOX was in the polyelectrolyte multilayer shell during the PAA coating step by forming PAA-DOX complexes *via* electrostatic interactions.[243] To understand the effects of concentration on DOX loading into the polyelectrolyte shells, a concentration range of 0-1000 μg/ml was investigated. **Figure 3.2D** shows that DOX loading increased in an exponential growth manner and reached saturation at 400 μg/ml. The maximum loading achieved after complexing the final layer of PBAE was 155 ± 5 ng DOX per 10^{11} vesicles. Based on these results, concentrations of 0.3 mg/ml and 0.6 mg/ml DOX (the saturated plateau) were selected as low and high dose groups, respectively, for the comparison of dose effects in subsequent studies.

3.3.3. Tumor Cell Selectivity of the LbL-eEVs

Intracellular delivery is essential for achieving the desired therapeutic effects, but selectivity of the delivery system for tumor cells is also critical to reduce cytotoxicity to normal cells. Therefore, we investigated the uptake efficiency of LbL-eEVs labeled with Deep Red dye in lung adenocarcinoma cells (A549) and non-cancerous lung fibroblasts (CCL-210) by confocal microscopy and flow cytometry quantification. However, prior to studying LbL-eEV uptake, we used a set of control liposomes to evaluate differences in uptake activity between the A549 and CCL-210 cells (**Figure S4**). Specifically, cationic DOTAP liposomes, zwitterionic POPC liposomes and anionic POPG liposomes were stained with Deep Red dye delivered to the cells. Interestingly, while the A549 cells exhibited approximately ~2-fold higher uptake efficiency of zwitterionic liposomes, uptake of the DOTAP and POPG liposomes was greater in the CCL-210 cells. Thus, while the uptake mechanisms may differ, neither cell line exhibited consistently higher uptake activity.

The confocal images in **Figure 3.3A** demonstrate extensive uptake of the LbL-eEVs by the A549 cells. In contrast, minimal uptake was observed in the CCL-210 cells. The corresponding merged brightfield images showed the LbL-eEVs were mainly located in cytoplasm. **Figure 3.3B** shows the flow cytometry histogram of FL4-H (Deep Red dye). A binary gating analysis was set to define LbL-eEV positive and negative cells, and it was found that LbL-eEVs were internalized by 78.1% of A549 cells compared to only 47.7% of CCL-210 cells. However, this gating analysis is inherently binary. To provide greater insight on LbL-eEV uptake, **Figure 3.3C** shows the quantitative flow cytometry results of

normalized geometric mean of fluorescence intensity (nGMFI) for LbL-eEVs with different polymer coatings (*i.e.*, only PLL, PLL/PAA, and PLL/PAA/PBAE). While our prior work on native EVs demonstrated 15.8 times greater uptake of EVs in A549 cells compared to CCL-210 cells, the data obtained here show that the internalization of eEVs in A549 cells remains 14.2-fold greater than that in CCL-210 cells. Thus, the eEVs exhibited inherent selectivity for the cancer cells. Surprisingly, uptake of the LbL-PBAE-eEVs in the A549 cells was not reduced when compared to eEVs. Moreover, a LbL-eEV uptake was 5.2-fold higher in A549 cells compared to CCL-210 cells, indicating that the selectivity of the eEVs was not compromised by the LbL coating. This result can likely be attributed to the exposure of tetraspanin proteins or exosomal integrins, which have been reported to direct the selective internalization of EVs in different cells.[81]

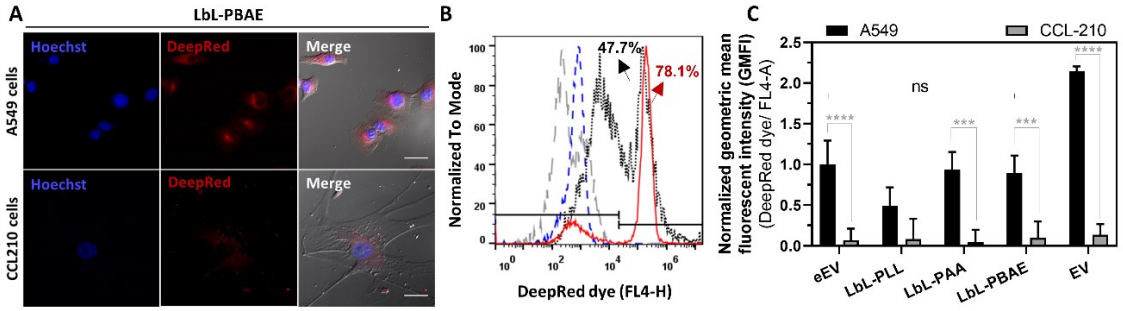

Figure 3.3 Visualization and quantification of LbL-eEV uptake in normal lung fibroblast (CCL-210) and lung adenocarcinoma cells (A549). (A) Confocal images of LbL-eEV staining with Deep Red dye in the cells. scale bar: 30 µm; (B) Flow cytometry histograms (FL4-H) of LbL-eEV uptake by A549 and CCL-210 cells. LbL-eEV in A549: Red, solid line; LbL-EV in CCL-210: black, dotted line; vesicles without dye in A549: blue, dashed line; vesicles without dye in CCL-210: gray, long-dashed line. (C) Normalized geometric mean fluorescence intensities (GMFI) indicating cellular uptake efficiency of LbL-eEVs in A549 and CCL-210 cells. ***p<0.001, ****p<0.0001.

3.3.4. Potential Antitumor Efficacy of LbL-eEVs

3.3.4.1. siRNA Delivery and Gene Silencing

Efficient cellular uptake and endosomal escape are crucial to translocate siRNA to the cytoplasmic region for RNAi-triggered gene silencing. To demonstrate the cargo siRNA within LbL-eEVs can be delivered intracellularly, Cy3-labelled siRNA was loaded in LbL-eEVs to evaluate the internalization of siRNA in both A549 and CCL-210 cells. Commercial RNAi silencing reagent LipofectamineRNAiMAX was used as a positive control and the uptake efficiency of siRNA was subsequently quantified by flow cytometry and comparisons of nGMFI (**Figure 3.4**). The confocal microscopy images of Cy3-siRNA internalization are shown in **Figure S5**. The histogram of FL2-H (Cy3-siRNA) (**Figure 3.4A)** confirms significantly enhanced uptake of LbL-PBAE-eEVs in A549 cells. Notably, the nGMFI in **Figure 3.4B** shows LbL-PBAE-eEVs more efficiently delivered siRNA intracellularly compared to other polyelectrolyte layered-eEVs. Moreover, the uptake amounts of Cy3-siRNA delivered by LbL-PBAE-eEVs in A549 was 2.27-fold higher than that in CCL-210 cells, whereas no significant difference between the uptake efficiency in A549 and CCL-210 cells was observed for the commercial lipofectamine RNAiMAX transfection reagents. These findings further confirm the potential of LbL-PBAE-eEVs for preferential delivery to tumor cells.

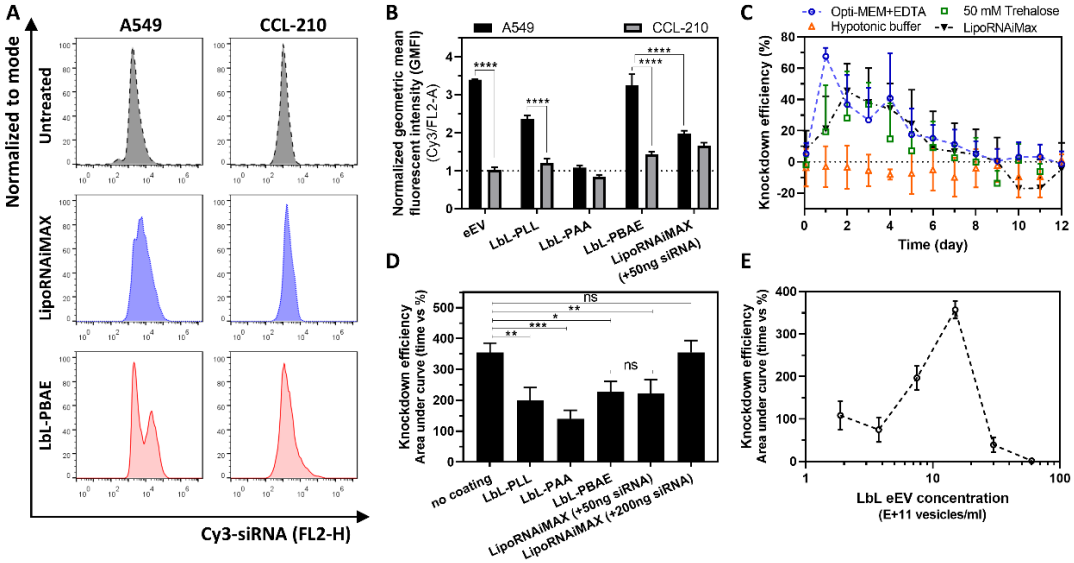

Figure 3.4 siRNA delivery and RNA interference knockdown with LbL- eEVs in CCL-210 and A549 cells. (A) Flow cytometry histograms (FL2-H) of Cy3-labelled siRNA uptake by A549 and CCL-210 cells; (B) Normalized geometric mean fluorescence intensities (GMFI) of LbL-eEV mediated siRNA uptake efficiency in A549 and CCL-210 cells. Lipofectamine RNAiMAX with 50 ng siRNA was prepared as a positive control group. GMFI was obtained by normalizing to the untreated cells. ****p<0.0001; (C) siRNA-mediated GFP knockdown of LbL eEVs (PBAE-layered) quantified over time in A549 cells by fluorescence measurements on a Cytation 5 plate reader. OptiMEM+EDTA, 50mM Trehalose and hypotonic electroporation buffer were used during electroporation for siRNA loading into the LbL-eEVs; (D) Overall knockdown efficiency (the area under the curves over time) of LbL-eEVs after different polyelectrolyte layers were added in A549 cells. OptiMEM+EDTA was used as the electroporation buffer. *p<0.05, **p<0.01, ***p<0.001; (E) Overall knockdown efficiency in A549 cells at varying LbL eEV dose (1.875-60 $\times 10^{11}$ vesicles/ml).

To validate that delivered siRNA can effectively suppress gene expression, siRNA against green fluorescence protein (siRNA-GFP) was delivered to GFP-expressing A549 cells. This model gene approach allowed for ease of monitoring as well as quantitative analysis of efficacy based on GFP fluorescence intensity. **Figure 3.4C** shows the knockdown efficiency in GFP expression over time in the cells treated with LbL-eEVs loaded using 3 different electroporation buffers. LbL-eEVs in Opti-MEM resulted in the most effective silencing, and the 67.5±5.5% knockdown efficiency on day 2 after delivery

was a 3.5-fold higher than the other formulations. On day 4, the knockdown efficiency of the LbL-eEV loaded using Opti-MEM was 40.9 ± 24.8%, which was comparable to the knockdown efficiency of commercial Lipofectamine RNAiMax with 50 ng siRNA delivery (34.0 ± 16.2%).

To investigate the influence of different layered LbL-eEVs on knockdown efficiency, the same electroporation procedure was repeated in Opti-MEM media. The decrease of GFP expression in the cells was quantified by integrating the area under the curve (knockdown efficiency over time), as shown in **Figure 3.4D**. The overall knockdown efficiency results show that the gene silencing capability of eEVs without polyelectrolyte shells was significantly higher than that of LbL-eEVs. However, the PBAE-layered eEVs were still able to effectively silence gene expression to the same degree compared with Lipofectamine treatment (50 ng siRNA/100 µl). Importantly, only about 0.6 nmol siRNA (~10 ng) was encapsulated in 10^{13} eEVs. Thus, matching the efficacy of Lipofectamine indicates that our LbL-eEVs are still a highly effective gene delivery platform.

We further evaluated the knockdown efficiency of LbL-eEVs at varying doses, as shown in **Figure 3.4E**. The results demonstrate that gene silencing increased with increasing vesicle/siRNA concentration and reached a maximum knockdown efficiency at a concentration of 1.5×10^{12} vesicles/ml. We found the knockdown efficiency decreased drastically at higher siRNA dose. This is likely due to the off-target effects of siRNA at higher dose, leads to the reduction of GFP expression in the control group treated with scramble siRNA, and therefore, limits the dose of siRNA can be applied. Consequently,

the concentration of 1.5 $\times 10^{12}$ vesicles/ml of LbL-eEV/siRNA complexes, exhibiting the maximum efficacy, was further used in the following co-delivery experiments.

3.3.4.2. DOX Delivery and Cancer Killing Efficiency

The primary mechanism of anti-tumor activity from DOX is the intercalation of DOX molecule into DNA, leading to inhibition of DNA synthesis. Therefore, it is necessary for DOX molecules to enter cell nuclei for therapeutic efficacy. Cellular internalization of DOX was evaluated by the same procedure as in the prior sections. **Figure 3.5A** demonstrates free DOX enters cell nuclei as a DNA intercalation agent for the induction of programmed cell death. Notably, the delivery of DOX by LbL-eEVs to CCL-210 showed decreased nuclear localization compared to in A549 cells. To further quantitively assess the preferential uptake and DOX delivery with LbL-eEVs, DOX-loaded poly (lactic-co-glycolic acid) nanoparticles (PLGA NPs), one of the most well-studied drug delivery systems, were tested using the same procedure for comparison. Consistent with the prior siRNA uptake results, DOX delivery by LbL-PBAE-eEVs resulted in significantly higher internalization in A549 cells (1.79-fold) than in CCL-210 cells, as shown in **Figure 3.5B**. In contrast, synthetic PLGA nanoparticles showed no significant difference in DOX delivery to A549 and CCL-210 cells, confirming the potential for preferential delivery to tumor cells with the LbL-eEV system. It is necessary to point out that the uptake efficiency (DOX) was significantly improved by LbL-PBAE, which was 2.15-fold higher than that by LbL-PAA, suggesting the necessity of the final cationic layer to facilitate cellular internalization. These results were also consistent with the siRNA internalization results in the previous section.

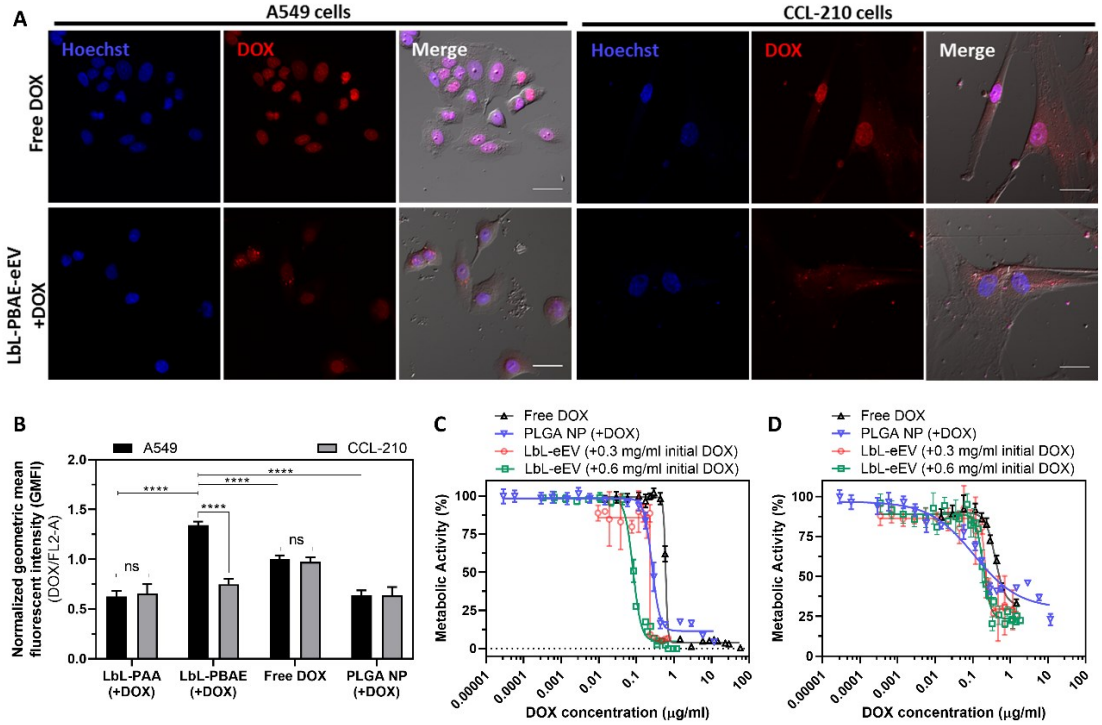

Figure 3.5 DOX delivery and cancer killing effects in A549 and CCL-210 cells. (A) Confocal images of Free DOX and LbL-eEV mediated DOX delivery in A549 and CCL-210 cells, Scale bar: 30 μm; (B) Normalized geometric mean fluorescence intensities (GMFI) of the DOX uptake efficiency in A549 and CCL-210 cells. DOX-loaded PLGA nanoparticles (PLGA NP) with the concentration of 0.488 μg DOX/ml were prepared for comparison. Equivalent amounts of DOX inLbL-PAA were also prepared to compare with LbL-PBAE. (C-D) Dose effects of free DOX, PLGA NP-delivered DOX, and LbL-eEV delivered DOX on (C) A549 and (D) CCL-210 cells after 3 days incubation. DOX concentration was calculated by: particle concentration (measured by NTA) × DOX loading/LbL-eEV particles.

We next used a cell proliferation assay (MTS assay) to evaluate the efficacy of DOX delivery with different formulations in cells. Prior to the experiment, the dose-dependent cytotoxicity of blank LbL-eEVs was examined in both A549 and CCL-210 cells. No toxicity was observed in the concentration range of 0-22×10^{12} particles/ml after

3 days incubation (**Figure S6**), confirming cytocompatibility of the vesicles. Subsequently, same experiment was repeated for DOX-loaded LbL-eEVs. **Figure 3.5C and D** shows the dose-responsive curves of free DOX, DOX-loaded PLGA NPs, and DOX-loaded LbL-eEVs in A549 and CCL-210 cells, respectively. The LbL-eEVs were loaded using a low or high concentration of DOX (0.3 and 0.6 mg/ml, respectively), based on the loading results (**Figure 3.2D**). For all treatment groups, the DOX amount in LbL-eEVs administered to the cells was quantified spectrophotometrically. The quantified inhibitory concentration (IC) values of DOX delivered by the various carriers are presented in **Table 3.1**. Both PLGA NPs and LbL-eEVs with DOX showed a higher antitumor efficacy at lower IC compared to free DOX, which can be attributed to the enhanced cellular internalization of drugs. Among all the therapeutic groups, LbL-eEVs prepared with the 0.6 mg/ml loading concentration of DOX were most effective, indicating the cancer killing efficiency depends on the amount of DOX complexed in the polyelectrolyte layers. In contrast to the conventional PLGA system, the IC_{50} of LbL-eEV (+0.6mg/ml DOX) was 3.2-fold decreased in A549 cells, indicating that LbL-eEV delivery system requires a substantially lower dose of DOX to achieve the same cancer cell killing efficiency. While the IC values in CCL-210 were also reduced, the IC values for LbL-eEV mediated DOX delivery were at least 1.8-fold lower in A549 cells than in CCL-210 cells.

Cell line	Treatment	Inhibitory concentration (μg/ml)		
		IC_{10}	IC_{50}	IC_{90}
A549	Free DOX	0.510	0.598±0.008	0.690
	PLGA NP	0.152	0.259±0.007	0.440
	LbL-eEV+ 0.3 mg/ml initial DOX	0.230	~0.232	0.233
	LbL-eEV+ 0.6 mg/ml initial DOX	0.050	0.081±0.002	0.140
CCL210	Free DOX	0.200	0.400±0.024	0.780
	PLGA NP	0.005	0.109±0.021	2.210
	LbL-eEV+ 0.3 mg/ml initial DOX	0.162	0.213±0.008	0.279
	LbL-eEV+ 0.6 mg/ml initial DOX	0.115	0.189±0.006	0.310

Table 3.1 IC10, IC50 and IC90 values calculated from inhibitor curves for free DOX, PLGA nanoparticles (PLGA NP), and LbL-eEVs loaded using low (0.3 mg/ml) and high (0.6 mg/ml) concentrations of DOX in A549 and CCL-210 cells. All the sigmoidal concentration response curves were fitted with Hill's equation using GraphPad software. Due to the high steep curve (large absolute value of Hill's slope), an ambiguous estimate (wide confidence interval) of the IC50 value (~0.232) was obtained in the fitting results of LbL-eEV+0.6 mg/ml initial DOX treated in A549 cells.

3.3.5. Co-Delivery of siRNA and DOX

The experimental results above demonstrated that LbL-eEVs are effective for preferential delivery of siRNA and DOX to A549 cancer cells separately. To confirm the utility of LbL-eEVs as a co-delivery system, GFP-expressing A549 cells were treated with LbL-eEVs and then quantitatively analyzed by flow cytometry. The cells were also stained with ethidium homodimer-1 (EthD-1) to assess the effects of DOX delivery. LbL-eEVs containing siRNA alone, DOX alone, and both siRNA and DOX. LbL-eEVs prepared with two different DOX loading concentrations were also tested (note: the overall DOX dose was held constant). Treatments with siRNA-GFP and control scramble siRNA were prepared in pairs for each individual condition. **Figure 3.6A** shows the qualitative results of A549 cells with LbL-eEV mediated co-delivery of siRNA/DOX. Morphological

changes were not observed in the cells with the delivery of either siRNA-GFP or control scramble siRNA, but considerable cell enlargement was observed in the DOX-delivery groups. On the other hand, remarkably reduced green fluorescence was observed in the groups treated with siRNA-GFP (i.e., Lipofectamine+siRNA-GFP, LbL-eEV+siRNA-GFP), indicating downregulation of GFP expression. The cell images in co-delivered formulations demonstrate both morphological changes and reduced green fluorescence in the cells, which verifies the co-delivery of siRNA and DOX. **Figure 3.6B** shows quadratic graphs from the flow cytometry analysis. The upper-right quadrant (Q1) represents GFP-positive and EthD-1/DOX positive cells. The upper left quadrant (Q2) corresponds to cells that are positive only for EthD-1/DOX. The bottom-left quadrant (Q3) represents double-negative cells. The bottom-right quadrant (Q4) represents cells that are positive only for GFP. The results show that siRNA-GFP/DOX co-delivery by LbL-eEVs markedly increased the percentages of cells located in Q1 and Q2 compared to untreated cells. The percentage of cells in Q2 was 23.5% and 31.1% in the siRNA-GFP/0.3 mg/ml DOX and siRNA-GFP/0.6 mg/ml DOX groups, respectively. In contrast, only 14.7% and 20.6% of the cells were in Q2 for the siRNA-scramble/0.3 mg/ml DOX and siRNA-scramble/0.6 mg/ml DOX groups, respectively. While these results provide evidence that the LbL-eEV particles achieved synchronous delivery of siRNA and DOX, further analysis was performed based on normalized GMFI measurements. Analysis of the FL3 channel indicated that DOX delivery was not hampered by the co-delivery of siRNA (**Figure 3.6C**). Moreover, the knockdown efficiency of single cells treated with siRNA/DOX co-loaded formulations was found to be comparable to the siRNA alone group (**Figure 3.6D)**.

Collectively, the results of these experiments confirm that co-loading siRNA and DOX does not compromise the efficacy of the LbL-eEV delivery system and that effective target gene silencing and DOX delivery are achieved simultaneously.

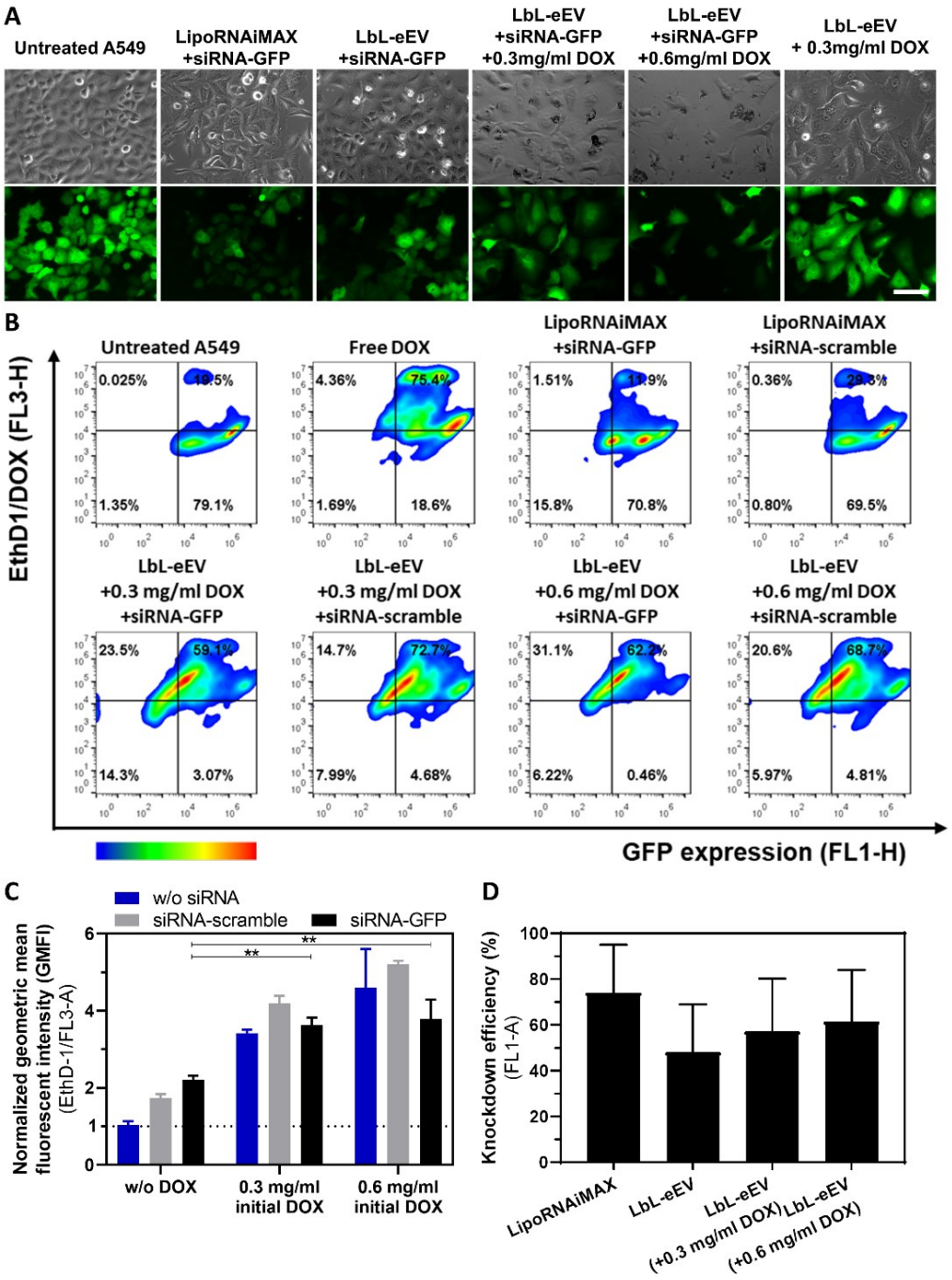

Figure 3.6 Co-delivery of DOX and siRNA-GFP/siRNA-scramble in A549 cells with different formulations. (A) Fluorescence microscope images of cells treated for 3 days with different formulations. Scale bar: 50 µm. (B-D) Fluorescence signals from green fluorescence protein expression (GFP/FL1-H) and a dead cell stain (EthD-1/FL3-H) in A549 cells were measured by flow cytometry and presented as (B) four quadrant diagrams, (C) normalized geometric fluorescence mean (nGMFI) of FL3-H (**p<0.01).

Figure 3.6 (Continued) (D) knockdown efficiency (FL1-H). No statistical difference of knockdown efficiency (FL1-A) was observed between all groups.

3.4. Conclusions

In summary, we developed a biocompatible and cancer cell-selective EV-based co-delivery system for combinatorial therapies, which we believe can potentially overcome challenges with drug resistance in cancer. To our knowledge, this study is the first to demonstrate LbL-eEVs, and our results provide valuable insight on their production as well as their efficacy for siRNA and DOX delivery. Moreover, our results show that the native selectivity of EVs for specific cells is preserved with LbL-eEVs, which is an important advantage compared to other deliver systems because it circumvents the need for surface modification with targeting ligands. However, further investigation of EVs' inherent selectivity is needed, including the preferential uptake of different EVs in different cells and their *in vivo* targeting efficacy. The long-term stability of engineered EV platforms and the synergistic effects of co-delivered therapeutic gene/drugs will also be the focus of our future studies. Nevertheless, we believe our studies provide a promising foundation for utilizing EVs as a multi-therapeutics carrier and for developing efficacious combinatorial therapies.

4. AZIDE/TETRAZINE FUNCTIONALIZATION OF EXTRACELLULAR VESICLES FOR IMMUNOMODULATORY THERAPY

4.1. Introduction

Mesenchymal stem/stromal cells (MSCs) have been widely studied for cell therapy in various diseases.[253] It was initially thought MSCs act therapeutically through cellular differentiation and cell replacement. However, recent research attention has been paid to MSC-derived extracellular vesicles (EVs), which have been identified as an active component in cells' secretomes.[254, 255] Various disease models have shown MSCs exert the therapeutic effects through migration to injured sites and release of EVs as immunomodulators.[256, 257] EVs are lipid bilayer vesicles consist of different cargo, such as nucleic acids (*e.g.,* non-coding RNA and coding RNA), pro-inflammatory/anti-inflammatory cytokines, and other proteins. Similar to the beneficial effects from human MSC (hMSC), hMSC-derived EVs (MSC-EVs) have also been demonstrated to present three major intrinsic regenerative functionalities, including anti-fibrotic effects, macrophage polarization, angiogenesis effects. Many studies have demonstrated MSC-derived exosomes are intrinsically able to polarize macrophages to the anti-inflammatory M2 phenotype in a variety of disease settings, such as cardiovascular infarction, lung injury, neurodegeneration, ischemia-induced renal injury, etc.[258] Kim *et al.* further performed a comparative molecular profiling of MSC EVs and demonstrated TGF-β1, PTX3, let-7b-5p and miR-21-5p are key effectors mediating the immunomodulatory function of EVs.[259] Compared to hMSCs, EVs have been found to cause less immunogenic effects due to a lower presence of MHC molecules on the exosomal membrane.[59]

Therefore, EVs are proposed to be a more convenient therapeutic alternative with respect to the whole cell-based therapy. The use of MSC-derived EVs can avoid the risk of DNA replication from stem cell transplantation. The cell-free therapy by EVs can possibly reduce the need to match the donor-recipient compatibility. Moreover, they can potentially be developed as off-shelf products, which can be categorized as biological medicinal products following the regulatory framework.[36, 260]

While hMSC EVs show great potential as cell-free therapeutics for tissue regenerative applications, effective delivery of EVs to tissue sites remains challenging. Rapid clearance of EVs at the defected/injured site was observed *in vivo*,[25, 68, 261] and therefore it is difficult for EVs to be retained and exert their therapeutic capability effectively. Several studies encapsulated EVs in bulk hydrogel (*e.g.,* hyaluronic acid-based hydrogel,[262, 263] chitosan-based hydrogel[264]) to enhance the retention of EVs at tissue site compared to EV injection. While encapsulating EVs in hydrogels relies mostly on diffusion-controlled release to local tissue, tethering EVs on a hydrogel *via* chemical conjugation is expected to provide a prolonged stimulative effect at the injured site. Our lab has previously developed methods for fabricating clickable microporous annealed particle (MAP) hydrogels displaying norbornene groups.[265, 266] The functional groups present on the hydrogel can be leveraged for any desired functional groups by using bio-orthogonal click chemistry (*e.g.,* tetrazine-norbornene reaction), which is desirable for biological system due to its fast kinetics, high specificity and low cytotoxicity. In the current study, we attempted to functionalize hMSC EV with bio-orthogonal moieties (*e.g.,*

tetrazine group) on the exosomal surface that will be covalently conjugated *via* click chemistry to the hydrogels for local delivery.

To enable EV surface modification for click labeling to hydrogels, functional groups for copper free azide-alkyne cycloaddition (*i.e.,* strain promoted alkyne-azide cycloaddition (SPAAC), azide-dibenzocyclooctyne (DBCO)) click reaction are commonly selected. The azide moieties can be introduced to EVs through transfection[139] or metabolic labeling[267] of the EV producer cells, or by direct chemical modification on the amine groups of EV surface.[135] Although the direct chemical modification is quite straightforward in that the reactive functional groups can be conjugated to the amine groups on exosome membrane through EDC/NHS coupling (*i.e.,* amine-carboxylic acid reaction), this reaction may modify the amine groups on surface proteins universally. This may impair the active site of proteins and lead to a compromised bioactivity of EVs after surface modification. To circumvent this issue, delivery of azide-functional chemicals/analogs to the EV producer cells and subsequently obtaining EVs displaying azide moieties from cell-conditioned media could be a more reasonable strategy.

To introduce functional groups to EV producer cells, Lee *et al.* functionalized cancer cell (B16F10 and MDA-MB-231) membranes with azide groups by transfecting membrane fusogenic liposome (MFL) containing SPE-PEG(2000)-azide lipids. The azide-presenting EVs were obtained after 2-days of liposome treatment.[139] On the other hand, utilizing cellular biosynthesis pathways by supplementing cell culture media with azide-modified (non-native) metabolites/analogs can be another strategy. For example, metabolic engineering of the surface expression of cells with azide moieties by the sialic

acid pathway (*i.e.,* glycosylation) has been recently studied for glycoprotein quantification and cell tracking.[268, 269] Through this natural pathway, azide-modified metabolites (*e.g.,* ManNAz sugars) are taken up by the cells and can be incorporated to the glycoproteins on cell membrane. Wang *et al.* first applied this metabolic labeling approach to functionalize EVs.[135] The azide precursors did not interfere cellular metabolism and were non-disruptively introduced onto EVs.[136, 267] In addition to glycoprotein engineering, incorporating azide-choline to membrane lipids through the synthesis pathway of choline-containing phospholipids has also been investigated.[137, 138, 270]

The objective of this work was to tether bio-orthogonal moieties, tetrazine groups, on hMSC EV surface for covalent conjugation on norbornene-containing MAP hydrogel. We proposed an *in situ* biorthogonal click chemistry approach to functionalize tetrazine groups on exosomal membrane *via* surface engineering of the EV producer cells (**Figure 4.1**). Specifically, we aimed to first introduce azide groups on hMSC membrane. Subsequently, tetrazine groups, which are reactive to norbornene, would be installed on the azide-presenting membrane by treatment with a DBCO-tetrazine linker to hMSC. After 2 days incubation, the DBCO-tetrazine labeled EVs secreted from hMSC would be collected. This *in situ* bio-orthogonal click reaction is expected to offer improved functionalization efficiency and retention of EV bioactivity,[136, 271] compared to direct chemical modification on EVs post-isolation from cell conditioned media.

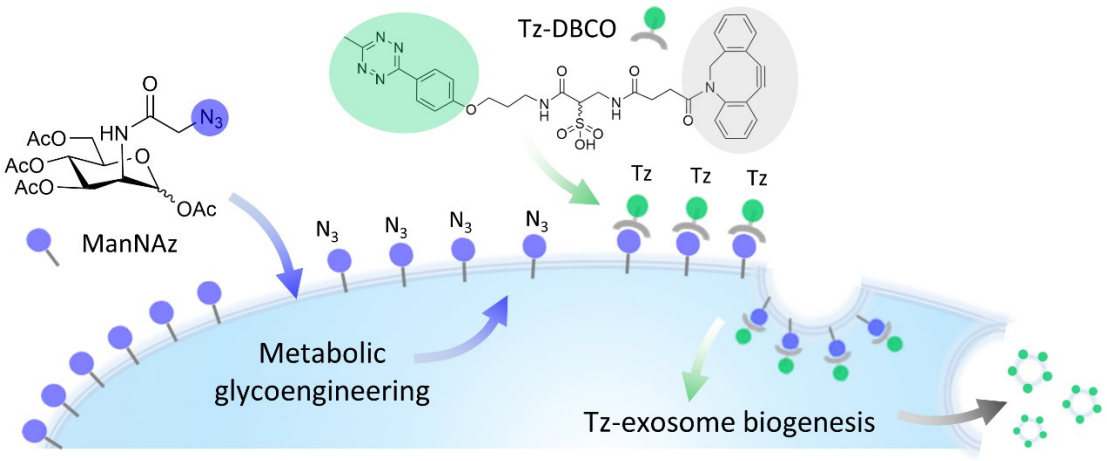

Figure 4.1 Schematic illustration of *in situ* bio-orthogonal click reaction of EVs from surface-engineered (metabolite-treated) hMSCs.

4.2. Materials and Methods

4.2.1. Materials

Ac4ManNAz (Click Chemistry Tools); 1-Azido-choline (Jena Bioscience); αMEM (Gibco), Bovine serum albumin (Thermo Fisher Scientific); CellMask^{TM} Deep Red plasma membrane stain (Invitrogen); DBCO-Cy5 (Click Chemistry Tools); DBCO-AF488 (Click Chemistry); Methyltetrazine-DBCO (BroadPharm); dynamic light scattering cuvette (Zetasizer); DSPE-PEG(2000)-azide (Avanti Polar Lipids); fetal bovine serum (FBS) (Gibco); micro bicinchoninic acid (Micro BCA) protein assay kit (Thermo Fisher Scientific); GlutaMax (Thermo Fisher Scientific); Hoechst 33258 (Invitrogen); paraformaldehyde (Thermo Fisher Scientific); penicillin-streptomycin (Invitrogen); phosphate buffered saline (PBS) (Gibco); Triton X-100 (Invitrogen); TCO-Cy5 (Click Chemistry Tools)

4.2.2. Cell Culture

Bone marrow-derived human mesenchymal stem cells were purchased from ATCC and maintained with passage number 2 to 5 for experimental testing. The cells were cultured in αMEM media supplemented with 20% v/v fetal bovine serum (FBS), 1% v/v GlutaMAX (100x), and 1% v/v 100 μg/ml penicillin-streptomycin. An incubator using cell culture conditions of 37°C and 5% CO_2 was maintained for cell incubation.

4.2.3. Azide Functionalization on hMSC by Various Methods

4.2.3.1. Azide-functionalization by Membrane Fusogenic Liposome (MFL) Transfection

Azide containing membrane fusogenic liposomes (MFL) were prepared using a film hydration method following the protocol from Lee *et al*.[139] MFL was prepared by loading a mixture of DMPC: DSPE-PEG(2000)-azide: DOTAP: DPhPE=71.15: 3.85: 20: 5 molar ratio (total: 1405 μM in chloroform) in a small glass vial. Dry lipid film was generated by evaporating chloroform from the lipid solution under vacuum. The lipid film was gently hydrated by adding 1 ml of PBS. The lipid aqueous solution was subsequently sonicated with 20% amplitude for 2 min. using a 120 Watt, 20kHz probe-type sonicator (Fisher Scientific FB120). Next, the mixture was extruded through pore size of 100 nm extruder more than 25 times. hMSC were seeded on 24-well plates at initial density of 500 cells/cm^2 and maintained until 80-90% confluence. Concentrations of ~250 μM and ~500 μM liposome mixture were delivered to the cells and incubated for 30 min. After 30 min. incubation, the cells were washed twice and fixed with 4% paraformaldehyde. The azide

functionalization level was evaluated by 10 μM DBCO-AlexaFluor488 (DBCO-AF488) labeling for 1 hr., followed by microscopy imaging.

4.2.3.2. Azide-functionalization by Metabolic Glycoengineering

hMSC were seeded on 24-well plates at an initial density of 500 cells/cm^2 and maintained until 60 % confluence. Then the cells were incubated in the presence of 10-50 μM ManNAz sugar for 1-3 days. The ManNAz concentration range without causing cytotoxicity was selected according to Layek, Sadhukha and Prabha.[269] After the incubation, the cells were washed twice with PBS and fixed with 4% paraformaldehyde. The fixed cells were then incubated with 5 μg/ml Hoechst (20 min.) and 10 μM DBCO-Cy5 for 1 hr, followed by microscopy imaging.

4.2.3.3. Azide-functionalization by Metabolic Choline-Phospholipid Engineering

hMSC were seeded on 24-well plates at an initial density of 500 cells/cm^2 and maintained until 60 % confluence. Then the cells were incubated in the presence of 50-500 μM Azido-Choline for 2 days. The Azido-Choline concentration range without causing cytotoxicity was selected according to Zhang *et al*.[137] After the incubation, the cells were washed twice with PBS and fixed with 4% paraformaldehyde. The fixed cells were then incubated with 5 μg/ml Hoechst (20 min.) and 10 μM DBCO-AF488 for 1 hr., followed by microscopy imaging.

4.2.4. Tetrazine Functionalization on hMSC by Metabolic Glycoengineering

To incorporate tetrazine groups on azide-presenting hMSCs, after the cells were treated with 50 μM ManNAz sugar for 2 days, the cells were supplemented with media containing DBCO-Tetrazine linker (2.5-50 μM) for 1 hr. at 37ºC. Then the hMSC were

washed, fixed with 4% paraformaldehyde, followed by staining with 5 μg/ml Hoechst solution (for 20 min.) to visualize the nucleus and 10 μM TCO-Cy5 solution (for 1hr.) to visualize the tetrazine conjugation on hMSC.

4.2.5. Isolation of EVs

To produce azide-integrated hMSC EVs, the cells were maintained in the culturing media composed of exosome-removed FBS in the presence of 50 μM ManNAz sugar or 500 μM Azido-Choline for 2 days. Exosome-removed FBS was prepared in lab by ultracentrifugation at 125000 ×g for 2 hrs, followed by 0.22 μm filtration. To isolate hMSC EVs from the collected conditioned media after 2 days of incubation, a PEG purification protocol was followed.[118, 272] Briefly, conditioned media was first centrifuged at 2000 ×g for 20 min. The obtained supernatant was filtered through 0.22 μm filter and then supplemented with 50% w/v stock solution of PEG 6000 to a final concentration of 10-12% PEG and with 3.75 M NaCl to final concentration of 75 mM NaCl. Samples were mixed and kept on ice on the horizontal shaker with slow mixing speed for 10-14 hrs. The EV-PEG mixture was spun down by centrifugation at 1500 ×g for 30 min. The supernatant was removed completely, and the pellet was resuspended in 1 ml 0.9% NaCl solution. The concentrated EV samples were further washed with ~30 ml 0.9% NaCl solution on a rotator or shaker overnight at 4 ºC prior to ultracentrifugation. To obtain the final EV pellet, the EV mixture with 0.9% NaCl was ultracentrifuged at 125000 ×g for 120 min. and washed 2-3 times.

4.2.6. Physicochemical Characterization of EVs derived from EVs

4.2.6.1. Nanoparticle Tracking Analysis

The size and concentration of EVs were characterized by nanoparticle tracking analysis (NTA) (NanoSight LM10, Amesbury, United Kingdom). The samples with a dilution factor within the measurable concentration range for NTA (10^{7-9} particles/ml) were prepared to determine the original concentration of EVs. Three individual measurements of each condition were performed immediately after the sample was injected into the chamber. Data were collected for 60 s at room temperature and analyzed using NanoSight NTA 3.2 software. The error bars shown are standard deviations of the mean size from three measurements.

4.2.6.2. On-bead Flow Cytometry Analysis

~3×10^9 EVs were incubated with ~3×10^6 aldehyde/sulfate latex bead (4 μm) in 100 μl PBS at 4ºC on a horizontal shaker for 12 hrs. to conjugate the EVs onto the beads. After incubation, the EV-bead pellet was washed by centrifugation at 5000 ×g for 5 min. twice, followed by incubation with 100 mM glycine/PBS for 30 min. at room temperature to block unreacted aldehyde groups. After the blocking procedure, the EV-bead samples were incubated with primary antibody for CD63 in 0.2% bovine serum albumin (BSA)/PBS for 1 hr. at room temperature. Subsequently, the antibody-labelled EV-beads were washed twice and then incubated with secondary antibody igG1-AlexaFluor 647 for 30 min. at room temperature. The concentration of antibodies was prepared according to the manufacturer's recommended protocol. Samples were further washed 3 times prior to flow cytometry analysis.

4.2.7. Azide-functionalization Characterization by Fluorescent Labeling and mPEG Labeling

4.2.7.1. Fluorescence labeling of EVs

The amounts of azide or tetrazine functional groups on the EV surface was quantified by conjugation to DBCO-Cy5/DBCO-AF488 dye or TCO-Cy5 dye, respectively, *via* click chemistry reactions. A particle concentration of 10^9-10^{11} EVs was used for incubation with 10 μM DBCO dye or TCO dye for 1 hr. After 1 hr. incubation, samples were purified by ultrafiltration (centrifugal column, Amicon 100 kDa) to remove the excess dye. NTA measurement was conducted to quantify the exact particle number of vesicles after purification. The control (un-functionalized) EVs and azide/tetrazine-functionalized EVs were adjusted to the same particle concentration according to the obtained NTA results, followed by fluorescence readings to detect the presence of functional groups.

Azide-presenting liposomes were prepared using the same protocol for MFL liposome preparation, but only consisting of azide-PEG(2000)-SPE. The azide-presenting liposome was used as a positive control and various concentrations were prepared (10^7-10^{11}) to determine the lowest detection limit of the plate reader measurement.

4.2.7.2. DBCO-mPEG Labeling of Azide-functionalized EVs

As an alternative method to validate the presence of azide functional group on EV surface. 10 μM DBCO-mPEG (20kDa) was incubated with control EVs and aEVs for 12 hr. to 24 hr., followed by centrifugal column filtration to remove unconjugated DBCO-

mPEG chains. NTA measurement was performed to determine the change in hydrodynamic radius of the samples before and after DBCO-mPEG incubation.

4.2.8. Statistics

Data are presented as the mean ± the standard deviation (SD). All experiments were conducted with at least triplicates. Statistical data analyses were performed using GraphPad Prism 7 software.

4.3. Results and Discussion

4.3.1. Azide Functionalization on hMSC by Various Methods

To expand the scope of methods that can be used to generate azide functionalized EVs from hMSC, multiple approaches for azide integration were conducted, including (1) transfection of azide-containing membrane fusogenic liposomes (MFL), (2) metabolic engineering of glycoprotein pathways by supplementing ManNAz sugar to the culturing media, and (3) metabolic engineering of choline-modified phospholipids by supplementing Azido-choline lipid.

First, we used azide-containing MFL to incorporate azide groups into the cell membrane following the protocol from Lee *et al*.[139] Optimized concentrations of ~250 μM and ~500 μM from their protocol were delivered to hMSC for 30 min. incubation. We evaluated the fusion of MFL by labeling azide-integrated cell membrane *via* click conjugation with fluorescent DBCO-AlexaFluor 488 or Cy5 dyes. The microscopy imaging (**Figure S1**) revealed that MFLs were efficiently delivered into hMSC and incorporated to cell membrane. However, after 30 min. incubation, normal hMSC changed their morphology from a spindle shape to an enlarged, flattened shape. While normal

morphology was shown in the studies from Lee *et al.* using the cancer cell lines B16F10 and MDA-MB-231 after MFL incubation, our results indicate the MFL treatments may alter the viability and cell functionality of hMSC. Although a lower dose of liposomes may be applied to circumvent this problem, in this work, we decided not to proceed with this approach for azide functionalization.

We next investigated the metabolic engineering approaches to incorporate azide functional groups to hMSC membranes. The applicability of this approach was first tested by metabolic labeling of glycoprotein using peracetylated N-azidoacetylmannosamine (ManNAz) sugar, which was reported to be the best metabolic precursor for exosome modification.[267] The precursor ManNAz containing azide groups is taken up by the cells and incorporated into cell surface sialylated glycans. Based on previous reports,[269] various concentrations (10-50 μM) and incubation times (1-3 day) were tested to optimize the conditions. DBCO-Cy5 labelled cell images (**Figure 4.2**) showed efficient incorporation of azide functional groups on the membrane. hMSCs treated with 50 μM ManNAz showed the highest (brightest) expression level of DBCO-Cy5 and the expression reached a maximum at day 2. Regardless of the ManNAz concentration, the azide expression on hMSC surface started to decline after 2 days of incubation. Therefore, the condition of 50 μM ManNAz with 2 days incubation was used in the subsequent experiments in this work. Additionally, another metabolic engineering approach using Azido-Choline to incorporate azide functional groups on Choline-modified phospholipidis was also tested (**Figure S2**). However, a higher dose of Azido-Choline (500 μM) was required to achieve efficient incorporation of azide groups. For the sake of cost effectiveness, the subsequent tetrazine

functionalization on an azide-integrated membrane was studied using the glycoprotein engineering approach.

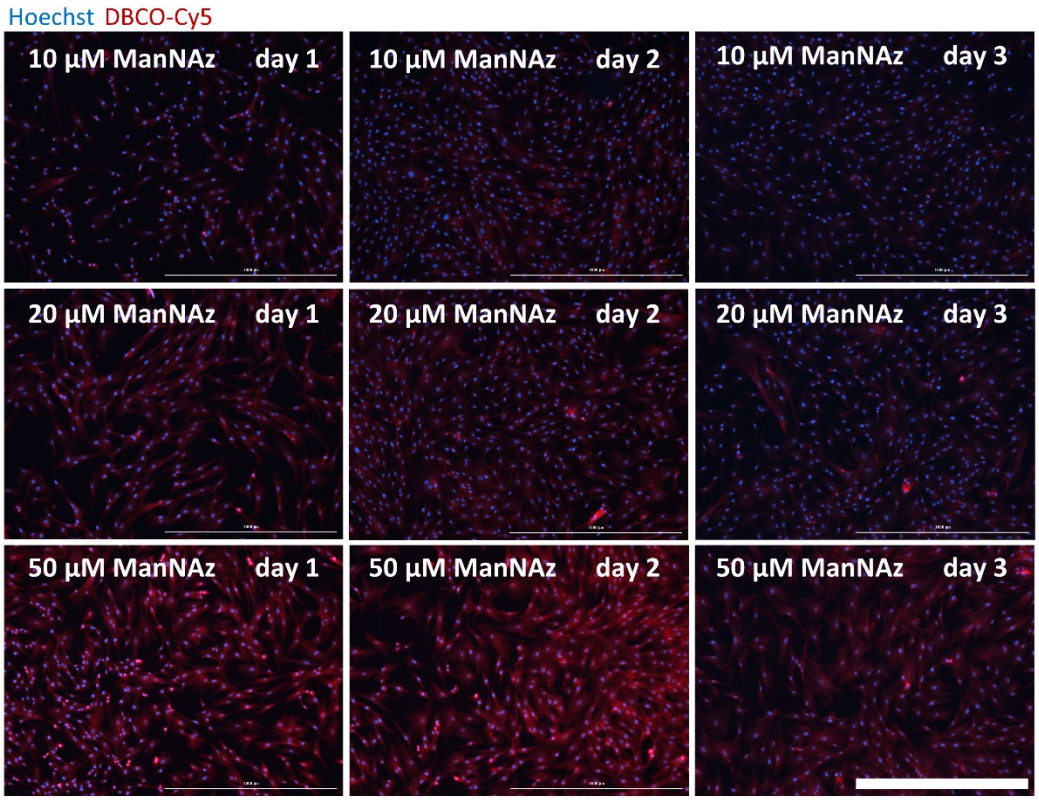

Figure 4.2 Optimization of azide functionalization on hMSC. Fluorescent images of DBCO-Cy5 labeled hMSC that were incubated with ManNAz sugar (10-50 μM) for 1 to 3 days (Scale bar=1000 μm).

4.3.2. Tetrazine Functionalization on hMSC by Metabolic Glycoengineering

In situ bio-orthogonal click chemistry approach to functionalize tetrazine groups was first begun with glycoprotein engineering by ManNAz sugar supplementation of hMSC. After 2 days incubation of ManNAz sugar, the azide-reactive DBCO-tetrazine

linker (DBCO-Tz) was delivered to azide-presenting cells. Since the azide-DBCO reaction is rapid and highly selective, a short incubation time of 1 hr. was conducted to reduce cellular internalization of excess DBCO-Tz. Following treatment with DBCO-Tz, the functionalization of Tz groups on cell membrane was examined by TCO-tetrazine labeling. The TCO-Cy5 labelled cell images (**Figure 4.3**) demonstrated the Tz groups can be decorated easily on the cells within a short time frame. However, compared to the positive group of DBCO-Cy5 labelled azide-displaying cells, the fluorescence intensity of TCO-Cy5 labelled cells was relatively low. This observation implied either low TCO-Cy5 labeling efficiency on the Tz-presenting surface or insufficient amounts of DBCO-tetrazine to cover the entire azide groups. We then used the condition with the highest concentration of 50 μM DBCO-Tz linker to further generate Tz-presenting hMSC EVs.

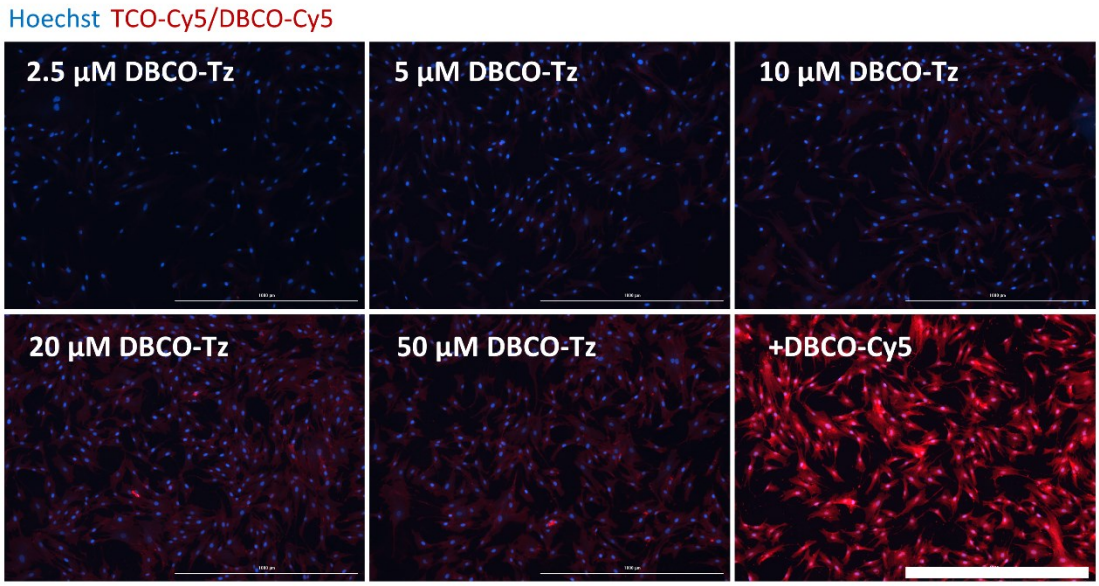

Figure 4.3 Optimization of Tetrazine (Tz) functionalization on hMSC. Fluorescent images of TCO-Cy5 labelled hMSC that were incubated with 50 µM ManNAz sugar for 2 days, followed by DBCO-Tz treatment at varying concentration (2.5-50 µM) for 1 hr incubation. Azide-presenting hMSC (w/ 50 µM ManNAz treatment) without DBCO-Tz treatment was incubated with DBCO-Cy5 for fluorescent labeling as a positive control.

4.3.3. Physicochemical Characterization of EVs derived from hMSC

Prior to the characterization of azide-functionalized EVs, we assessed the physicochemical properties of isolated hMSC EVs. The isolated EV populations were characterized by nanoparticle tracking analysis (NTA), total protein content (BCA assay) and on-bead flow cytometry analysis. A production yield of isolated EVs was quantified by the measured concentration using the NTA technique. We obtained a significantly higher amount of EVs released from hMSC than our previous studies with A549 cells (**Figure 4.4A**), possibly due to the nature of active EV secretion from hMSC.[100-102] On the other hand, there was no obvious difference in the representative protein amounts within

A549 EV and hMSC EV (**Figure 4.4B**). In addition, the expression of the exosomal surface marker CD63 on the hMSC EV surface was quantified by fluorescence measurement using flow cytometry. Surprisingly, there was a significant difference in CD63 expression between A549 EV and hMSC EV. While CD63 was highly enriched in isolated A549 EV samples, a 10-fold decrease of CD63 expression was shown in isolated hMSC EV (**Figure 4.4C**). Because the surface compositions of isolated EV populations are still poorly defined in the EV research field, it cannot be concluded if this finding is just the intrinsic properties of hMSC EV populations or if the purity/integrity of hMSC EVs may have been altered during the culture and isolation processes. Further investigations on the surface components and quality of hMSC EV over multiple batches are required to provide a better explanation of the current findings.

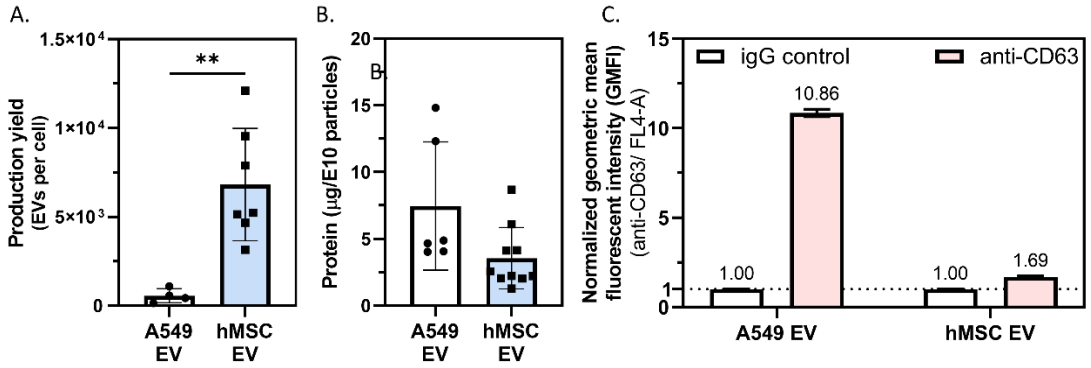

Figure 4.4 Characterization of hMSC EVs and A549 EVs. (A) Production yield of EVs secreted by hMSC and A549 cells. The number of vesicles was quantified by NTA measurement. (B) Affiliated protein per EV quantified by Micro BCA assay. (C) Flow cytometric analysis of EVs stained with fluorescent labelled antibodies (Alexa Fluor 647) targeting CD63. The negative isotype control was normalized to 1.

4.3.4. Azide-functionalization Characterization by Fluorescent Labeling and DBCO-mPEG Labeling

To characterize the azide functionalization of the isolated hMSC EVs, we labelled fluorescent dye *via* azide-specific click chemistry reaction with DBCO. The same procedure of the DBCO-AF488 labelling on cells was conducted on EVs for azide group characterization. As a control, EVs isolated from untreated hMSC cells were also labeled with DBCO-Cy5. We further prepared azide containing liposomes using the azide-PEG(2000)-SPE lipid as a positive control to evaluate the azide functionalization efficiency of hMSC EV. Various concentrations of azide-presenting liposomes from 10^7 particles/ml to 10^9 particles/ml were prepared to determine the lowest detection limits of the fluorescence reading assay. The resultant concentration curve of azide-liposomes (**Figure 4.5A**) demonstrated a minimum of 10^7 particles/ml is required to obtain a distinguishable signal from the control (no azide) vesicles. With increasing azide liposome concentration, the fluorescent intensity of DBCO-AF488 drastically increased, indicating a greater amount of azide groups was coupled with DBCO dye under the incubation conditions. Nevertheless, there was little signal detected from azide-functionalized hMSC EVs, which were either treated with ManNAZ sugar or Azido-choline. The background fluorescence of control EVs was also higher than the liposome samples, likely due to the non-specific binding of dyes in the presence of membrane proteins. However, even elevating the EV concentration to 10^{11} particles/ml for fluorescence measurement, the intensity of DBCO-AF488 was still low and undistinguishable from the background

control groups. The same results of low fluorescent intensity were obtained from Tz functionalized EVs (**Figure 4.5B**). These results may indicate the insufficient azide functionalization on hMSC EVs or it may be attributed to low sensitivity of the fluorescence reading technique.

We next performed another method to characterize the presence of azide groups on exosomal membrane. DBCO-mPEG with 20 kDa molecular weight was employed to label the azide groups. It is hypothesized that the hydrodynamic radius of azide-presenting EVs would increase after DBCO-mPEG conjugation, due to the extension of mPEG chains in aqueous solution (**Figure 4.5C**). It is expected an ~10 nm size increase with 20 kDa mPEG can be observed by NTA measurement. **Figure 4.5D** showed the diameter change of EVs before and after DBCO-mPEG incubation. A 13 nm increase of the mean diameter on azide-presenting EVs (obtained by ManNAz delivery) after mPEG labeling was observed compared to the unconjugated azide EVs. A similar increase was observed with azide liposomes. This can possibly indicate the presence of azide functional groups. However, the isolated EV samples are inherently heterogenous populations, which may explain the large variability observed in the control EVs. Thus, more samples over multiple batches should be tested to confirm the azide incorporation efficacy.

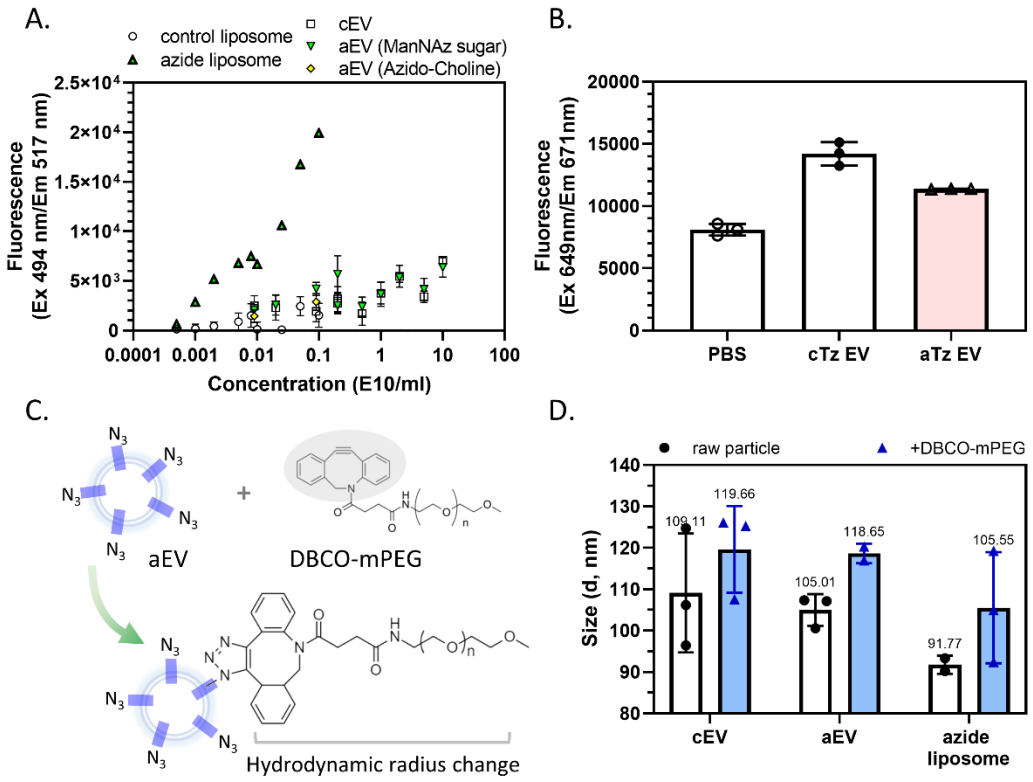

Figure 4.5 Characterization of Azide-functionalization on hMSC EVs. (A) Fluorescence intensity of DBCO-AlexaFluor488 labelled control EVs (cEV) and aEVs (obtained from ManNAz sugar-delivered or Azido-Choline-delivered hMSC). (B) Fluorescence intensity of TCO-Cy5 labelled control EVs (cTz EV) and aTz EV (obtained from DBCO-Tz delivered azide-presenting hMSC). (C) Illustration of azide-DBCO reaction between aEV and DBCO-mPEG. (D) The hydrodynamic radius change of aEVs after mPEG conjugation was determined by size measurement using NTA technique.

4.4. Conclusions

Mesenchymal stem cells have been studied as cell therapeutics for inflammatory and degenerative diseases. It has been suggested that most of the therapeutic effects of MSCs are attributed to the secretion of extracellular vesicles (MSC-EVs). MSC-EVs contain the bioactive molecules from their parental cells to modulate immunosuppressive and regenerative responses. In this study, we aimed to surface-modify MSC EV with bio-

orthogonal moieties by cellular metabolic engineering and *in situ* click chemistry (Azide-DBCO) reaction, which ultimately could be used for covalent conjugation to norbornene-containing MAP hydrogels.

Various approaches of azide functionalization on hMSC were examined. We performed fluorescence labeling using bio-orthogonal reactions, specifically azide-DBCO and tetrazine-TCO reaction to characterize the incorporation efficiency of azide groups and tetrazine groups on cell membrane. Successful incorporation of azide groups were observed in hMSC for both the liposome transfection method and metabolic engineering method. However, the minimum dose required and the cytotoxicity of azide reagents are a critical consideration for further applicability. We then performed physicochemical characterization on purified hMSC EVs obtained from cell conditioned media. However, low CD63 expression was observed in the EV samples. Moreover, azide functionalization was difficult to confirm, although the increase in size after incubation with mPEG-DBCO was encouraging. A systemic investigation of the EV contents and the quality over multiple batches is needed and could help solve the current pitfall. Lipidomic or proteomic analysis of the EV components may be required to definitively confirm the presence of functional groups on the exosomal membrane.

5. CONCLUSIONS

5.1. Summary of Present Findings

This dissertation lays out a path for the rational design of both semi-artificial extracellular vesicles (EVs) and native EVs for drug delivery and therapeutics applications. Engineering the surface composition of EVs can combine phospholipids and synthetic polymeric materials for efficient gene delivery (Chapter II), enable a combination of different therapeutics to be loaded (Chapter III), and provide a foundation for a bio-orthogonal conjugation reactable platform (Chapter IV). These studies present insights for the development of EV-based therapies.

First, we sought to establish a simple synthetic lipid fusion technique with EVs to solve the limitation of low yield EV production (Chapter II). We generated semi-artificial, lipid-hybridized EV carriers by fusing the surface composition of EVs with lipid-based materials (DOTAP, POPC, DPPC, and POPG) *via* a sonication and membrane extrusion technique. We performed several assessments to evaluate the membrane fusion efficacy, including quantification of lipid-to-protein content, alternation of surface marker expression on exosomal membrane, and fluorescence intensity changes in a single vesicle by fluorescent nanoparticle tracking analysis. The results demonstrated lipids were successfully incorporated into the exosomal membrane. We were able to achieve a 6- to 43-fold increase in numbers of vesicles post- isolation, depending on the applied lipid of interest. Further, we successfully loaded exogenous siRNA into these engineered vesicles with ~15% – 20% encapsulation efficiency using electroporation technique. We further demonstrated engineered extracellular vesicles sustained the preferential uptake capability

to lung cancer cells (A549) and achieved an effective gene silencing effect comparable to commercial Lipofectamine RNAiMax. These results demonstrated EVs can be fused with lipid materials while retaining their innate properties for gene delivery applications.

Second, we sought to develop a cell-selective EV-based co-delivery system for combination therapies (Chapter III). We combined the engineered lipid-hybridized EVs (eEVs) with a polymer coating technique to establish a carrier system capable of siRNA and doxorubicin (DOX) co-delivery to cancer cells. We first loaded siRNA into engineered lipid-hybridized EVs to serve as a core. Subsequently, we incorporated DOX into a polyelectrolyte shell surrounding eEVs by polymer layer-by-layer (LbL) assembly. We assessed cellular uptake, cytotoxicity, and gene silencing efficacy in A549 cancer cells, with non-cancerous fibroblast cells (CCL-210) used as a control. We demonstrated siRNA and DOX can be synchronously delivered to cells and the cell selectivity of EVs can still be retained after polymer deposition.

In addition to engineering EVs as drug delivery carriers, we also sought to modify functional groups (*e.g.,* tetrazine) on mesenchymal stem cell-derived EVs for future development of an EV-decorated, implantable hydrogel for cell-free therapeutic applications. Chapter IV describes a proof-of-concept experiment to generate bio-orthogonal reactive EVs through natural cellular metabolic pathways. These surface functionalized EVs are proposed to be covalently conjugated to a hydrogel *via* click chemistry. We attempted to functionalize azide groups and tetrazine groups on exosomal membrane by an *in-situ* bio-orthogonal click chemistry approach. First, we introduced azide groups on the hMSC membrane by supplementing azide-modified metabolites in

culturing media. The azide analog was taken up by the cells and expressed on the cellular membrane. Subsequently, we delivered DBCO-tetrazine linker to the cells, which is reactive to azide-displaying cell membranes and can be conjugated on the cells rapidly, resulting in a tetrazine functionalized cell surface. We demonstrated the azide and tetrazine groups were successfully integrated to almost the entire cell membrane. Therefore, it is postulated that azide- and tetrazine-functionalized EVs can be produced from the cells. However, an appropriate characterization method for surface functionalized EVs is yet needed to be studied. Further investigation on the quality control and components in the isolated EV samples are also required.

5.2. Recommendations for Future Work

The present studies show the proof of concept that EVs can be incorporated with different materials while retaining their inherent capability of cellular tropism to specific recipient cells. However, further understanding of EVs' molecular compositions and cellular selective capabilities are needed. For example, the critical factors affecting the selectivity of EVs' internalization process need to be identified for the rational design of membrane-fused EVs. The influence of lipid fusion ratios on the cell-selectivity of engineered EV may also provide information on the fundamental mechanisms of EVs' properties. A thorough characterization on lipidome or proteome levels can help further understanding of the composition and bioactivity relationships of the engineered EVs.

Despite promising results suggesting that the engineered EVs and polymer-coated eEVs could be used to selectively deliver to cancer cells, the addition of these synthetic materials may alter particle stability and EVs' bioactivity during modification. This

concern may be overcome by systematic screening of lipids/polymer used for EV membrane fusion and evaluating the corresponding membrane fusion efficiency, stability and aggregation properties. Additionally, the purification procedure after membrane fusion is critical to obtain effective carriers. Due to the similarity of membrane structure between liposomes and exosomes, current techniques for separating lipid materials by centrifugation or filtration columns may not be sufficient to remove excess residual materials. This may lead to a compromised therapeutic effect in the formulation.

While surface functionalization and characterization of native EVs remains challenging, the impurities (*e.g.,* inherent exosomes from fetal bovine serum) or non-classical EVs (*e.g.,* non-membranous exomeres) within isolated heterogenous samples may cause side effects to EVs' functionality. The quality of EVs may vary from batch-to-batch, so there is also a need to establish a standardized protocol to assay the identity and purity of MSC EVs. Chemically defined media may reduce the variability of cell culture, and yet a systematic investigation of the EV contents from collected media at varying conditions of cell growth is required to better understand EVs' therapeutic potency.

REFERENCES

1. Valadi H, Ekström K, Bossios A, et al. Exosome-mediated transfer of mRNAs and microRNAs is a novel mechanism of genetic exchange between cells. *Nature cell biology* 2007; 9: 654-659.
2. Sun D, Zhuang X, Zhang S, et al. Exosomes are endogenous nanoparticles that can deliver biological information between cells. *Advanced drug delivery reviews* 2013; 65: 342-347.
3. Corrado C, Raimondo S, Chiesi A, et al. Exosomes as intercellular signaling organelles involved in health and disease: basic science and clinical applications. *International journal of molecular sciences* 2013; 14: 5338-5366.
4. Cicero AL, Stahl PD and Raposo G. Extracellular vesicles shuffling intercellular messages: for good or for bad. *Current opinion in cell biology* 2015; 35: 69-77.
5. Vader P, Mol EA, Pasterkamp G, et al. Extracellular vesicles for drug delivery. *Advanced drug delivery reviews* 2016; 106: 148-156.
6. Stremersch S, De Smedt SC and Raemdonck K. Therapeutic and diagnostic applications of extracellular vesicles. *Journal of Controlled Release* 2016; 244: 167-183.
7. Fuhrmann G, Herrmann IK and Stevens MM. Cell-derived vesicles for drug therapy and diagnostics: opportunities and challenges. *Nano Today* 2015; 10: 397-409.
8. Tan A, Rajadas J and Seifalian AM. Exosomes as nano-theranostic delivery platforms for gene therapy. *Advanced drug delivery reviews* 2013; 65: 357-367.
9. Kalra H, Drummen GP and Mathivanan S. Focus on Extracellular Vesicles: Introducing the Next Small Big Thing. *International journal of molecular sciences* 2016; 17: 170.
10. Heusermann W, Hean J, Trojer D, et al. Exosomes surf on filopodia to enter cells at endocytic hot spots, traffic within endosomes, and are targeted to the ER. *Journal of Cell Biology* 2016; 213: 173-184.
11. Liang Q, Bie N, Yong T, et al. The softness of tumour-cell-derived microparticles regulates their drug-delivery efficiency. *Nature biomedical engineering* 2019; 3: 729-740.
12. Herzog RW, Cao O and Srivastava A. Two decades of clinical gene therapy–success is finally mounting. *Discovery medicine* 2010; 9: 105.
13. Prakash V, Moore M and Yáñez-Muñoz RJ. Current Progress in Therapeutic Gene Editing for Monogenic Diseases. *Molecular Therapy* 2016; 24: 465-474.
14. Ghosh S, Thrasher AJ and Gaspar HB. Gene therapy for monogenic disorders of the bone marrow. *British journal of haematology* 2015; 171: 155-170.
15. Vogelstein B, Papadopoulos N, Velculescu VE, et al. Cancer genome landscapes. *science* 2013; 339: 1546-1558.
16. Yin H, Kanasty RL, Eltoukhy AA, et al. Non-viral vectors for gene-based therapy. *Nature Reviews Genetics* 2014; 15: 541-555.
17. Gaudet D, Méthot J, Déry S, et al. Efficacy and long-term safety of alipogene tiparvovec (AAV1-LPLS447X) gene therapy for lipoprotein lipase deficiency: an open-label trial. *Gene therapy* 2013; 20: 361-369.

18. Thomas SM and Grandis JR. The current state of head and neck cancer gene therapy. *Human gene therapy* 2009; 20: 1565-1575.
19. Hsu PD, Lander ES and Zhang F. Development and applications of CRISPR-Cas9 for genome engineering. *Cell* 2014; 157: 1262-1278.
20. McNeer NA, Anandalingam K, Fields RJ, et al. Nanoparticles that deliver triplex-forming peptide nucleic acid molecules correct F508del CFTR in airway epithelium. *Nature communications* 2015; 6: 6952-6952.
21. Rapti K, Louis-Jeune V, Kohlbrenner E, et al. Neutralizing antibodies against AAV serotypes 1, 2, 6, and 9 in sera of commonly used animal models. *Molecular Therapy* 2012; 20: 73-83.
22. Louis Jeune V, Joergensen JA, Hajjar RJ, et al. Pre-existing anti–adeno-associated virus antibodies as a challenge in AAV gene therapy. *Human gene therapy methods* 2013; 24: 59-67.
23. Kim JH, Lee J, Park J, et al. Gram-negative and Gram-positive bacterial extracellular vesicles. In: *Seminars in cell & developmental biology* 2015, pp.97-104. Elsevier.
24. van der Pol E, Böing AN, Harrison P, et al. Classification, functions, and clinical relevance of extracellular vesicles. *Pharmacological reviews* 2012; 64: 676-705.
25. Zhou X, Xie F, Wang L, et al. The function and clinical application of extracellular vesicles in innate immune regulation. *Cellular & Molecular Immunology* 2020; 17: 323-334.
26. Kowal J, Arras G, Colombo M, et al. Proteomic comparison defines novel markers to characterize heterogeneous populations of extracellular vesicle subtypes. *Proceedings of the National Academy of Sciences* 2016; 113: E968-E977.
27. Zhang H, Freitas D, Kim HS, et al. Identification of distinct nanoparticles and subsets of extracellular vesicles by asymmetric flow field-flow fractionation. *Nature cell biology* 2018; 20: 332-343.
28. Jeppesen DK, Fenix AM, Franklin JL, et al. Reassessment of exosome composition. *Cell* 2019; 177: 428-445. e418.
29. Mathieu M, Martin-Jaular L, Lavieu G, et al. Specificities of secretion and uptake of exosomes and other extracellular vesicles for cell-to-cell communication. *Nature cell biology* 2019; 21: 9-17.
30. Théry C, Witwer KW, Aikawa E, et al. Minimal information for studies of extracellular vesicles 2018 (MISEV2018): a position statement of the International Society for Extracellular Vesicles and update of the MISEV2014 guidelines. *Journal of extracellular vesicles* 2018; 7: 1535750.
31. Meldolesi J. Ectosomes and Exosomes-Two Extracellular Vesicles That Differ Only in Some Details. *Biochemistry & Molecular Biology Journal* 2016; 2: 1-3.
32. Abels ER and Breakefield XO. Introduction to extracellular vesicles: biogenesis, RNA cargo selection, content, release, and uptake. Springer, 2016, p. 301-312.
33. Bebelman MP, Smit MJ, Pegtel DM, et al. Biogenesis and function of extracellular vesicles in cancer. *Pharmacology & therapeutics* 2018; 188: 1-11.
34. Trajkovic K, Hsu C, Chiantia S, et al. Ceramide triggers budding of exosome vesicles into multivesicular endosomes. *Science* 2008; 319: 1244-1247.

35. Skotland T, Sandvig K and Llorente A. Lipids in exosomes: current knowledge and the way forward. *Progress in lipid research* 2017; 66: 30-41.
36. Lener T, Gimona M, Aigner L, et al. Applying extracellular vesicles based therapeutics in clinical trials–an ISEV position paper. *Journal of extracellular vesicles* 2015; 4: 30087.
37. Revenfeld ALS, Bæk R, Nielsen MH, et al. Diagnostic and prognostic potential of extracellular vesicles in peripheral blood. *Clinical therapeutics* 2014; 36: 830-846.
38. György B, Szabó TG, Pásztói M, et al. Membrane vesicles, current state-of-the-art: emerging role of extracellular vesicles. *Cellular and molecular life sciences* 2011; 68: 2667-2688.
39. Pollet H, Conrard L, Cloos A-S, et al. Plasma membrane lipid domains as platforms for vesicle biogenesis and shedding? *Biomolecules* 2018; 8: 94.
40. Haraszti RA, Miller R, Dubuke ML, et al. Serum deprivation of mesenchymal stem cells improves exosome activity and alters lipid and protein composition. *Iscience* 2019; 16: 230-241.
41. Cocca BA, Cline AM and Radic MZ. Blebs and apoptotic bodies are B cell autoantigens. *The Journal of Immunology* 2002; 169: 159-166.
42. Savill J, Dransfield I, Gregory C, et al. A blast from the past: clearance of apoptotic cells regulates immune responses. *Nature Reviews Immunology* 2002; 2: 965-975.
43. Visnovitz T, Osteikoetxea X, Sódar BW, et al. An improved 96 well plate format lipid quantification assay for standardisation of experiments with extracellular vesicles. *Journal of extracellular vesicles* 2019; 8: 1565263.
44. Osteikoetxea X, Balogh A, Szabó-Taylor K, et al. Improved characterization of EV preparations based on protein to lipid ratio and lipid properties. *PLoS One* 2015; 10: e0121184.
45. Greening DW, Gopal SK, Xu R, et al. Exosomes and their roles in immune regulation and cancer. In: *Seminars in cell & developmental biology* 2015, pp.72-81. Elsevier.
46. Natasha G, Gundogan B, Tan A, et al. Exosomes as immunotheranostic nanoparticles. *Clinical therapeutics* 2014; 36: 820-829.
47. Chaput N and Théry C. Exosomes: immune properties and potential clinical implementations. In: *Seminars in immunopathology* 2011, pp.419-440. Springer.
48. Zitvogel L, Regnault A, Lozier A, et al. Eradication of established murine tumors using a novel cell-free vaccine: dendritic cell derived exosomes. *Nature medicine* 1998; 4: 594.
49. Hao S, Yuan J and Xiang J. Nonspecific CD4+ T cells with uptake of antigen-specific dendritic cell-released exosomes stimulate antigen-specific CD8+ CTL responses and long-term T cell memory. *Journal of leukocyte biology* 2007; 82: 829-838.
50. Hao S, Liu Y, Yuan J, et al. Novel exosome-targeted CD4+ T cell vaccine counteracting CD4+ 25+ regulatory T cell-mediated immune suppression and stimulating efficient central memory CD8+ CTL responses. *The Journal of Immunology* 2007; 179: 2731-2740.

51. Viaud S, Terme M, Flament C, et al. Dendritic cell-derived exosomes promote natural killer cell activation and proliferation: a role for NKG2D ligands and IL-15Rα. *PloS one* 2009; 4: e4942.
52. Pitt JM, André F, Amigorena S, et al. Dendritic cell–derived exosomes for cancer therapy. *The Journal of clinical investigation* 2016; 126: 1224-1232.
53. Wolfers J, Lozier A, Raposo G, et al. Tumor-derived exosomes are a source of shared tumor rejection antigens for CTL cross-priming. *Nature medicine* 2001; 7: 297-303.
54. Zech D, Rana S, Büchler MW, et al. Tumor-exosomes and leukocyte activation: an ambivalent crosstalk. *Cell Communication and Signaling* 2012; 10: 1.
55. Veerman RE, Akpinar GG, Eldh M, et al. Immune cell-derived extracellular vesicles–functions and therapeutic applications. *Trends in molecular medicine* 2019; 25: 382-394.
56. Li X, Li J-J, Yang J-Y, et al. Tolerance induction by exosomes from immature dendritic cells and rapamycin in a mouse cardiac allograft model. *PloS one* 2012; 7.
57. Pullan JE, Confeld MI, Osborn JK, et al. Exosomes as drug carriers for cancer therapy. *Molecular Pharmaceutics* 2019; 16: 1789-1798.
58. Meng W, He C, Hao Y, et al. Prospects and challenges of extracellular vesicle-based drug delivery system: considering cell source. *Drug Delivery* 2020; 27: 585-598.
59. Vishnubhatla I, Corteling R, Stevanato L, et al. The development of stem cell-derived exosomes as a cell-free regenerative medicine. *Journal of Circulating Biomarkers* 2014; 3: 3-2.
60. Xie M, Xiong W, She Z, et al. Immunoregulatory Effects of Stem Cell-Derived Extracellular Vesicles on Immune Cells. *Frontiers in Immunology* 2020; 11: 13.
61. Henao Agudelo JS, Braga TT, Amano MT, et al. Mesenchymal stromal cell-derived microvesicles regulate an internal pro-inflammatory program in activated macrophages. *Frontiers in immunology* 2017; 8: 881.
62. Cheng L, Wang Y and Huang L. Exosomes from M1-polarized macrophages potentiate the cancer vaccine by creating a pro-inflammatory microenvironment in the lymph node. *Molecular Therapy* 2017; 25: 1665-1675.
63. Noy R and Pollard JW. Tumor-associated macrophages: from mechanisms to therapy. *Immunity* 2014; 41: 49-61.
64. Morishita M, Takahashi Y, Nishikawa M, et al. Pharmacokinetics of exosomes—an important factor for elucidating the biological roles of exosomes and for the development of exosome-based therapeutics. *Journal of pharmaceutical sciences* 2017; 106: 2265-2269.
65. Smyth T, Kullberg M, Malik N, et al. Biodistribution and delivery efficiency of unmodified tumor-derived exosomes. *Journal of Controlled Release* 2015; 199: 145-155.
66. Takahashi Y, Nishikawa M, Shinotsuka H, et al. Visualization and in vivo tracking of the exosomes of murine melanoma B16-BL6 cells in mice after intravenous injection. *Journal of biotechnology* 2013; 165: 77-84.
67. Charoenviriyakul C, Takahashi Y, Morishita M, et al. Cell type-specific and common characteristics of exosomes derived from mouse cell lines: Yield,

physicochemical properties, and pharmacokinetics. *European Journal of Pharmaceutical Sciences* 2017; 96: 316-322.
68. Imai T, Takahashi Y, Nishikawa M, et al. Macrophage-dependent clearance of systemically administered B16BL6-derived exosomes from the blood circulation in mice. *Journal of extracellular vesicles* 2015; 4: 26238.
69. Peinado H, Alečković M, Lavotshkin S, et al. Melanoma exosomes educate bone marrow progenitor cells toward a pro-metastatic phenotype through MET. *Nature medicine* 2012; 18: 883-891.
70. Wiklander OP, Nordin JZ, O'Loughlin A, et al. Extracellular vesicle in vivo biodistribution is determined by cell source, route of administration and targeting. *Journal of extracellular vesicles* 2015; 4: 26316.
71. Munagala R, Aqil F, Jeyabalan J, et al. Bovine milk-derived exosomes for drug delivery. *Cancer letters* 2016; 371: 48-61.
72. Maumus M, ROZIER P, Boulestreau J, et al. Mesenchymal stem cells derived extracellular vesicles: opportunities and challenges for clinical translation. *Frontiers in Bioengineering and Biotechnology* 2020; 8: 997.
73. Perets N, Betzer O, Shapira R, et al. Golden exosomes selectively target brain pathologies in neurodegenerative and neurodevelopmental disorders. *Nano letters* 2019; 19: 3422-3431.
74. Lara P, Chan AB, Cruz LJ, et al. Exploiting the Natural Properties of Extracellular Vesicles in Targeted Delivery towards Specific Cells and Tissues. *Pharmaceutics* 2020; 12: 1022.
75. Feng D, Zhao WL, Ye YY, et al. Cellular internalization of exosomes occurs through phagocytosis. *Traffic* 2010; 11: 675-687.
76. Toda Y, Takata K, Nakagawa Y, et al. Effective internalization of U251-MG-secreted exosomes into cancer cells and characterization of their lipid components. *Biochemical and biophysical research communications* 2015; 456: 768-773.
77. Hazan-Halevy I, Rosenblum D, Weinstein S, et al. Cell-specific uptake of mantle cell lymphoma-derived exosomes by malignant and non-malignant B-lymphocytes. *Cancer letters* 2015; 364: 59-69.
78. Svensson KJ, Christianson HC, Wittrup A, et al. Exosome uptake depends on ERK1/2-heat shock protein 27 signaling and lipid Raft-mediated endocytosis negatively regulated by caveolin-1. *Journal of Biological Chemistry* 2013; 288: 17713-17724.
79. Yong T, Wang D, Li X, et al. Extracellular vesicles for tumor targeting delivery based on five features principle. *Journal of Controlled Release* 2020; 322: 555-565.
80. Sancho-Albero M, Navascués N, Mendoza G, et al. Exosome origin determines cell targeting and the transfer of therapeutic nanoparticles towards target cells. *Journal of nanobiotechnology* 2019; 17: 16.
81. Qiao L, Hu S, Huang K, et al. Tumor cell-derived exosomes home to their cells of origin and can be used as Trojan horses to deliver cancer drugs. *Theranostics* 2020; 10: 3474-3487.
82. Xu L, Faruqu FN, Liam-or R, et al. Design of experiment (DoE)-driven in vitro and in vivo uptake studies of exosomes for pancreatic cancer delivery enabled by

copper-free click chemistry-based labelling. *Journal of Extracellular Vesicles* 2020; 9: 1779458.
83. Rana S, Yue S, Stadel D, et al. Toward tailored exosomes: the exosomal tetraspanin web contributes to target cell selection. *The international journal of biochemistry & cell biology* 2012; 44: 1574-1584.
84. Morelli AE, Larregina AT, Shufesky WJ, et al. Endocytosis, intracellular sorting, and processing of exosomes by dendritic cells. *Blood* 2004; 104: 3257-3266.
85. Hoshino A, Costa-Silva B, Shen T-L, et al. Tumour exosome integrins determine organotropic metastasis. *Nature* 2015; 527: 329-335.
86. Watson DC, Bayik D, Srivatsan A, et al. Efficient production and enhanced tumor delivery of engineered extracellular vesicles. *Biomaterials* 2016; 105: 195-205.
87. Saunderson SC, Dunn AC, Crocker PR, et al. CD169 mediates the capture of exosomes in spleen and lymph node. *Blood, The Journal of the American Society of Hematology* 2014; 123: 208-216.
88. Kamerkar S, LeBleu VS, Sugimoto H, et al. Exosomes facilitate therapeutic targeting of oncogenic KRAS in pancreatic cancer. *Nature* 2017; 546: 498-503.
89. Faruqu FN, Wang JT-W, Xu L, et al. Membrane Radiolabelling of Exosomes for Comparative Biodistribution Analysis in Immunocompetent and Immunodeficient Mice-A Novel and Universal Approach. *Theranostics* 2019; 9: 1666.
90. Willis GR, Kourembanas S and Mitsialis SA. Toward exosome-based therapeutics: isolation, heterogeneity, and fit-for-purpose potency. *Frontiers in Cardiovascular Medicine* 2017; 4: 63.
91. Gimona M, Pachler K, Laner-Plamberger S, et al. Manufacturing of human extracellular vesicle-based therapeutics for clinical use. *International journal of molecular sciences* 2017; 18: 1190.
92. de Jong B, Barros ER, Hoenderop JG, et al. Recent Advances in Extracellular Vesicles as Drug Delivery Systems and Their Potential in Precision Medicine. *Pharmaceutics* 2020; 12: 1006.
93. Gandham S, Su X, Wood J, et al. Technologies and standardization in research on extracellular vesicles. *Trends in biotechnology* 2020; 38: 1066-1098.
94. Jang SC, Kim OY, Yoon CM, et al. Bioinspired exosome-mimetic nanovesicles for targeted delivery of chemotherapeutics to malignant tumors. *ACS nano* 2013; 7: 7698-7710.
95. Ren J, He W, Zheng L, et al. From structures to functions: insights into exosomes as promising drug delivery vehicles. *Biomaterials science* 2016; 4: 910-921.
96. Katsuda T, Tsuchiya R, Kosaka N, et al. Human adipose tissue-derived mesenchymal stem cells secrete functional neprilysin-bound exosomes. *Scientific reports* 2013; 3: 1197.
97. Kordelas L, Rebmann V, Ludwig A, et al. MSC-derived exosomes: a novel tool to treat therapy-refractory graft-versus-host disease. *Leukemia* 2014; 28: 970-973.
98. Haraszti RA, Miller R, Stoppato M, et al. Exosomes produced from 3D cultures of MSCs by tangential flow filtration show higher yield and improved activity. *Molecular Therapy* 2018; 26: 2838-2847.

99. Batrakova EV and Kim MS. Development and regulation of exosome-based therapy products. *Wiley Interdisciplinary Reviews: Nanomedicine and Nanobiotechnology* 2016; 8: 744-757.
100. Yeo RWY, Lai RC, Zhang B, et al. Mesenchymal stem cell: an efficient mass producer of exosomes for drug delivery. *Advanced drug delivery reviews* 2013; 65: 336-341.
101. Chen TS, Arslan F, Yin Y, et al. Enabling a robust scalable manufacturing process for therapeutic exosomes through oncogenic immortalization of human ESC-derived MSCs. *Journal of translational medicine* 2011; 9: 47.
102. Yeo RWY, Lai RC, Zhang B, et al. Mesenchymal stem cell: an efficient mass producer of exosomes for drug delivery. 2013; 65: 336-341.
103. Usman WM, Pham TC, Kwok YY, et al. Efficient RNA drug delivery using red blood cell extracellular vesicles. *Nature communications* 2018; 9: 1-15.
104. Aqil F, Munagala R, Jeyabalan J, et al. Milk exosomes-Natural nanoparticles for siRNA delivery. *Cancer letters* 2019; 449: 186-195.
105. Jafari D, Malih S, Eini M, et al. Improvement, scaling-up, and downstream analysis of exosome production. *Critical Reviews in Biotechnology* 2020; 40: 1098-1112.
106. Sun L, Wang H-x, Zhu X-j, et al. Serum deprivation elevates the levels of microvesicles with different size distributions and selectively enriched proteins in human myeloma cells in vitro. *Acta Pharmacologica Sinica* 2014; 35: 381-393.
107. Lamparski HG, Metha-Damani A, Yao J-Y, et al. Production and characterization of clinical grade exosomes derived from dendritic cells. *Journal of immunological methods* 2002; 270: 211-226.
108. Witwer KW, Buzas EI, Bemis LT, et al. Standardization of sample collection, isolation and analysis methods in extracellular vesicle research. *Journal of extracellular vesicles* 2013; 2: 20360.
109. Wang J, Bonacquisti EE, Brown AD, et al. Boosting the biogenesis and secretion of mesenchymal stem cell-derived exosomes. *Cells* 2020; 9: 660.
110. Andrews SH, Maughon T, Marklein RA, et al. Priming of MSCs with inflammation-relevant signals affects extracellular vesicle biogenesis, surface markers, and modulation of T cell subsets. *bioRxiv* 2020. DOI: 10.1101/2020.04.30.066456.
111. Wang X, Gu H, Huang W, et al. Hsp20-mediated activation of exosome biogenesis in cardiomyocytes improves cardiac function and angiogenesis in diabetic mice. *Diabetes* 2016; 65: 3111-3128.
112. Schiller LT, Lemus-Diaz N, Ferreira RR, et al. Enhanced production of exosome-associated AAV by overexpression of the Tetraspanin CD9. *Molecular Therapy-Methods & Clinical Development* 2018; 9: 278-287.
113. Hurwitz SN, Nkosi D, Conlon MM, et al. CD63 regulates Epstein-Barr virus LMP1 exosomal packaging, enhancement of vesicle production, and noncanonical NF-κB signaling. *Journal of virology* 2017; 91: e02251-02216.
114. Sinha S, Hoshino D, Hong NH, et al. Cortactin promotes exosome secretion by controlling branched actin dynamics. *Journal of Cell Biology* 2016; 214: 197-213.

115. Mitchell JP, Court J, Mason MD, et al. Increased exosome production from tumour cell cultures using the Integra CELLine Culture System. *Journal of immunological methods* 2008; 335: 98-105.
116. Weng Y, Sui Z, Shan Y, et al. Effective isolation of exosomes with polyethylene glycol from cell culture supernatant for in-depth proteome profiling. *Analyst* 2016; 141: 4640-4646.
117. Rider MA, Hurwitz SN and Meckes Jr DG. ExtraPEG: a polyethylene glycol-based method for enrichment of extracellular vesicles. *Scientific reports* 2016; 6: 23978.
118. Ludwig A-K, De Miroschedji K, Doeppner TR, et al. Precipitation with polyethylene glycol followed by washing and pelleting by ultracentrifugation enriches extracellular vesicles from tissue culture supernatants in small and large scales. *Journal of extracellular vesicles* 2018; 7: 1528109.
119. Yang Z, Shi J, Xie J, et al. Large-scale generation of functional mRNA-encapsulating exosomes via cellular nanoporation. *Nature Biomedical Engineering* 2020; 4: 69-83.
120. Salunkhe S, Basak M, Chitkara D, et al. Surface functionalization of exosomes for target-specific delivery and in vivo imaging & tracking: Strategies and significance. *Journal of Controlled Release* 2020; 326: 599-614.
121. Rayamajhi S and Aryal S. Surface functionalization strategies of extracellular vesicles. *Journal of Materials Chemistry B* 2020; 9: 4552-4569.
122. Armstrong JP, Holme MN and Stevens MM. Re-Engineering extracellular vesicles as smart nanoscale therapeutics. *ACS nano* 2017; 11: 69-83.
123. Alvarez-Erviti L, Seow Y, Yin H, et al. Delivery of siRNA to the mouse brain by systemic injection of targeted exosomes. *Nature biotechnology* 2011; 29: 341-345.
124. Tian Y, Li S, Song J, et al. A doxorubicin delivery platform using engineered natural membrane vesicle exosomes for targeted tumor therapy. *Biomaterials* 2014; 35: 2383-2390.
125. Ohno S-i, Takanashi M, Sudo K, et al. Systemically injected exosomes targeted to EGFR deliver antitumor microRNA to breast cancer cells. *Molecular Therapy* 2013; 21: 185-191.
126. Hung ME and Leonard JN. Stabilization of exosome-targeting peptides via engineered glycosylation. *Journal of Biological Chemistry* 2015; 290: 8166-8172.
127. Stickney Z, Losacco J, McDevitt S, et al. Development of exosome surface display technology in living human cells. *Biochemical and biophysical research communications* 2016; 472: 53-59.
128. Kooijmans SA, Aleza CG, Roffler SR, et al. Display of GPI-anchored anti-EGFR nanobodies on extracellular vesicles promotes tumour cell targeting. *Journal of extracellular vesicles* 2016; 5: 31053.
129. Zeelenberg IS, Ostrowski M, Krumeich S, et al. Targeting tumor antigens to secreted membrane vesicles in vivo induces efficient antitumor immune responses. *Cancer research* 2008; 68: 1228-1235.
130. Hartman ZC, Wei J, Glass OK, et al. Increasing vaccine potency through exosome antigen targeting. *Vaccine* 2011; 29: 9361-9367.

131. Rountree RB, Mandl SJ, Nachtwey JM, et al. Exosome targeting of tumor antigens expressed by cancer vaccines can improve antigen immunogenicity and therapeutic efficacy. *Cancer research* 2011; 71: 5235-5244.
132. Kooijmans SA, Gitz-Francois JJ, Schiffelers RM, et al. Recombinant phosphatidylserine-binding nanobodies for targeting of extracellular vesicles to tumor cells: a plug-and-play approach. *Nanoscale* 2018; 10: 2413-2426.
133. Smyth T, Petrova K, Payton NM, et al. Surface functionalization of exosomes using click chemistry. *Bioconjugate chemistry* 2014; 25: 1777-1784.
134. Tian T, Zhang H-X, He C-P, et al. Surface functionalized exosomes as targeted drug delivery vehicles for cerebral ischemia therapy. *Biomaterials* 2018; 150: 137-149.
135. Wang M, Altinoglu S, Takeda YS, et al. Integrating protein engineering and bioorthogonal click conjugation for extracellular vesicle modulation and intracellular delivery. 2015; 10: e0141860.
136. Alberti D, Grange C, Porta S, et al. Efficient Route to Label Mesenchymal Stromal Cell-Derived Extracellular Vesicles. *ACS omega* 2018; 3: 8097-8103.
137. Zhang P, Dong B, Zeng E, et al. In vivo tracking of multiple tumor exosomes labeled by phospholipid-based bioorthogonal conjugation. *Analytical chemistry* 2018; 90: 11273-11279.
138. Nie W, Wu G, Zhang J, et al. Responsive exosome nano-bioconjugates for synergistic cancer therapy. *Angewandte Chemie* 2020; 132: 2034-2038.
139. Lee J, Lee H, Goh U, et al. Cellular engineering with membrane fusogenic liposomes to produce functionalized extracellular vesicles. *ACS applied materials & interfaces* 2016; 8: 6790-6795.
140. Di H, Zeng E, Zhang P, et al. General Approach to Engineering Extracellular Vesicles for Biomedical Analysis. *Analytical chemistry* 2019; 91: 12752-12759.
141. Sato YT, Umezaki K, Sawada S, et al. Engineering hybrid exosomes by membrane fusion with liposomes. *Scientific reports* 2016; 6: 21933.
142. Rayamajhi S, Nguyen TDT, Marasini R, et al. Macrophage-derived exosome-mimetic hybrid vesicles for tumor targeted drug delivery. *Acta biomaterialia* 2019; 94: 482-494.
143. Tamura R, Uemoto S and Tabata Y. Augmented liver targeting of exosomes by surface modification with cationized pullulan. *Acta biomaterialia* 2017; 57: 274-284.
144. Nakase I and Futaki S. Combined treatment with a pH-sensitive fusogenic peptide and cationic lipids achieves enhanced cytosolic delivery of exosomes. *Scientific reports* 2015; 5: 10112.
145. Batrakova EV and Kim MS. Using exosomes, naturally-equipped nanocarriers, for drug delivery. *Journal of Controlled Release* 2015; 219: 396-405.
146. Peng H, Ji W, Zhao R, et al. Exosome: a significant nano-scale drug delivery carrier. *Journal of Materials Chemistry B* 2020; 8: 7591-7608.
147. Mehryab F, Rabbani S, Shahhosseini S, et al. Exosomes as a next-generation drug delivery system: an update on drug loading approaches, characterization, and clinical application challenges. *Acta biomaterialia* 2020; 113: 42-62.
148. Liu C and Su C. Design strategies and application progress of therapeutic exosomes. *Theranostics* 2019; 9: 1015.

149. Pascucci L, Coccè V, Bonomi A, et al. Paclitaxel is incorporated by mesenchymal stromal cells and released in exosomes that inhibit in vitro tumor growth: a new approach for drug delivery. *Journal of Controlled Release* 2014; 192: 262-270.
150. Zhang Y, Li L, Yu J, et al. Microvesicle-mediated delivery of transforming growth factor β1 siRNA for the suppression of tumor growth in mice. *Biomaterials* 2014; 35: 4390-4400.
151. Yim N and Choi CJBr. Extracellular vesicles as novel carriers for therapeutic molecules. 2016; 49: 585.
152. Huang C-C, Kang M, Lu Y, et al. Functionally Engineered Extracellular Vesicles Improve Bone Regeneration. *Acta Biomaterialia* 2020; 109: 182-194.
153. Shen B, Wu N, Yang J-M, et al. Protein targeting to exosomes/microvesicles by plasma membrane anchors. 2011; 286: 14383-14395.
154. Yim N, Ryu S-W, Choi K, et al. Exosome engineering for efficient intracellular delivery of soluble proteins using optically reversible protein–protein interaction module. *Nature communications* 2016; 7: 12277.
155. Kennedy MJ, Hughes RM, Peteya LA, et al. Rapid blue-light–mediated induction of protein interactions in living cells. *Nature methods* 2010; 7: 973.
156. Luan X, Sansanaphongpricha K, Myers I, et al. Engineering exosomes as refined biological nanoplatforms for drug delivery. *Acta Pharmacologica Sinica* 2017; 38: 754.
157. Sun D, Zhuang X, Xiang X, et al. A novel nanoparticle drug delivery system: the anti-inflammatory activity of curcumin is enhanced when encapsulated in exosomes. *Molecular Therapy* 2010; 18: 1606-1614.
158. Haney MJ, Klyachko NL, Zhao Y, et al. Exosomes as drug delivery vehicles for Parkinson's disease therapy. *Journal of Controlled Release* 2015; 207: 18-30.
159. Kim MS, Haney MJ, Zhao Y, et al. Development of exosome-encapsulated paclitaxel to overcome MDR in cancer cells. *Nanomedicine: Nanotechnology, Biology and Medicine* 2016; 12: 655-664.
160. Fuhrmann G, Serio A, Mazo M, et al. Active loading into extracellular vesicles significantly improves the cellular uptake and photodynamic effect of porphyrins. *Journal of Controlled Release* 2015; 205: 35-44.
161. Lamichhane TN, Raiker RS and Jay SM. Exogenous DNA loading into extracellular vesicles via electroporation is size-dependent and enables limited gene delivery. *Molecular pharmaceutics* 2015; 12: 3650-3657.
162. Kooijmans SA, Stremersch S, Braeckmans K, et al. Electroporation-induced siRNA precipitation obscures the efficiency of siRNA loading into extracellular vesicles. *Journal of controlled release* 2013; 172: 229-238.
163. Lamichhane TN, Jeyaram A, Patel DB, et al. Oncogene knockdown via active loading of small RNAs into extracellular vesicles by sonication. *Cellular and molecular bioengineering* 2016; 9: 315-324.
164. Haraszti RA, Miller R, Didiot M-C, et al. Optimized cholesterol-siRNA chemistry improves productive loading onto extracellular vesicles. *Molecular Therapy* 2018; 26: 1973-1982.
165. Syn NL, Wang L, Chow EK-H, et al. Exosomes in cancer nanomedicine and immunotherapy: Prospects and challenges. *Trends in Biotechnology* 2017; 35: 665-676.

166. Ruigrok M, Frijlink H and Hinrichs W. Pulmonary administration of small interfering RNA: The route to go? *Journal of Controlled Release* 2016; 235: 14-23.
167. Charoenphol P, Oswalt K and Bishop CJ. Therapeutics incorporating blood constituents. *Acta biomaterialia* 2018; 73: 64-80.
168. Lee SJ, Kim MJ, Kwon IC, et al. Delivery strategies and potential targets for siRNA in major cancer types. *Advanced drug delivery reviews* 2016; 104: 2-15.
169. Kim Y-D, Park T-E, Singh B, et al. Nanoparticle-mediated delivery of siRNA for effective lung cancer therapy. *Nanomedicine* 2015; 10: 1165-1188.
170. Harding CV, Heuser JE and Stahl PDJJCB. Exosomes: looking back three decades and into the future. 2013; 200: 367-371.
171. Jiang X-C and Gao J-Q. Exosomes as novel bio-carriers for gene and drug delivery. *International journal of pharmaceutics* 2017; 521: 167-175.
172. Gilligan KE and Dwyer RM. Engineering exosomes for cancer therapy. *International journal of molecular sciences* 2017; 18: 1122.
173. Srivastava A, Babu A, Filant J, et al. Exploitation of exosomes as nanocarriers for gene-, chemo-, and immune-therapy of cancer. *Journal of biomedical nanotechnology* 2016; 12: 1159-1173.
174. Andaloussi SE, Mäger I, Breakefield XO, et al. Extracellular vesicles: biology and emerging therapeutic opportunities. *Nature reviews Drug discovery* 2013; 12: 347-357.
175. Maas SL, Breakefield XO and Weaver AM. Extracellular vesicles: unique intercellular delivery vehicles. *Trends in cell biology* 2017; 27: 172-188.
176. Andaloussi SE, Lakhal S, Mäger I, et al. Exosomes for targeted siRNA delivery across biological barriers. *Advanced drug delivery reviews* 2013; 65: 391-397.
177. Maheshwari R, Tekade M, Gondaliya P, et al. Recent advances in exosome-based nanovehicles as RNA interference therapeutic carriers. *Nanomedicine* 2017; 12: 2653-2675.
178. Ohno S-i, Drummen GP and Kuroda M. Focus on Extracellular Vesicles: Development of Extracellular Vesicle-Based Therapeutic Systems. *International journal of molecular sciences* 2016; 17: 172.
179. Conlan RS, Pisano S, Oliveira MI, et al. Exosomes as reconfigurable therapeutic systems. 2017; 23: 636-650.
180. Armstrong JP and Stevens MM. Strategic design of extracellular vesicle drug delivery systems. *Advanced drug delivery reviews* 2018; 130: 12-16.
181. Fuhrmann G, Chandrawati R, Parmar PA, et al. Engineering Extracellular Vesicles with the Tools of Enzyme Prodrug Therapy. 2018; 30: 1706616.
182. Greening DW, Xu R, Ji H, et al. A protocol for exosome isolation and characterization: evaluation of ultracentrifugation, density-gradient separation, and immunoaffinity capture methods. *Proteomic Profiling*. Springer, 2015, pp.179-209.
183. Szatanek R, Baran J, Siedlar M, et al. Isolation of extracellular vesicles: determining the correct approach. *International journal of molecular medicine* 2015; 36: 11-17.

184. Löf L, Ebai T, Dubois L, et al. Detecting individual extracellular vesicles using a multicolor in situ proximity ligation assay with flow cytometric readout. *Scientific reports* 2016; 6: 34358.
185. Properzi F, Logozzi M and Fais S. Exosomes: the future of biomarkers in medicine. *Biomarkers in medicine* 2013; 7: 769-778.
186. Théry C, Amigorena S, Raposo G, et al. Isolation and characterization of exosomes from cell culture supernatants and biological fluids. *Current protocols in cell biology* 2006; 30: 3.22. 21-23.22. 29.
187. El-Andaloussi S, Lee Y, Lakhal-Littleton S, et al. Exosome-mediated delivery of siRNA in vitro and in vivo. *Nature protocols* 2012; 7: 2112-2126.
188. Golzio M, Mora M-P, Raynaud C, et al. Control by osmotic pressure of voltage-induced permeabilization and gene transfer in mammalian cells. *Biophysical journal* 1998; 74: 3015-3022.
189. Usaj M and Kanduser M. The systematic study of the electroporation and electrofusion of B16-F1 and CHO cells in isotonic and hypotonic buffer. *The Journal of membrane biology* 2012; 245: 583-590.
190. Ušaj M, Trontelj K, Hudej R, et al. Cell size dynamics and viability of cells exposed to hypotonic treatment and electroporation for electrofusion optimization. *Radiology and Oncology* 2009; 43: 108-119.
191. Navakanitworakul R, Hung W-T, Gunewardena S, et al. Characterization and small RNA content of extracellular vesicles in follicular fluid of developing bovine antral follicles. *Scientific reports* 2016; 6: 25486.
192. Pi F, Binzel DW, Lee TJ, et al. Nanoparticle orientation to control RNA loading and ligand display on extracellular vesicles for cancer regression. 2018; 13: 82.
193. Kamerkar S, LeBleu VS, Sugimoto H, et al. Exosomes facilitate therapeutic targeting of oncogenic KRAS in pancreatic cancer. 2017; 546: 498.
194. Gregory J. Monitoring particle aggregation processes. *Adv Colloid Interfac* 2009; 147: 109-123.
195. Lu M, Zhao X, Xing H, et al. Comparison of exosome-mimicking liposomes with conventional liposomes for intracellular delivery of siRNA. 2018; 550: 100-113.
196. Zhang Q, Ran R, Zhang L, et al. Simultaneous delivery of therapeutic antagomirs with paclitaxel for the management of metastatic tumors by a pH-responsive anti-microbial peptide-mediated liposomal delivery system. *Journal of Controlled Release* 2015; 197: 208-218.
197. Jamaluddin MP and Krishman LK. A spectrophotometric method for following initial rate kinetics of blood platelet aggregation. *Journal of Biochemical and Biophysical Methods* 1987; 14: 191-200.
198. Hood JL, Scott MJ and Wickline SA. Maximizing exosome colloidal stability following electroporation. *Analytical biochemistry* 2014; 448: 41-49.
199. Tran T-H, Mattheolabakis G, Aldawsari H, et al. Exosomes as nanocarriers for immunotherapy of cancer and inflammatory diseases. *Clinical Immunology* 2015; 160: 46-58.
200. Bishop CJ, Tzeng SY and Green JJ. Degradable polymer-coated gold nanoparticles for co-delivery of DNA and siRNA. *Acta biomaterialia* 2015; 11: 393-403.

201. Takov K, Yellon DM and Davidson SM. Confounding factors in vesicle uptake studies using fluorescent lipophilic membrane dyes. *Journal of extracellular vesicles* 2017; 6: 1388731.
202. Dominkuš PP, Stenovec M, Sitar S, et al. PKH26 labeling of extracellular vesicles: characterization and cellular internalization of contaminating PKH26 nanoparticles. *Biochimica et Biophysica Acta (BBA)-Biomembranes* 2018; 1860: 1350-1361.
203. Simonsen JB. Pitfalls associated with lipophilic fluorophore staining of extracellular vesicles for uptake studies. *Journal of extracellular vesicles* 2019; 8: 1582237.
204. Xu R, Greening DW, Zhu H-J, et al. Extracellular vesicle isolation and characterization: toward clinical application. *Journal of Clinical Investigation* 2016; 126: 1152.
205. Christianson HC, Svensson KJ, van Kuppevelt TH, et al. Cancer cell exosomes depend on cell-surface heparan sulfate proteoglycans for their internalization and functional activity. *Proceedings of the National Academy of Sciences* 2013; 110: 17380-17385.
206. Turinetto V, Vitale E and Giachino C. Senescence in human mesenchymal stem cells: functional changes and implications in stem cell-based therapy. *International journal of molecular sciences* 2016; 17: 1164.
207. Jin HJ, Bae YK, Kim M, et al. Comparative analysis of human mesenchymal stem cells from bone marrow, adipose tissue, and umbilical cord blood as sources of cell therapy. *International journal of molecular sciences* 2013; 14: 17986-18001.
208. Kanada M, Bachmann MH, Hardy JW, et al. Differential fates of biomolecules delivered to target cells via extracellular vesicles. *Proceedings of the National Academy of Sciences* 2015; 112: E1433-E1442.
209. Jhan Y-Y, Prasca-Chamorro D, Zuniga GP, et al. Engineered extracellular vesicles with synthetic lipids via membrane fusion to establish efficient gene delivery. *International Journal of Pharmaceutics* 2020; 573: 118802.
210. Watson DC, Bayik D, Srivatsan A, et al. Efficient production and enhanced tumor delivery of engineered extracellular vesicles. 2016; 105: 195-205.
211. Antimisiaris S, Mourtas S and Papadia K. Targeted si-RNA with liposomes and exosomes (extracellular vesicles): how to unlock the potential. *international Journal of pharmaceutics* 2017; 525: 293-312.
212. Piffoux M, Silva AK, Wilhelm C, et al. Modification of extracellular vesicles by fusion with liposomes for the design of personalized biogenic drug delivery systems. *ACS nano* 2018; 12: 6830-6842.
213. Marimpietri D, Petretto A, Raffaghello L, et al. Proteome profiling of neuroblastoma-derived exosomes reveal the expression of proteins potentially involved in tumor progression. *PloS one* 2013; 8: e75054.
214. Lv H, Zhang S, Wang B, et al. Toxicity of cationic lipids and cationic polymers in gene delivery. *Journal of controlled release* 2006; 114: 100-109.
215. Stapulionis RJB and bioenergetics. Electric pulse-induced precipitation of biological macromolecules in electroporation. 1999; 48: 249-254.

216. Scherer TM, Leung S, Owyang L, et al. Issues and challenges of subvisible and submicron particulate analysis in protein solutions. *The AAPS journal* 2012; 14: 236-243.
217. Cho EC, Zhang Q and Xia Y. The effect of sedimentation and diffusion on cellular uptake of gold nanoparticles. *Nature nanotechnology* 2011; 6: 385-391.
218. O'Loughlin AJ, Mäger I, de Jong OG, et al. Functional delivery of lipid-conjugated siRNA by extracellular vesicles. *Molecular Therapy* 2017; 25: 1580-1587.
219. Tekade RK, Tekade M, Kesharwani P, et al. RNAi-combined nano-chemotherapeutics to tackle resistant tumors. *Drug discovery today* 2016; 21: 1761-1774.
220. Wang M, Wang J, Li B, et al. Recent advances in mechanism-based chemotherapy drug-siRNA pairs in co-delivery systems for cancer: a review. *Colloids and Surfaces B: Biointerfaces* 2017; 157: 297-308.
221. Yoon HY, Son S, Lee SJ, et al. Glycol chitosan nanoparticles as specialized cancer therapeutic vehicles: Sequential delivery of doxorubicin and Bcl-2 siRNA. *Scientific reports* 2014; 4: 6878.
222. Jiang J, Yang S-j, Wang J-c, et al. Sequential treatment of drug-resistant tumors with RGD-modified liposomes containing siRNA or doxorubicin. *European journal of pharmaceutics and biopharmaceutics* 2010; 76: 170-178.
223. Sakurai Y, Hatakeyama H, Akita H, et al. Improvement of doxorubicin efficacy using liposomal anti-polo-like kinase 1 siRNA in human renal cell carcinomas. *Molecular pharmaceutics* 2014; 11: 2713-2719.
224. Tsouris V, Joo MK, Kim SH, et al. Nano carriers that enable co-delivery of chemotherapy and RNAi agents for treatment of drug-resistant cancers. *Biotechnology advances* 2014; 32: 1037-1050.
225. Zhang RX, Wong HL, Xue HY, et al. Nanomedicine of synergistic drug combinations for cancer therapy–Strategies and perspectives. *Journal of Controlled Release* 2016; 240: 489-503.
226. Bhise NS, Shmueli RB, Gonzalez J, et al. A novel assay for quantifying the number of plasmids encapsulated by polymer nanoparticles. *Small* 2012; 8: 367-373.
227. Li Y, Thambi T and Lee DS. Co-delivery of drugs and genes using polymeric nanoparticles for synergistic cancer therapeutic effects. *Advanced healthcare materials* 2018; 7: 1700886. DOI: 10.1002/adhm.201700886.
228. Taratula O, Kuzmov A, Shah M, et al. Nanostructured lipid carriers as multifunctional nanomedicine platform for pulmonary co-delivery of anticancer drugs and siRNA. *Journal of Controlled Release* 2013; 171: 349-357.
229. Chen L, Qian M, Zhang L, et al. Co-delivery of doxorubicin and shRNA of Beclin1 by folate receptor targeted pullulan-based multifunctional nanomicelles for combinational cancer therapy. *RSC advances* 2018; 8: 17710-17722.
230. Xia Y, Xu T, Wang C, et al. Novel functionalized nanoparticles for tumor-targeting co-delivery of doxorubicin and siRNA to enhance cancer therapy. *International journal of nanomedicine* 2018; 13: 143-159.

231. Cheng Q, Du L, Meng L, et al. The promising nanocarrier for doxorubicin and siRNA co-delivery by PDMAEMA-based amphiphilic nanomicelles. *ACS applied materials & interfaces* 2016; 8: 4347-4356.
232. Dong D-W, Xiang B, Gao W, et al. pH-responsive complexes using prefunctionalized polymers for synchronous delivery of doxorubicin and siRNA to cancer cells. *Biomaterials* 2013; 34: 4849-4859.
233. Gao Y, Jia L, Wang Q, et al. pH/Redox Dual-Responsive Polyplex with Effective Endosomal Escape for Co-Delivery of siRNA and Doxorubicin against Drug-Resistant Cancer Cells. *ACS applied materials & interfaces* 2019; 11: 16296-16310.
234. Jia H-Z, Zhang W, Zhu J-Y, et al. Hyperbranched–hyperbranched polymeric nanoassembly to mediate controllable co-delivery of siRNA and drug for synergistic tumor therapy. *Journal of controlled release* 2015; 216: 9-17.
235. Yin T, Wang L, Yin L, et al. Co-delivery of hydrophobic paclitaxel and hydrophilic AURKA specific siRNA by redox-sensitive micelles for effective treatment of breast cancer. *Biomaterials* 2015; 61: 10-25.
236. Wang J, Zheng Y and Zhao M. Exosome-based cancer therapy: implication for targeting cancer stem cells. *Frontiers in pharmacology* 2017; 7: 533.
237. Richardson JJ and Ejima H. Surface Engineering of Extracellular Vesicles through Chemical and Biological Strategies. *Chemistry of Materials* 2019; 31: 2191-2201.
238. Li Y, Zhang Y, Li Z, et al. Exosomes as Carriers for Antitumor Therapy. *ACS Biomaterials Science & Engineering* 2019; 5: 4870-4881.
239. Alhasan AH, Patel PC, Choi CHJ, et al. Exosome encased spherical nucleic acid gold nanoparticle conjugates as potent microRNA regulation agents. *Small* 2014; 10: 186-192.
240. Alkekhia D, Hammond PT and Shukla A. Layer-by-layer biomaterials for drug delivery. *Annual Review of Biomedical Engineering* 2020; 22: 1-24. DOI: 10.1146/annurev-bioeng-060418-052350.
241. Am Hong C, Son HY and Nam YS. Layer-by-layer siRNA/poly (L-lysine) multilayers on polydopamine-coated surface for efficient cell adhesion and gene silencing. *Scientific reports* 2018; 8: 1-7.
242. Wohl BM and Engbersen JF. Responsive layer-by-layer materials for drug delivery. *Journal of controlled release* 2012; 158: 2-14.
243. Kitaeva M, Melik-Nubarov N, Menger F, et al. Doxorubicin− Poly (acrylic acid) Complexes: Interaction with Liposomes. 2004; 20: 6575-6579.
244. Chen Y, Qi Y and Liu BJJoN. Polyacrylic acid functionalized nanographene as a nanocarrier for loading and controlled release of doxorubicin hydrochloride. 2013; 2013: 16. DOI: 10.1155/2013/345738.
245. Bishop CJ, Liu AL, Lee DS, et al. Layer-by-layer inorganic/polymeric nanoparticles for kinetically controlled multigene delivery. *Journal of Biomedical Materials Research Part A* 2016; 104: 707-713.
246. Routkevitch D, Sudhakar D, Conge MJ, et al. Efficiency of Cytosolic Delivery with Poly (beta-amino ester) Nanoparticles is Dependent on the Effective pKa of the Polymer. *ACS Biomaterials Science & Engineering* 2020; 6: 3411-3421.

247. Kozielski KL, Tzeng SY, Hurtado De Mendoza BA, et al. Bioreducible cationic polymer-based nanoparticles for efficient and environmentally triggered cytoplasmic siRNA delivery to primary human brain cancer cells. *ACS nano* 2014; 8: 3232-3241.
248. Betancourt T, Brown B and Brannon-Peppas L. Doxorubicin-loaded PLGA nanoparticles by nanoprecipitation: preparation, characterization and in vitro evaluation. 2007; 2: 219-232.
249. Sui Z, Salloum D and Schlenoff JB. Effect of molecular weight on the construction of polyelectrolyte multilayers: stripping versus sticking. *Langmuir* 2003; 19: 2491-2495.
250. Seyrek E, Hierrezuelo J, Sadeghpour A, et al. Molecular mass dependence of adsorbed amount and hydrodynamic thickness of polyelectrolyte layers. *Physical Chemistry Chemical Physics* 2011; 13: 12716-12719.
251. Vader P, Mol EA, Pasterkamp G, et al. Extracellular vesicles for drug delivery. *Advanced drug delivery reviews* 2016; 106: 148-156.
252. Ramasamy T, Tran TH, Choi JY, et al. Layer-by-layer coated lipid–polymer hybrid nanoparticles designed for use in anticancer drug delivery. *Carbohydrate polymers* 2014; 102: 653-661.
253. Wu X, Jiang J, Gu Z, et al. Mesenchymal stromal cell therapies: immunomodulatory properties and clinical progress. *Stem Cell Research & Therapy* 2020; 11: 1-16.
254. Barreca MM, Cancemi P and Geraci F. Mesenchymal and Induced Pluripotent Stem Cells-Derived Extracellular Vesicles: The New Frontier for Regenerative Medicine? *Cells* 2020; 9: 1163.
255. Witwer KW, Van Balkom BW, Bruno S, et al. Defining mesenchymal stromal cell (MSC)-derived small extracellular vesicles for therapeutic applications. *Journal of extracellular vesicles* 2019; 8: 1609206.
256. Sagaradze G, Basalova N, Efimenko A, et al. Mesenchymal stromal cells as critical contributors to tissue regeneration. *Frontiers in Cell and Developmental Biology* 2020; 8: 917.
257. Xunian Z and Kalluri R. Biology and therapeutic potential of mesenchymal stem cell-derived exosomes. *Cancer Science* 2020; 111: 3100.
258. Wang J, Xia J, Huang R, et al. Mesenchymal stem cell-derived extracellular vesicles alter disease outcomes via endorsement of macrophage polarization. *Stem Cell Research & Therapy* 2020; 11: 1-12.
259. Kim H, Lee M, Bae E, et al. Comprehensive Molecular Profiles of Functionally Effective MSC-Derived Extracellular Vesicles in Immunomodulation. *Molecular therapy: the journal of the American Society of Gene Therapy* 2020; 28: 1628-1644.
260. Maumus M, Rozier P, Boulestreau J, et al. Mesenchymal Stem Cell-Derived Extracellular Vesicles: Opportunities and Challenges for Clinical Translation. *Frontiers in Bioengineering and Biotechnology* 2020; 8: 1-12.
261. Riau A, Ong HS, Yam GH, et al. Sustained delivery system for stem cell-derived exosomes. *Frontiers in pharmacology* 2019; 10: 1368.

262. Liu X, Yang Y, Li Y, et al. Integration of stem cell-derived exosomes with in situ hydrogel glue as a promising tissue patch for articular cartilage regeneration. *Nanoscale* 2017; 9: 4430-4438.
263. Wang C, Wang M, Xu T, et al. Engineering bioactive self-healing antibacterial exosomes hydrogel for promoting chronic diabetic wound healing and complete skin regeneration. *Theranostics* 2019; 9: 65.
264. Zhang K, Zhao X, Chen X, et al. Enhanced therapeutic effects of mesenchymal stem cell-derived exosomes with an injectable hydrogel for hindlimb ischemia treatment. *ACS applied materials & interfaces* 2018; 10: 30081-30091.
265. Xin S, Chimene D, Garza JE, et al. Clickable PEG hydrogel microspheres as building blocks for 3D bioprinting. *Biomaterials science* 2019; 7: 1179-1187.
266. Isaac A, Jivan F, Xin S, et al. Microporous Bio-orthogonally Annealed Particle Hydrogels for Tissue Engineering and Regenerative Medicine. *ACS Biomaterials Science & Engineering* 2019; 5: 6395-6404.
267. Lee TS, Kim Y, Zhang W, et al. Facile metabolic glycan labeling strategy for exosome tracking. *Biochimica et Biophysica Acta (BBA)-General Subjects* 2018; 1862: 1091-1100.
268. Nagahama K, Kimura Y and Takemoto A. Living functional hydrogels generated by bioorthogonal cross-linking reactions of azide-modified cells with alkyne-modified polymers. *Nature communications* 2018; 9: 1-11.
269. Layek B, Sadhukha T and Prabha S. Glycoengineered mesenchymal stem cells as an enabling platform for two-step targeting of solid tumors. *Biomaterials* 2016; 88: 97-109.
270. Liang Y, Jiang X, Yuan R, et al. Metabolism-based click-mediated platform for specific imaging and quantification of cell surface sialic acids. *Analytical chemistry* 2017; 89: 538-543.
271. Song S, Shim MK, Lim S, et al. In situ one-step fluorescence labeling strategy of exosomes via bioorthogonal click chemistry for real-time exosome tracking in vitro and in vivo. *Bioconjugate Chemistry* 2020; 31: 1562-1574.
272. Börger V, Staubach S, Dittrich R, et al. Scaled Isolation of Mesenchymal Stem/Stromal Cell-Derived Extracellular Vesicles. *Current protocols in stem cell biology* 2020; 55: e128.
273. McMahon A, Lu H and Butovich IAJL. The spectrophotometric sulfo-phospho-vanillin assessment of total lipids in human meibomian gland secretions. 2013; 48: 513-525.
274. Cheng YS, Zheng Y and VanderGheynst JS. Rapid quantitative analysis of lipids using a colorimetric method in a microplate format. *Lipids* 2011; 46: 95-103.
275. Knight JA, Anderson S and Rawle JM. Chemical basis of the sulfo-phospho-vanillin reaction for estimating total serum lipids. *Clinical chemistry* 1972; 18: 199-202.
276. Bishop C, Abubaker-Sharif B, Guiriba T, et al. Gene delivery polymer structure–function relationships elucidated via principal component analysis. *Chemical Communications* 2015; 51: 12134-12137.
277. Haney MJ, Klyachko NL, Zhao Y, et al. Exosomes as drug delivery vehicles for Parkinson's disease therapy. 2015; 207: 18-30.

278. Boethling R, Meylan WJEt and chemistry. How accurate are physical property estimation programs for organosilicon compounds? 2013; 32: 2433-2440.

APPENDIX A. SUPPORTING INFORMATION OF CHAPTER II

A.1. Graphical Abstract

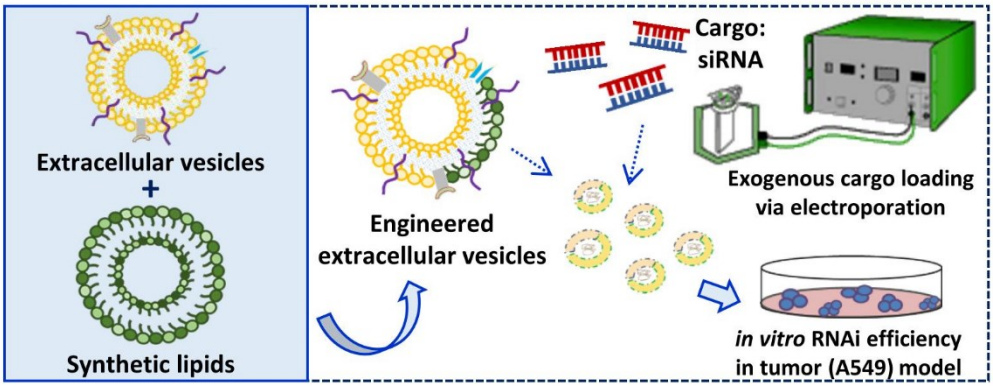

A.2. Experimental Sections

A.2.1. Transmission Electron Microscopy – Morphology

A 400 mesh Formvar/carbon-coated copper grid was transferred on top of the drop with their carbon-coated side facing the EV suspension. The EVs were then fixed with 2% paraformaldehyde and 1% glutaraldehyde, followed by a repetitive PBS wash procedure. Subsequently, the contrast of the samples was enhanced by transferring the grid to a drop of uranyl oxalate solution, which was prepared by the following: 1:1 v/v of 4% uranyl acid and 0.15 M oxalic acid (adjusted to pH 7). Subsequently, the grid was then embedded in a drop of methyl cellulose/uranyl acetate, which was prepared as follows: 1:1 v/v of 2%

of methyl cellulose and 4% uranyl acetate. To remove the excess solution from the grids, a Whatman no. 1 filter paper was used.

A.2.2. Membrane Composition Quantification Assay – Lipid Quantification

A sulfo-phospho-vanillin (SPV) assay was used to quantify the lipid amount within the vesicles, which is a two-step micro-colorimetric assay to detect the presence of double bonds or free hydroxyl groups within the lipids.[273-275] The quantification was conducted in simple 96 well plate format using cholesterol as a lipid standard for EVs.[44] Pure lipid solutions (DOTAP, DPPC, POPC and POPG) were also prepared individually as standards for each individual lipid-extruded eEV system. Different concentrations (0.1-2 μg/μl) of lipid solutions were prepared in chloroform, which were aliquoted (70 μl). The defined aliquoted lipid standard solutions (70μl in chloroform) and the EV/eEV solutions (70μl in PBS) were evaporated at 90°C to dryness for 25 minutes. Subsequently, 250 μl of 96% sulfuric acid was added to each tube and incubated at 95°C for 20 min. After reaction, the reaction mixtures were cooled and 220 μl of mixture were transferred to new microtubes. Then 110 μl of 0.2 mg/ml vanillin in 17% aqueous phosphoric acid solution was added to each of the reaction mixtures and incubated at room temperature for 10 min. Finally, 100 μl of mixture was transferred to a 96 well plate. Absorbance of each of the wells were quantified using a plate reader (Cytation 5, BioTek Instruments, Inc.) at 540 nm.

A.2.3. Loaded siRNA Content Quantification – Modified TRIzol RNA Isolation

In brief, the pellets of EVs/eEVs after ultracentrifugation were homogenized in 200 μl of TRIzol reagent for 10 min. at room temperature. Samples were then centrifuged at 12000 ×g for 15 min. at 4°C. The supernatant was discarded and after 40 μl of

chloroform was added to the microtube, vigorous shaking was applied. Vigorous shaking helps introduce many pockets of different phases with a high surface area between the phases within the microtube and is accomplished to help the siRNA fully transport into the proper phase. Samples were then centrifuged again at 12000 ×g for 15 min. at 4°C to obtain 2 phases, thus minimizing the surface area between the 2 phases. The aqueous phase of samples (upper phase) was transferred to a new microtube. Subsequently, 100 µl of isopropanol and 1 µl of glycogen (20 µg/µl) was added to the aqueous solution and incubated at -80°C for 1 hr., followed by 12000 ×g for 15 min. at 4°C centrifugation. Glycogen was used to extract the short RNA fragments. After centrifugation, the supernatant was discarded, and the pellet was washed with 70% ethanol. A pellet was obtained by centrifugation at 7500 ×g for 15 min. at 4°C. The RNA pellet was then dried under a hood at room temperature and was then re-suspended in 10 µl of RNase-free water for further RNA quantification.

A.2.4. Particle Size Analysis — Dynamic Light Scattering (DLS)

Particle size measurements were performed using DLS with a Malvern Zetasizer Nano-ZS. Sample concentrations of ~10^{11} particle/ml were prepared and were loaded in disposable polystyrene cuvettes. Data were collected after 2 min. of temperature equilibration at 25°C and acquired in an automatic mode to ensure enough photon signals were recorded. The Z-average diameter (nm) and relative percent (intensity) of size distribution profiles were determined.

A.2.5. siRNA Gel Retardation Assay

eEVs were prepared at different dosage amounts from 3.06×10^{10} particles to 18.36×10^{10} particles. All the samples contained 200 ng of siRNA and a total volume of 200 µl Opti-MEM or hypotonic electroporation buffer were used for electroporation. The electroporated eEV samples were wash-centrifuged after the electroporation processes and resuspended in a total volume of 10 µl of ultrapure water. The samples were then mixed with 2 µl of 6x DNA loading dye (Thermo Fisher Scientific) and electrophoresed in a 3% agarose gel in TAE buffer containing 10,000x SYBR Safe (Invitrogen). Electrophoresis was performed at 120 V for 1 hr. The resulting gels were photographed under ultraviolet illumination. 2 µg and 200 ng of naked siRNA were used as a control. 1.5 µg of Gene Ruler 100 bp DNA ladder (Thermo Fisher Scientific) was used as a standard. Resulting gel images were semi-quantified by ImageJ to obtain the amounts of siRNA retained in the gel well.

A.2.6. Cell Culture/ Flow Cytometric-Cell Sorting for a High GFP-expressing Tumor Cell Model

NIH/3T3 fibroblast cells (ATCC, P5-P10) were cultured in Dulbecco's Modified Eagle's Media (DMEM, Corning). The media was supplemented with 10% volume to volume (v/v) fetal bovine serum (FBS, Gibco) and 1% v/v 100 µg/ml penicillin/streptomycin (Gibco). The A549 lung cancer cells (P5-P15) were cultured in DMEM high glucose (4.5 g/ml glucose, Corning) media supplemented with 10% v/v FBS (Gibco); 1% v/v 0.1 mM Non-essential amino acids (MEM-NEAA, Gibco); and 1% v/v 100 µg/ml penicillin-streptomycin (Gibco). CCL-210 cells were cultured in Modified

Eagle's Media (EMEM, Lonza, #12-662F) supplemented with 10% v/v FBS (Gibco); 1% v/v GlutaMax (Thermofisher, #35050061); and 1% v/v 100 µg/ml penicillin-streptomycin (Gibco). All the cell types were grown in an incubator using cell culture conditions of 37°C and 5% CO_2.

GFP expressing A549 lung cancer cells were purchased from Cell Biolab, Inc. (#AKR-209) and further sorted by flow cytometry to obtain a higher percentage of GFP expressing A549 cell population. A549 GFP expressing cells were detached from the culturing flask by trypsinization, followed by centrifugation for 5 min. at 200 ×g. After centrifugation, the cells were resuspended in PBS buffer containing 2% (v/v) FBS for cell sorting. To obtain a more stable and a higher expressing GFP cell population, cell sorting was carried out on a Beckman Coulter MoFlo® AstriosTM High-Speed Cell Sorter and Becton Dickinson FACSCalibur TM Analyzer. A plot of FSC-H versus SSC-H was used to exclude debris and identify the singlet population of cells. By plotting the FL1-H versus the FL3-H channels, the higher GFP-expressing cell population was identified. The FL1-H versus FL3-H and the FL1-A histogram plots were used to determine the percentage of GFP expressing cells and to quantify the geometric mean of the fluorescence intensity. Post-cell sorting, the flow cytometry analysis for sorted cells were also performed using a BD AccuriTM C6 Flow Cytometer. The fold-increase of the normalized geometric mean fluorescent intensity (GMFI) was calculated by the following equation:

$$\mathrm{GMFI} = \frac{\frac{\mathrm{GM}_{\text{sorted A549}}}{\mathrm{GM}_{\text{background}}}}{\frac{\mathrm{GM}_{\text{pre-sorted A549}}}{\mathrm{GM}_{\text{background}}}} = \mathrm{GM}_{\text{sorted A549}} \Big/ \mathrm{GM}_{\text{pre-sorted A549}} \tag{A.1}$$

Non-GFP expressing A549 cells from Essen BioScience (#4491) Inc. was used to normalize to the background fluorescence of the cells.

A.3. Supporting Scheme

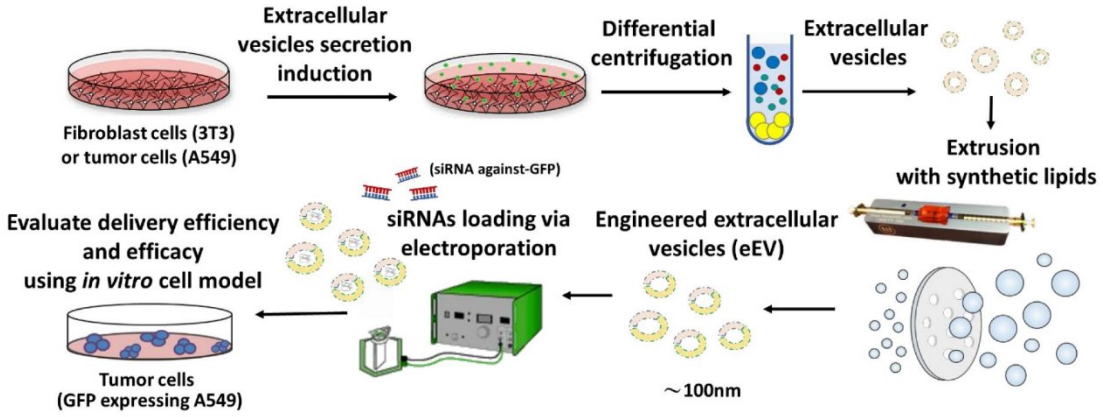

Scheme S1 Schematic illustration of the procedure for the generation of engineered lipid/extracellular vesicles (EVs). Reprinted with permission from © 2020 Elsevier from Jhan *et al*.[209]

A.4. Supporting Figures (S1-S21)

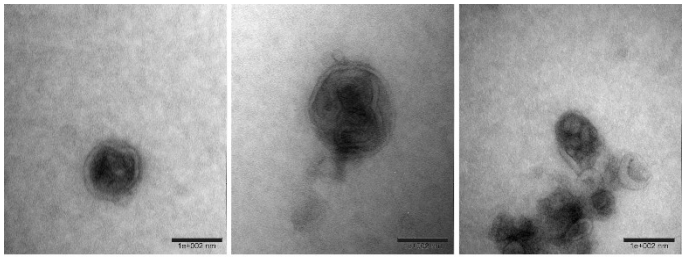

Figure S1 TEM images of native EVs. Spherical structure was shown in the images. Scale bar: 200 nm. Reprinted with permission from © 2020 Elsevier from Jhan *et al*.[209]

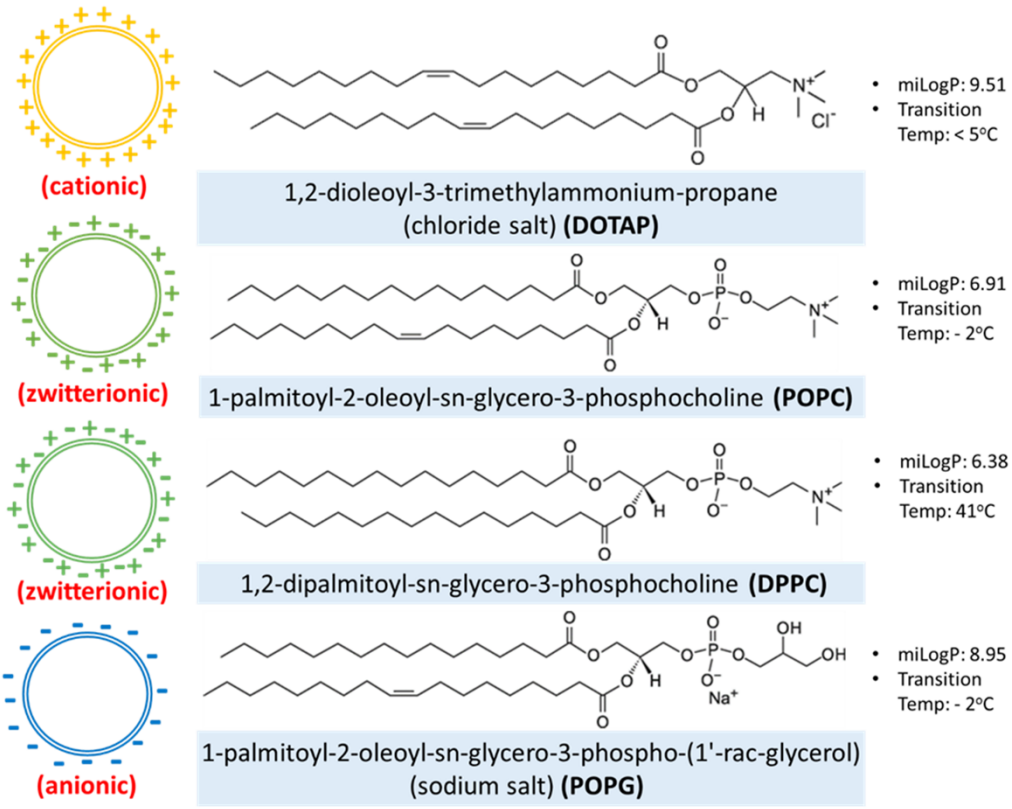

Figure S2 Lipids used to engineer the exosomeipid hybridized membrane. Note DOTAP, POPC, DPPC, and POPG are cationic, zwitterionic, zwitterionic, and anionic, respectively (left). The lipophilicity of lipids was calculated from open source LogP [276] prediction software, namely, Molinspiration (version: miLogP2.2 2005) [277, 278]. The LogP values generated from the mentioned software are referred to as "miLogP" values in the figure (right). The transition temperatures are also found within the figure (right). Reprinted with permission from © 2020 Elsevier from Jhan *et al*.[209]

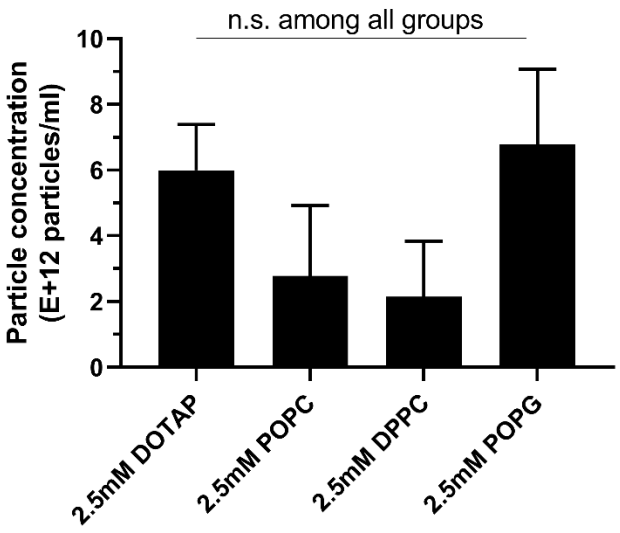

Figure S3 Particle number quantification of different lipids by NTA measurement. Reprinted with permission from © 2020 Elsevier from Jhan *et al*.[209]

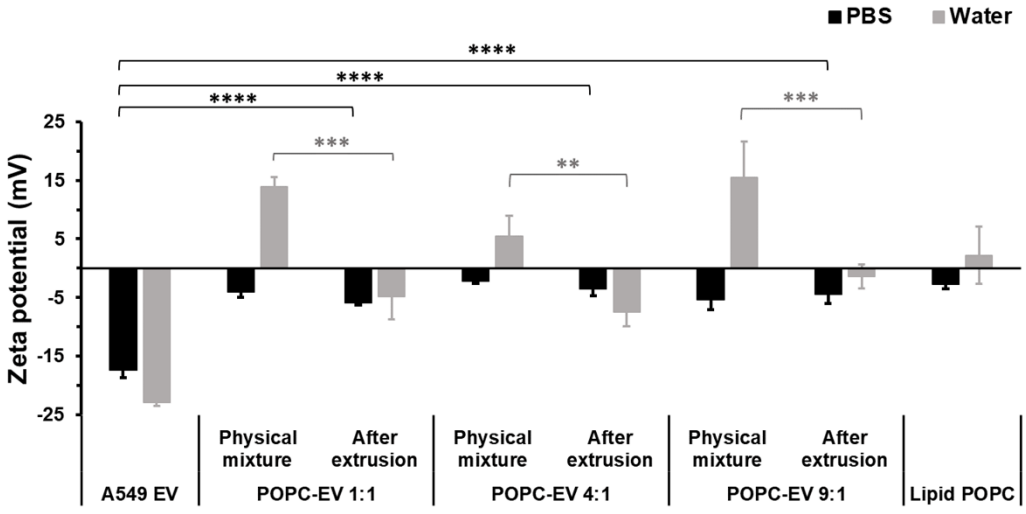

Figure S4 Zeta potential measurement of POPC-EV with POPC:EV mixing ratio from 1:1 to 9:1 before (physical mixture in the absence of sonication-extrusion processes) and after sonication-extrusion processes. Zeta potential values were determined in phosphate buffered saline (PBS) or water using a Malvern Zetasizer Nano ZS 90. ***p<0.01,* ****p <0.001* significant differences were shown between the groups of physical mixture and after extrusion (in water). *****p <0.0001* significant differences of samples after extrusion (in PBS) were shown compared to native A549 EV. Reprinted with permission from © 2020 Elsevier from Jhan *et al*.[209]

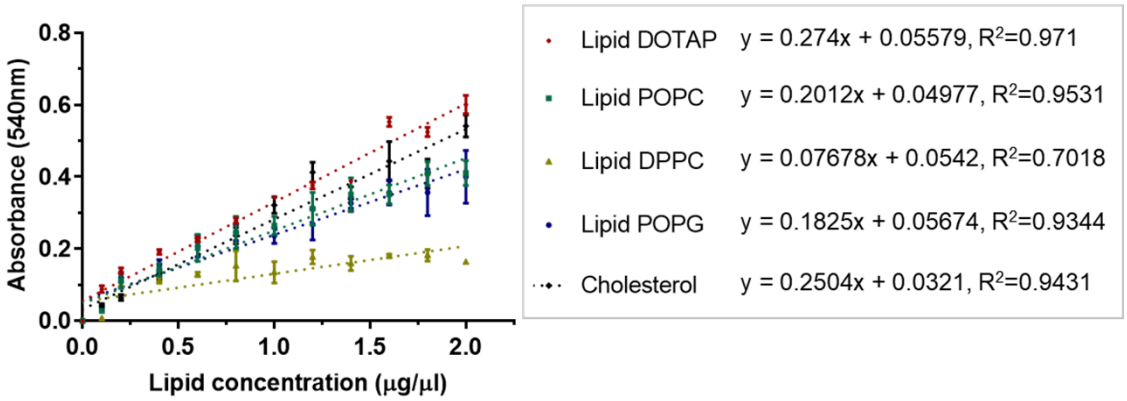

Figure S5 Absorbance linearity of different lipid types. Cholesterol is used as a standard for lipid quantification in EVs. Samples were incubated with H_2SO_4 at 90°C for 20 min. Vanillin-phosphoric acid (0.2 mg/ml vanillin in 17% phosphoric acid) was added for color development after the samples were cooled down to room temperature. Absorbance was measured at 540nm using Cytation 5 plate reader system. Data points represent measurement of triplicate samples. Reprinted with permission from © 2020 Elsevier from Jhan *et al*.[209]

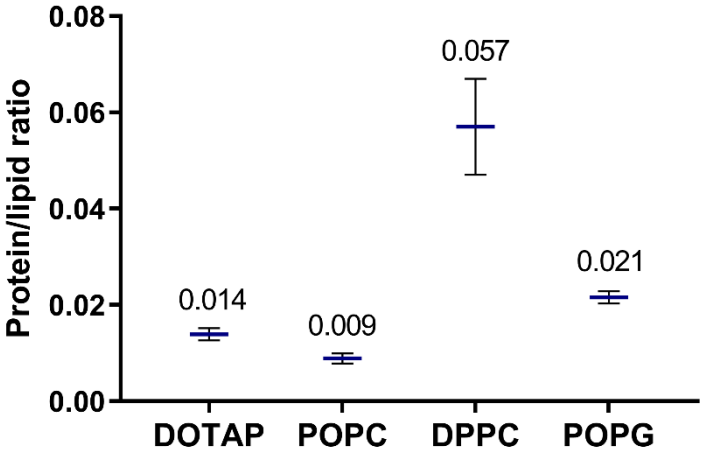

Figure S6. Protein to lipid ratios of pure lipid aqueous solutions. Protein to lipid ratios are presented for 2.5mM lipid (DOTAP, POPC, DPPC and POPG) in PBS aqueous solution determined by protein micro BCA assay and SPV assay. Mean values of three independent samples are indicated by horizontal lines. No big interference of lipid solution on protein microBCA determination was observed. Slightly higher background interference of lipids on protein micro BCA determination in DPPC samples was found. Reprinted with permission from © 2020 Elsevier from Jhan *et al*.[209]

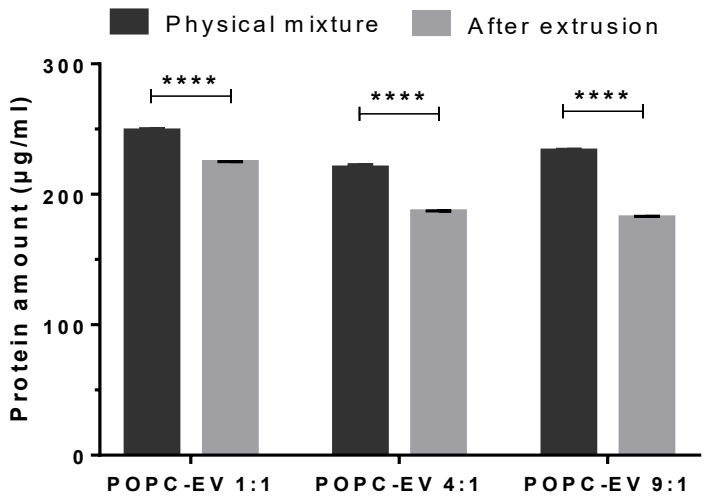

Figure S7 Protein quantification of engineered extracellular vesicles POPC-EV. EVs (50 µg/ml affiliated protein concentration) were mixed with POPC lipids (5mM) from 1:1 to 9:1 volumetric ratio prior to extrusion. The amounts of protein (µg/ml) of POPC-EV mixture before (physical mixture) and after the sonication-extrusion processes were quantified by Micro BCA protein assay kit. ****$p < 0.0001$ significant differences were shown between the groups of physical mixture and after extrusion. Reprinted with permission from © 2020 Elsevier from Jhan *et al*.[209]

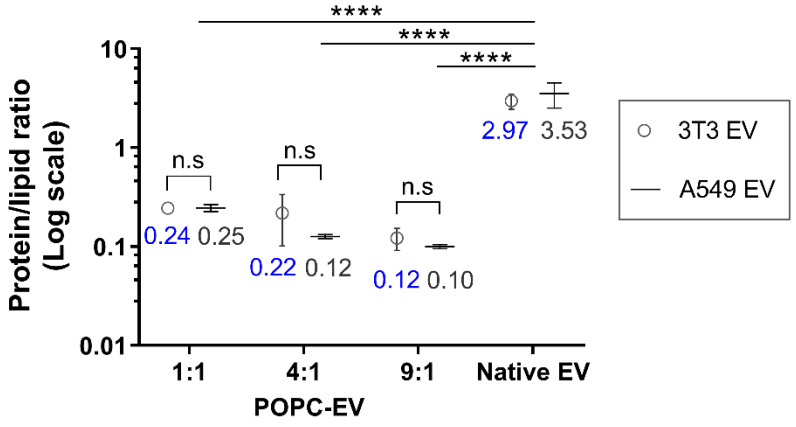

Figure S8 Protein to lipid ratios of eEVs at varying extruded ratio using EVs from two different parental cells (3T3 and A549 cells). Reprinted with permission from © 2020 Elsevier from Jhan *et al*.[209]

Figure S8 (Continued) The concentration of protein and lipids were determined by Micro BCA protein assay kit and sulfophosphovanillin (SPV) assay, respectively. EVs (50 μg/ml) were mixed with POPC lipids (5 mM) with different volumetric ratios prior to extrusion (*i.e.* 9:1 means lipid to EV with 9:1 mixing ratio). *****p <0.0001* significant differences were shown for compared to 3T3 EVs and A549 EVs.

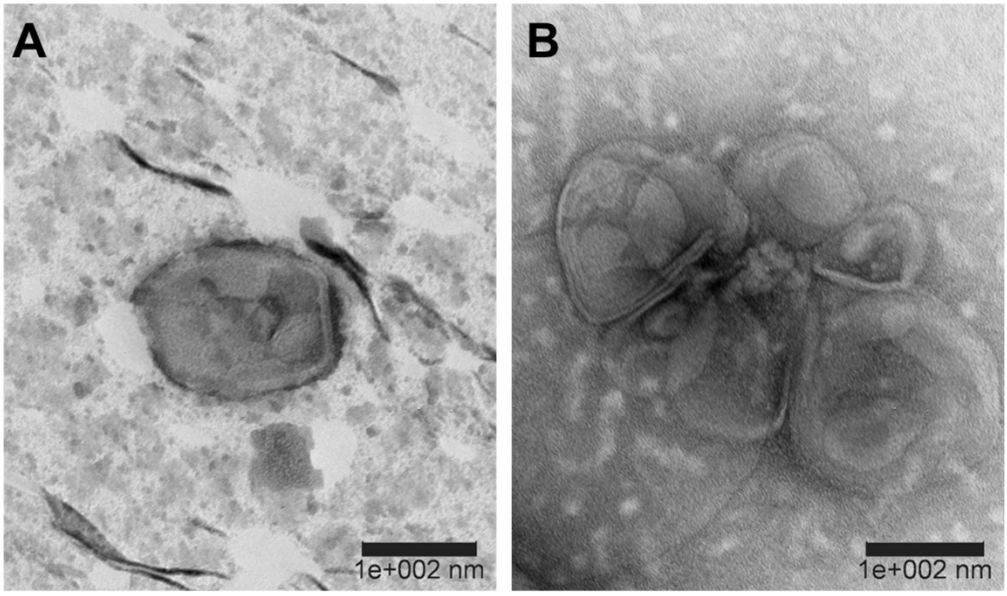

Figure S9 Morphology characterization of eEVs (POPC-EV) after electroporation using TEM. (A) POPC-EV with siRNA loading using electroporation; (B) aggregation was observed in electroporated samples. Scale bar: 200 nm. Reprinted with permission from © 2020 Elsevier from Jhan *et al*.[209]

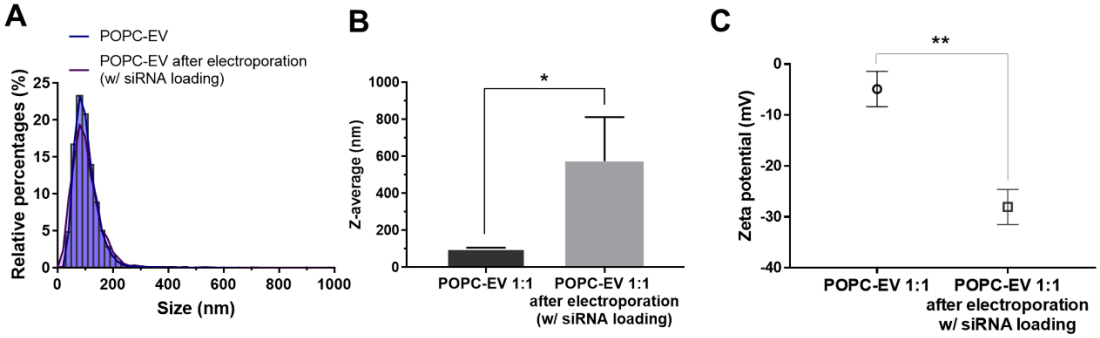

Figure S10 Size and zeta potential characterization of eEVs (POPC-EV) before and after electroporation. (A) NTA measurement; (B) DLS measurement; (C) zeta potential measurement. Reprinted with permission from © 2020 Elsevier from Jhan *et al*.[209]

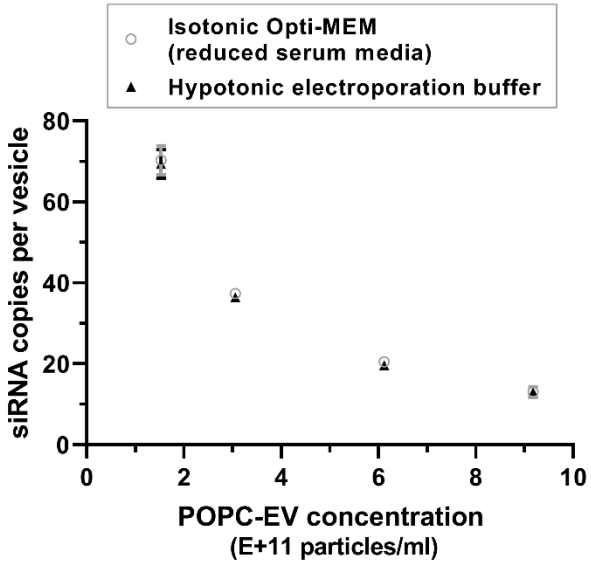

Figure S11 Effects of electroporation solution on siRNA loading efficiency at various POPC-EV concentrations. POPC-EV in the range of 1.53-9.18 × 10^{11} particles/ml concentration containing 200ng siRNA were prepared in isotonic Opti-MEM (reduced serum media) and hypotonic electroporation buffer with a total volume of 200 µl. The samples were electroporated, followed by siRNA isolation using TRIzol purification and quantification using Ribogreen quantification assay. Loading efficiency is determined by $\frac{\text{Numbers of siRNA in vesicles}}{\text{Numbers of vesicles}} \times 100\%$, which represents as siRNA copies per vesicle. Statistical differences were evaluated using an unpaired, two-tailed student t-test. No statistical difference was shown in the results. Reprinted with permission from © 2020 Elsevier from Jhan *et al*.[209]

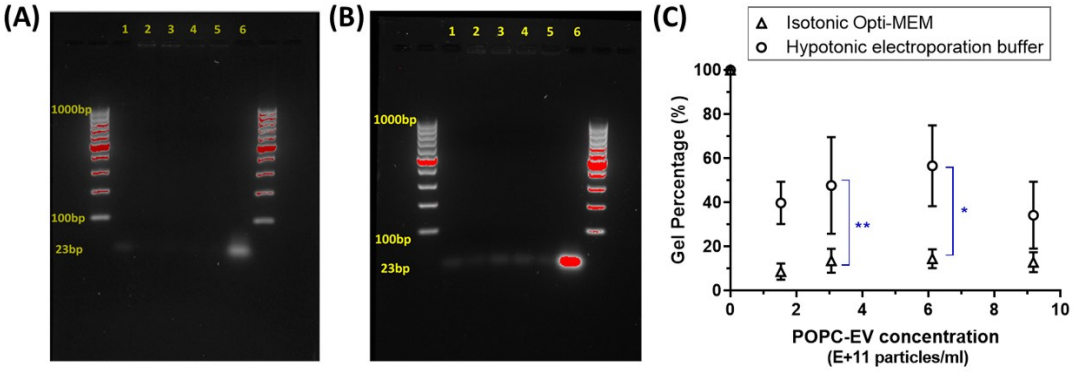

Figure S12 Gel retardation assay of POPC-EV with siRNA loading.

Figure S12 (Continued) Gel images of POPC-EV at various particle concentration in 200 µl (A) Opti-MEM media and (B) hypotonic electroporation buffer containing 200 ng siRNA. ****p <0.0001 significant differences were shown for each data point compared to the control group (200 ng siRNA only, at data point 0). (C) Quantitative results of POPC-EV at various particle concentration. Gel percentage was determined by the quantified results from the gel bands of each data point normalized to the results of control group (200 ng siRNA only, at data point 0) × 100%. *p <0.05 and **p <0.01 significant differences were shown between Opti-MEM and electroporation buffer. (A, B, C, D) Lane 1: siRNA 200 ng only; Lane 2: POPC-EV at 9.18×10^{11} particles/ml; Lane 3: POPC-EV at 6.12×10^{11} particles/ml; Lane 4: POPC-EV at 3.06×10^{11} particles/ml; Lane 5: POPC-EV at 1.53×10^{11} particles/ml; Lane 6: siRNA 2µg only. Reprinted with permission from © 2020 Elsevier from Jhan *et al*.[209]

A.4.1. Results of Figure S13: Flow Cytometric-Cell Sorting for A High GFP-expressing Tumor Cell Model

To demonstrate the cargo siRNA within eEVs can be delivered and be functioned intracellularly to suppress a gene expression, siRNA against green fluorescence protein (siRNA-GFP) was selected as model gene due to ease of knockdown the fluorescence expression in the GFP-expressing A549 cells. The GFP expression in the commercial A549 cells were characterized prior to cell studies. A representative bivariate dot plot of the cells (FL1-H versus FL3-H) and its histogram of FL1-A are presented in **Figure S12A** and **B**, respectively. We found two populations of GFP-expressing cells co-existed in the commercial A549 cells, where the higher GFP expressing population constituted 52.0% of the cells. Using the flow cytometry sorting method, we established a homogeneously (defined by a single FL1-A peak) expressing and high GFP-expressing tumor cell line (14.8 ± 3.5-fold higher in comparison to the commercial) (**Figure S12C**). We expected the homogenous expression would enable us to understand the variability of our future experiments to a higher degree, given that there would be less variability of GFP

expression on a per cell-basis. The sorted A549 cells were then used as an *in vitro* RNAi knockdown platform.

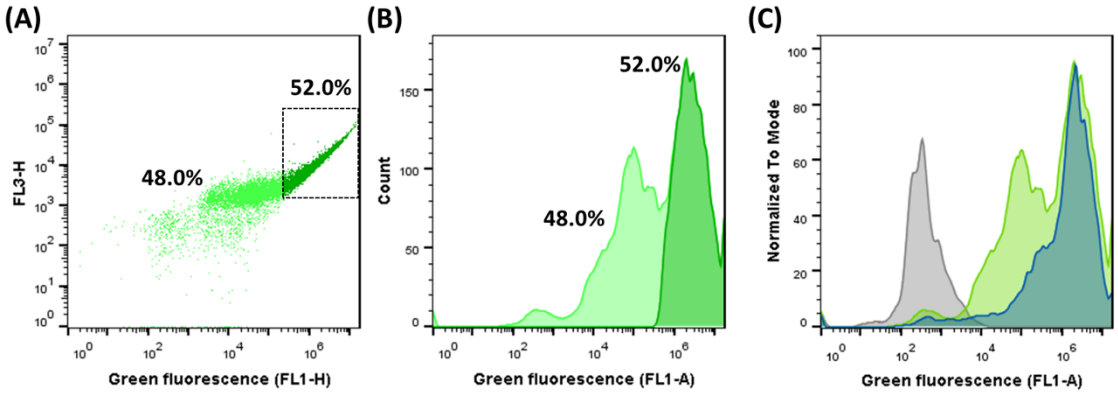

Figure S13 Flow cytometric analysis of A549 cells before (A and B) and after sorting (C). (Please note that A and B both have the same gating applied and the percentages of the populations shown are the same (48% and 52%.)) (A) A histogram of the fluorescence intensity showed two populations presented in the pre-sorted A549 cells (dark green: high GFP, dim green: low GFP). (B) Bivariate dot plot of FL1-H versus FL3-H for two populations. (C) FL1-A channel demonstrated the green fluorescence expression in all events after cell sorting. The y-axis, entitled, "Normalized to Mode", can also be considered the "% Population" (Gray: non-GFP expressing A549 cells, green: pre-sorted GFP expressing A549 cells, blue: sorted GFP expressing A549 cells.). Reprinted with permission from © 2020 Elsevier from Jhan *et al*.[209]

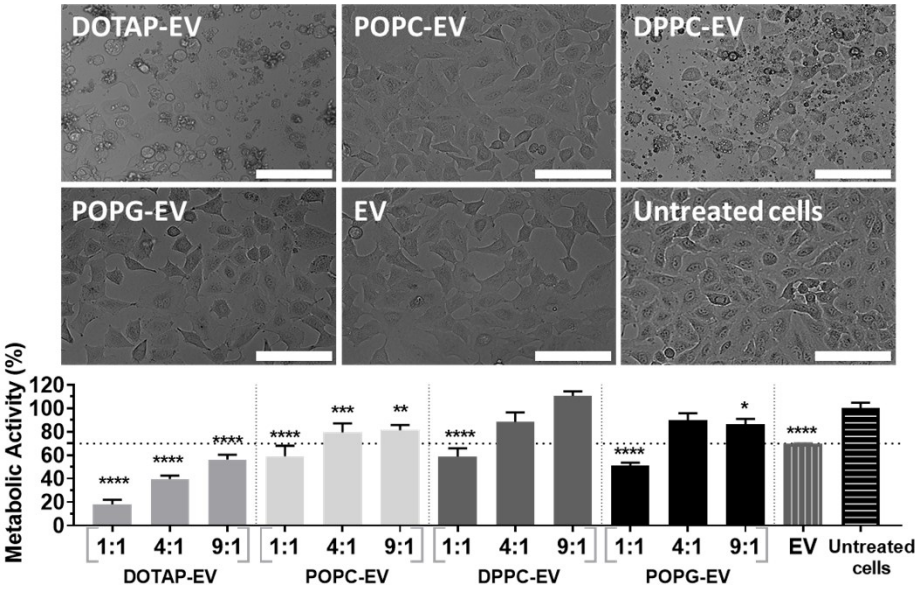

Figure S14 Cell viability of A549 cells incubated with various eEVs. (Top) Brightfield images of the eEV and EV formulations are shown (scale bar = 100 μm). (Bottom) The relative metabolic activities for each of the lipid-doped eEVs are quantified. EV/eEV in the concentration of 10^{10}-10^{11} vesicles/ml) were used as a single dose in a total loading volume of 200 μl Opti-MEM containing 1 ng/μl siRNA. **p< 0.05, **p< 0.01, ***p<0.001, ****p <0.0001* compared to the untreated cells. Reprinted with permission from © 2020 Elsevier from Jhan *et al*.[209]

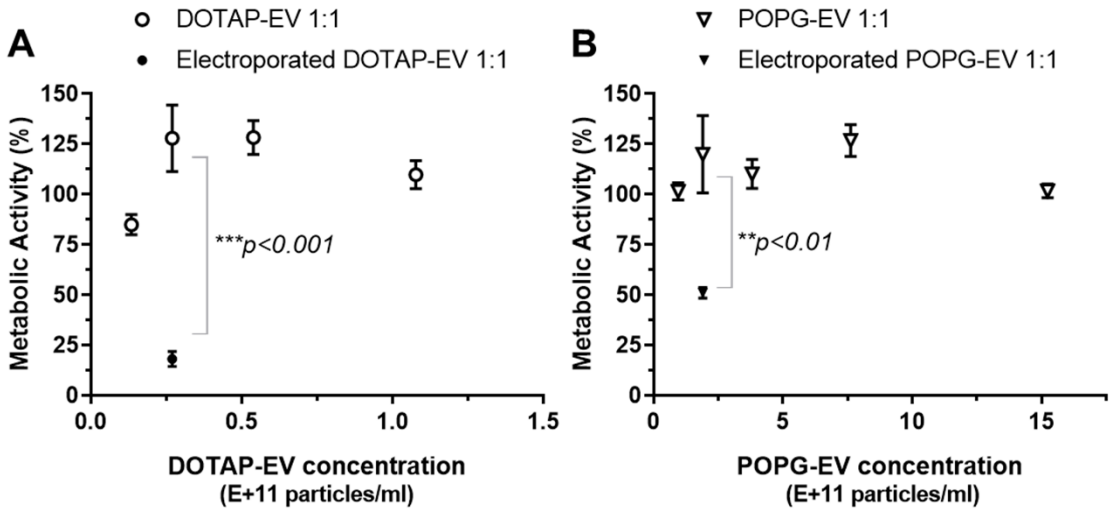

Figure S15 Cell viability of A549 cells treated with various concentrations of eEVs. (A) DOTAP-EV 1:1 with various concentration.

Figure S15 (Continued) (B) POPG-EV 1:1 with various concentrations (10^{10}-10^{11} vesicles/ml; 1 ng/µl siRNA in Opti-MEM) were either electroporated (closed symbols) or not (open symbols) before being added to the cells. Reprinted with permission from © 2020 Elsevier from Jhan *et al*.[209]

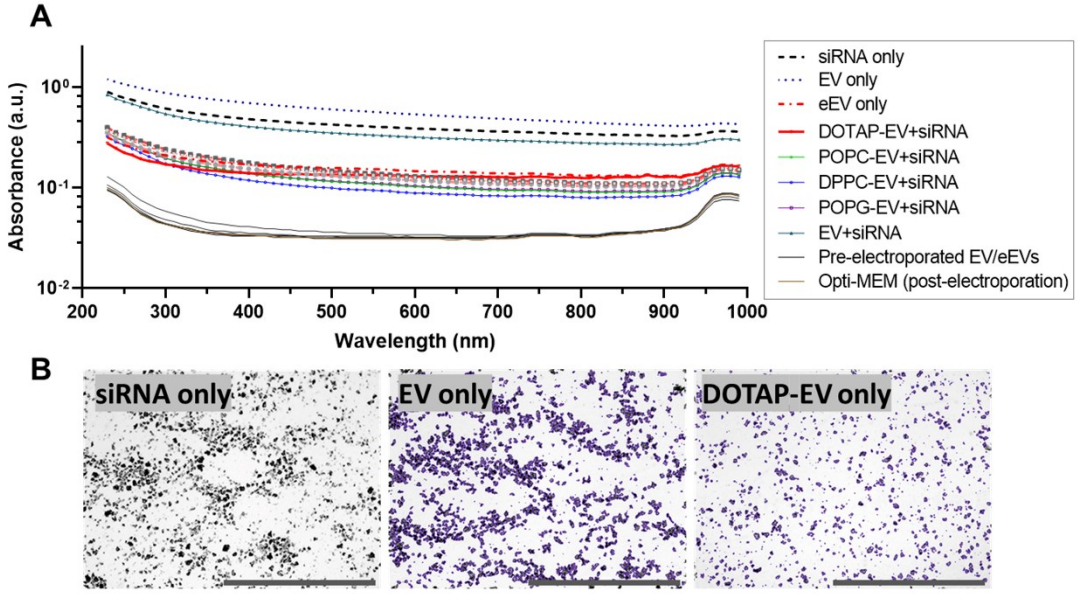

Figure S16 Characterization of aggregation by spectroscopic assays and microscopy image analysis. (A) Absorption spectra of siRNA (1 ng/µl) and EV/eEV (10^{10}-10^{11} vesicles/ml) in Opti-MEM after electroporation. (B) Image analysis of submicron aggregates in Opti-MEM media after electroporation processes. 10-fold diluted concentration from the initial concentration (Initial concentration: EV/eEV: 10^{10} – 10^{11} particle/ml; siRNA: 1 ng/µl). Purple outline shapes (pictures of EV only and DOTAP-EV only) indicated the boundary of objects defined by image analysis. 5000 for bright field intensity and particle size range of 0.5 to 100 µm were applied as thresholds to distinguish between background and particles using the build-in image analysis in a Cytation 5. Scale bar: 1000 µm. Reprinted with permission from © 2020 Elsevier from Jhan *et al*.[209]

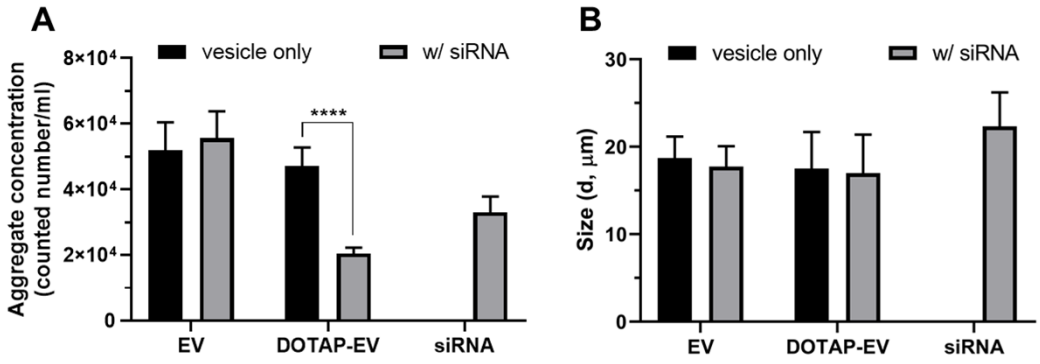

Figure S17 Quantification of aggregation by microscopy image analysis (A, B) show the semi-quantitative particle counts per ml and aggregate size (diameter) quantified by applying image analysis to digitized optical micrographs. Reprinted with permission from © 2020 Elsevier from Jhan *et al*.[209]

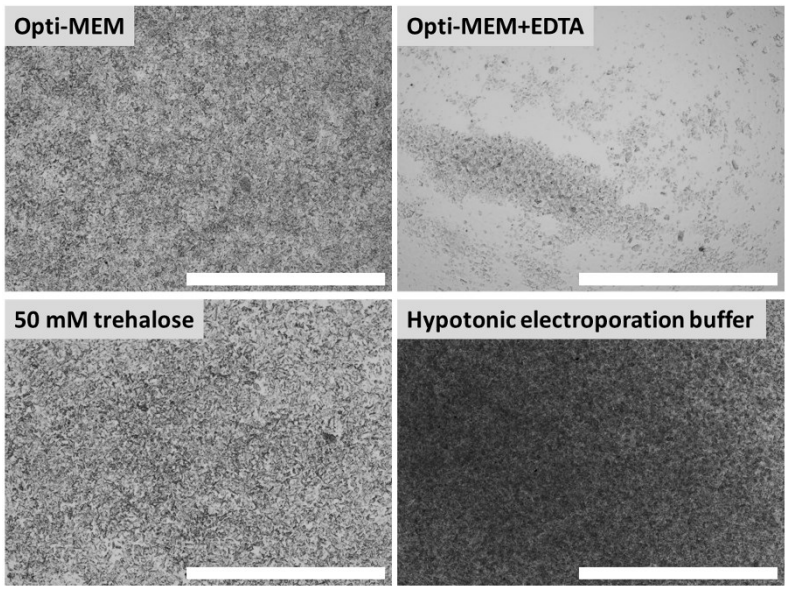

Figure S18 Visualization of submicron aggregates by microscopy images. POPG-EV (10^{11} particle/ml) in (A) Opti-MEM, (B) Opti-MEM+EDTA, (C) 50 mM trehalose, and (D) hypotonic electroporation buffer after electroporation. For Opti-MEM+EDTA group, 5mM EDTA was added to the electroporated mixture immediately after electroporation as the protocol from Lamichhane, Raiker and Jay, who reported similar effects can obtain for EDTA addition before and after electroporation.[161] Scale bar: 1000 μm. Reprinted with permission from © 2020 Elsevier from Jhan *et al*.[209]

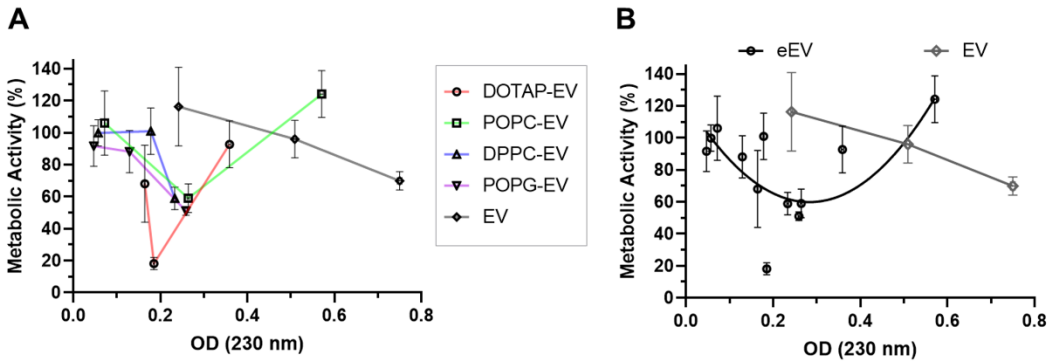

Figure S19 Cell viability of eEVs at different values of turbidity (OD at 230 nm). (A) Cell viability v.s. turbidity of eEV electroporated in various media. (B) Data points of all eEV samples were combined and analyzed by non-linear fitting using a quadratic equation, y= 789.5 x^2-445.5x=123, R^2=0.42. Reprinted with permission from © 2020 Elsevier from Jhan *et al*.[209]

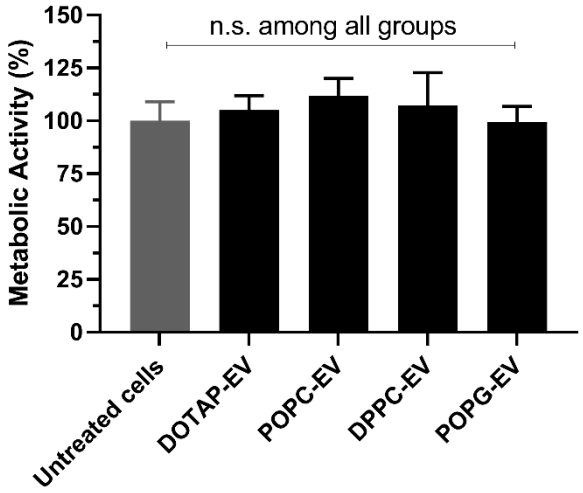

Figure S20 Cell viability of eEVs on CCL-210 cells. eEV in the concentration of 10^{10}-10^{11} vesicles/ml) were used as a single dose in Opti-MEM containing 1 ng/µl siRNA. 5mM EDTA was added to the samples after electroporation. Reprinted with permission from © 2020 Elsevier from Jhan *et al*.[209]

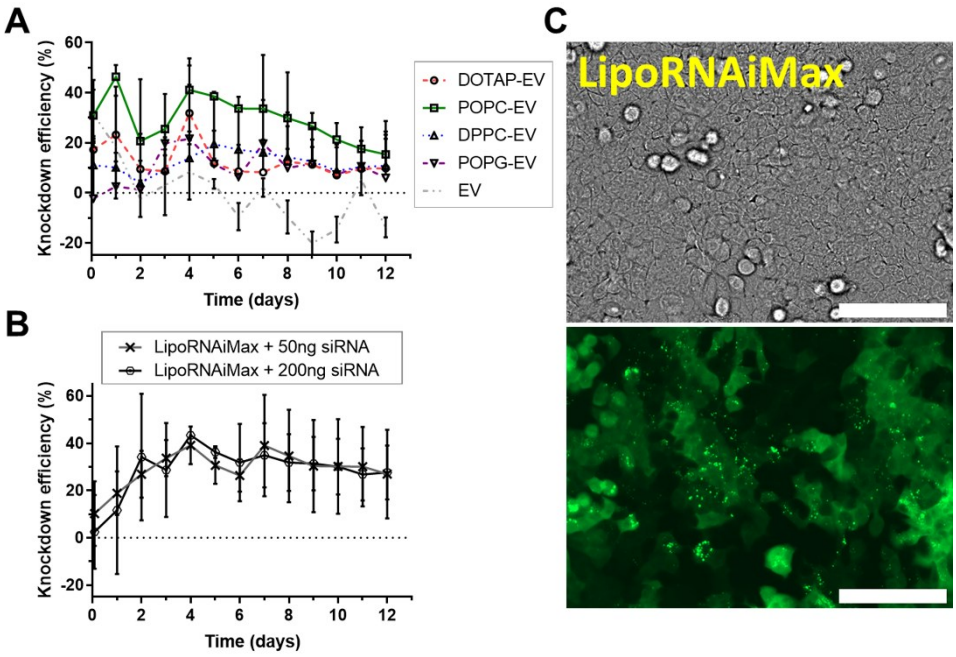

Figure S21 RNA interference knockdown over time in lung tumor cells (A549). (A) Knockdown efficiency of EV and eEV formulations over time in Opti-MEM+EDTA. The data were obtained using 10^{11} vesicles/ml in 100 µl Opti-MEM containing 1 ng/µl siRNA for electroporation. (B, C) Knockdown efficiency of positive control: commercial Lipofectamine RNAiMax over time in Opti-MEM. The formulation of lipofectamine with 50 ng siRNA or 100 ng siRNA was prepared following the manufacturer's instruction. Knockdown efficiency was quantified by green fluorescence using a Cytation 5 plate reader. Fluorescent images showed the delivery of anti-GFP siRNA with eEVs to A549 cells at 3 days post transfection. Scale bar: 100 µm. Reprinted with permission from © 2020 Elsevier from Jhan *et al*.[209]

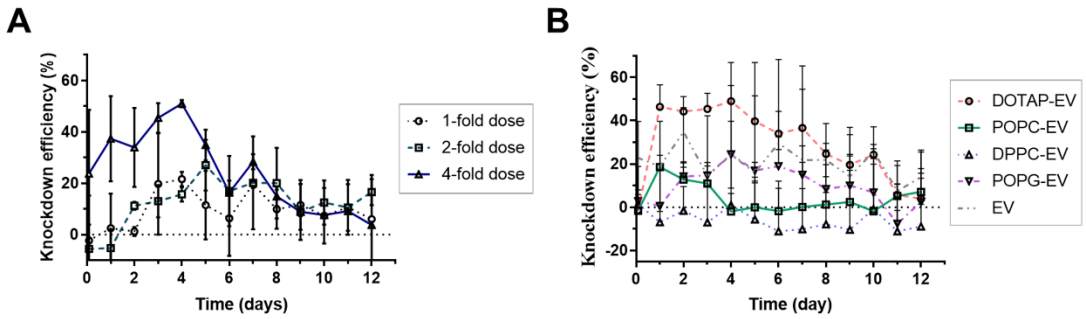

Figure S22 RNA interference knockdown of eEVs over time in lung tumor cells (A549). Knockdown efficiency of (A) POPG-EV with 1 to 4-fold amounts of dose in Opti-MEM (with EDTA addition following electroporation), (B) eEVs in Trehalose electroporation media. Reprinted with permission from © 2020 Elsevier from Jhan *et al*.[209]

APPENDIX B. SUPPORTING INFORMATION OF CHAPTER III

B.1. Graphical Abstract

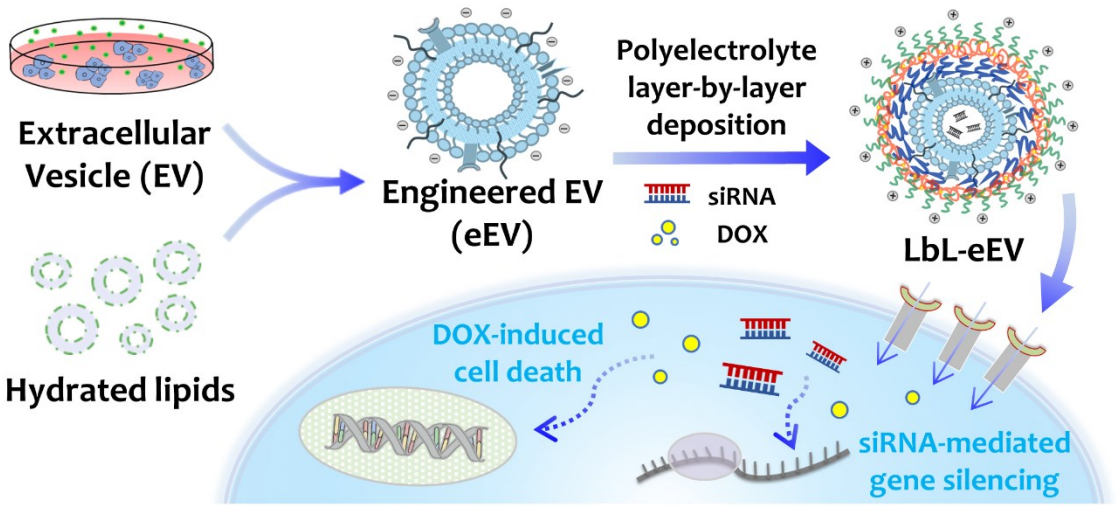

B.2. Experimental Sections

B.2.1. Immuno-gold Labelled Transmission Electron Microscopy

LbL-eEVs (~10^8 particles) aliquots were fixed in 2% paraformaldehyde and stained on a Formvar/carbon-coated copper grid (Electron Microscopy Sciences) following a protocol in previous literature.[186] Briefly, 5 µl of the sample was placed on a grid for 20 min., followed by a repetitive wash procedure for a total of 3 washes. The grid was then transferred to fresh drops of PBS/50 mM glycine to quench free aldehyde groups. For immunogold staining, the grid was then placed onto a drop of blocking buffer (PBS/5%BSA) for 10 min. After 10 min., without washing, the grid was transferred to a

fresh drop of antibody diluent (PBA/1%BSA) with the primary antibody CD63 (4 µg/ml; sc-5275, Santa Cruz) and incubated for 30 min. The grid was then rinsed with PBS and floated on a drop of secondary antibody anti-mouse IgG-gold 10 nm (G7652, Sigma) for 20 min. Subsequently, the sample grid was stained with uranyl-oxalate solution (Thermo Fisher Scientific), followed by methyl cellulose (Sigma) embedding. The sample grid was then allowed to vacuum dry overnight and observed *via* TEM (JEOL 1200EX) under 100 kV of energy and 100,000× to 150,000× magnification.

B.3. Supporting Scheme

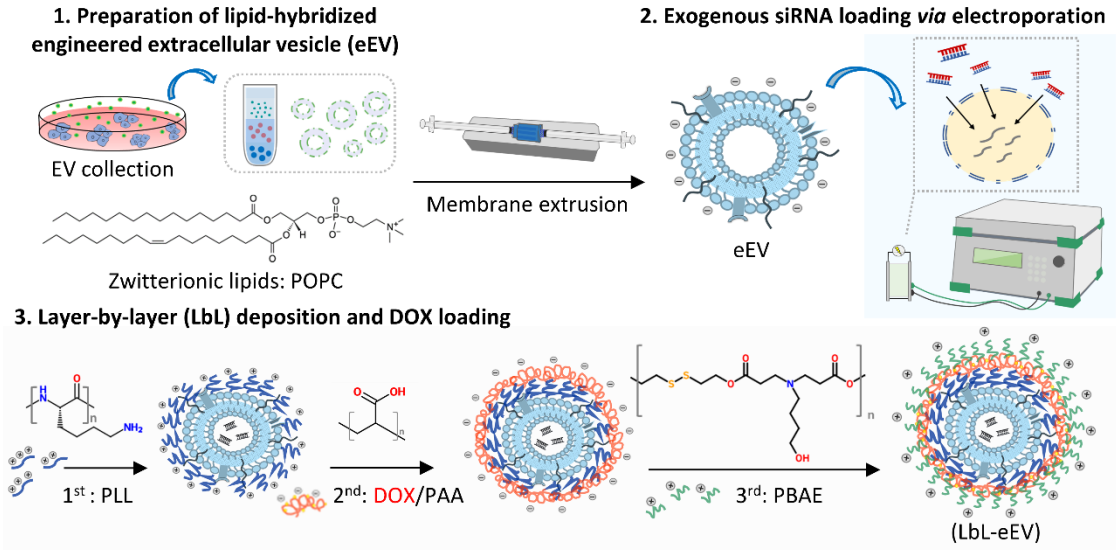

Scheme S1 Diagram illustrating the preparation of layer-by-layer coated engineered extracellular vesicles (LbL-eEVs) containing drug/siRNA complexes. Lipid-hybridized engineered extracellular vesicle (eEV) developed from our previous work,[209] serves as the core for siRNA loading. Tri-layered shell assembly of polyelectrolytes formed by LbL deposition, serves as the carrier for DOX loading. 1st layer: cationic poly (L-lysine) (PLL); 2nd layer: anionic poly (acrylic acids) (PAA); 3rd layer: Poly (β-amino ester)s (PBAE). PBAE was used in the final layer of polymer deposition to facilitate endosomal release.

B.4. Supporting Figures (S1-S6)

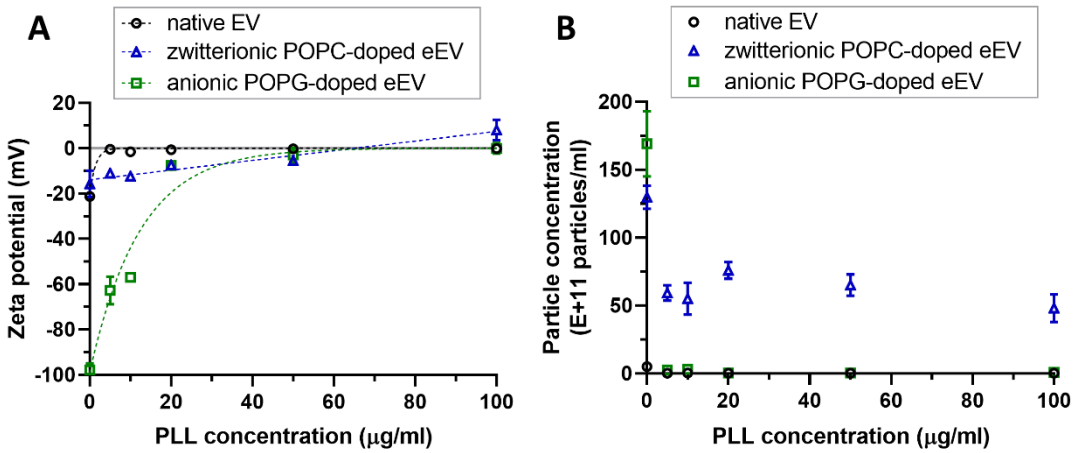

Figure S1 Preliminary tests of PLL deposition on native EV, zwitterionic POPC-doped eEV and anionic POPG-doped eEV *via* LbL assembly. (A) zeta potential and (B) particle concentration changes with the addition of PLL in the concentration range of 0-100μg/ml.

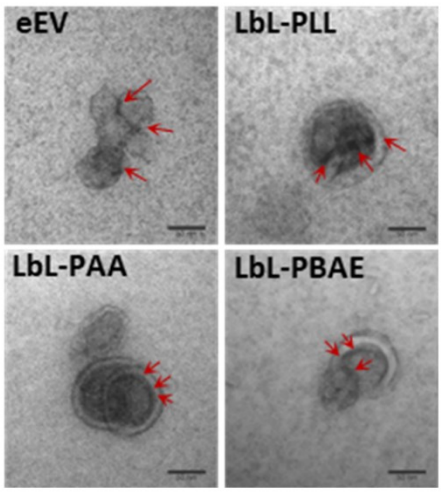

Figure S2 TEM observation of vesicle morphology. Scale bar=50 nm. Black dots indicate the immunogold labeling of CD63 molecules.

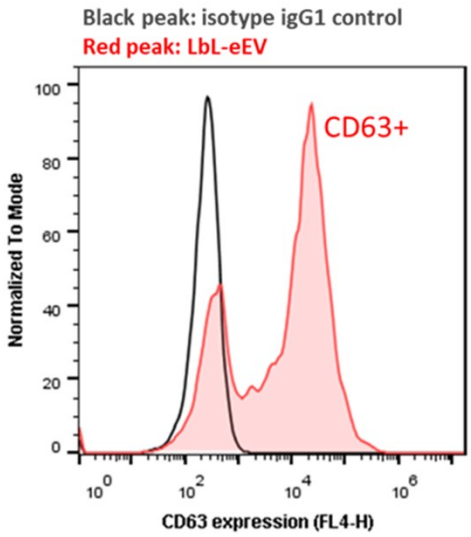

Figure S3 CD63 characterization of LbL-eEV using on bead flow cytometry analysis. LbL-eEV was incubated with 4 µm sulfate-latex beads, followed by protein blocking and anti-CD63-eFluor660 labeling. The histogram reports negative isotype control (black line) and CD63 positive LbL-eEV (red line).

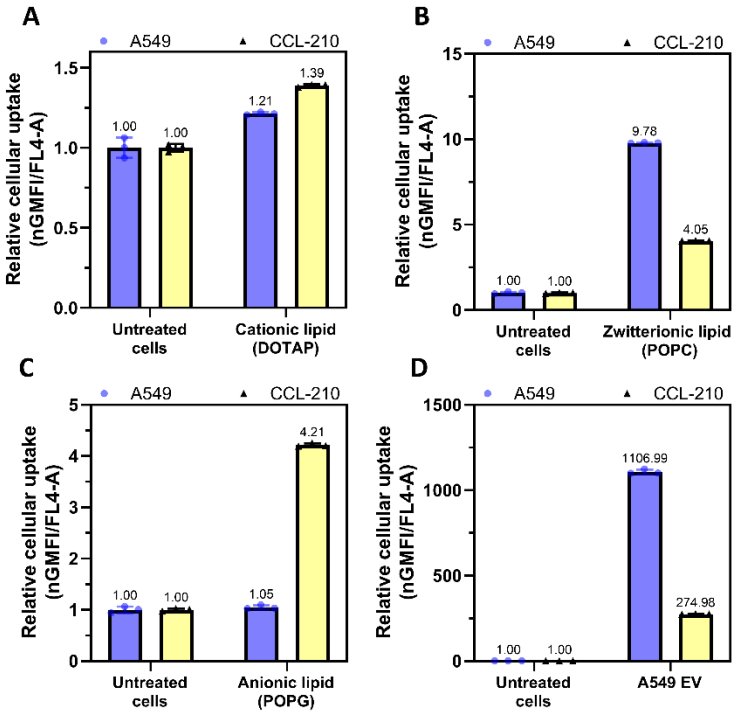

Figure S4 The uptake intensity of A549 cells and CCL-210 after treatment with fluorescence labelled (CellMask DeepRed® dye)-liposomes. (A) cationic DOTAP, (B) zwitterionic POPC, (C) anionic POPG, and (D) anionic A549 EVs for 2 hours at concentration of 1.8×E10 particles/ml. The normalized geometric mean fluorescence intensity was calculated by: $nGMFI = {GMFI_{\text{liposome or EV in A549 or CCL-210}}}/{GMFI_{\text{untreated A549 or CCL-210}}}$. The gene transfection reagent DOTAP liposome and POPG liposome showed a greater amount of vesicle internalization in CCL-210 cells, whereas a higher uptake intensity of POPC liposome was observed in A549 cells. It is worth noting that the preferential uptake of EVs to their parental is likely dose-dependent as discussed in the literature from Xu *et al*.[82] While a 15-fold greater of A549 EV internalization in A549 cells than CCL-210 cells was reported in the previous studies (10^{11} particles/ml), A 4 to 7-fold greater of A549 EV internalization was observed in A549 cells than CCL-210 cells at 10^{9}-10^{10} particles/ml.

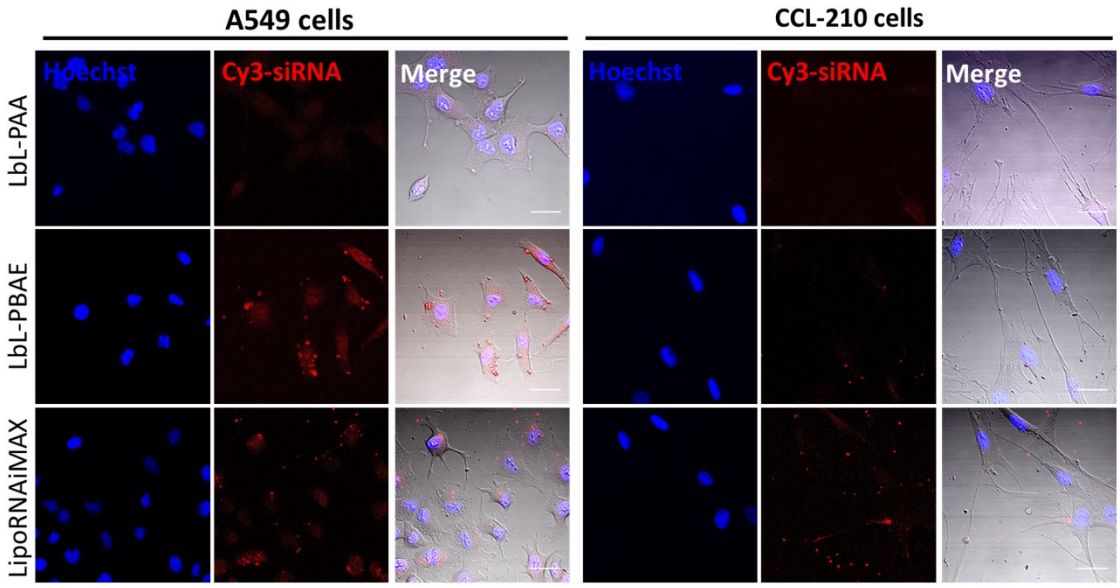

Figure S5 Confocal microscope images of cells treated by different formulations with Cy3-siRNA delivery. Fluorescent images showed Cy3-siRNA in cell cytoplasm. Scale bar: 30 μm.

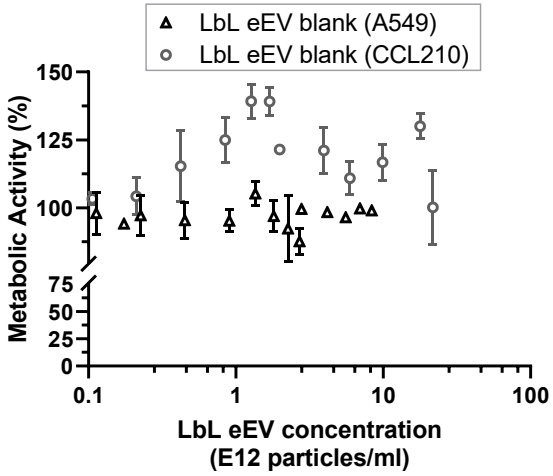

Figure S6 Cell viability of A549 cells and CCL-210 cells incubated with LbL-eEVs at varying concentration for 3 days. The metabolic activity of the cells with different were normalized to untreated A549 or CCL-210 cells.

APPENDIX C. SUPPORTING INFORMATION OF CHAPTER IV

C.1. Supporting Figures (S1-S2)

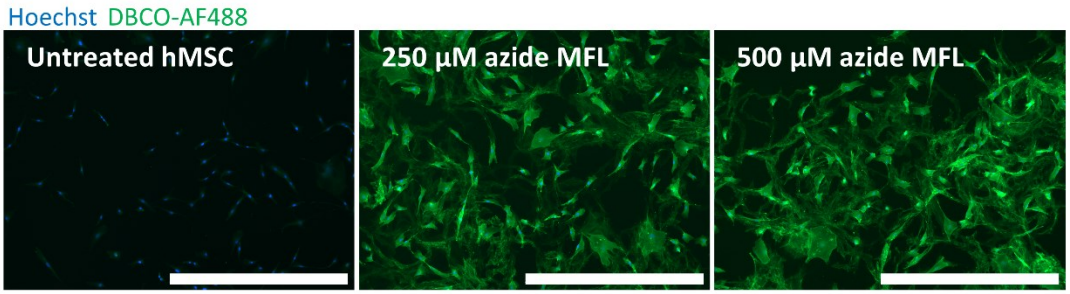

Figure S1 Fluorescent images of DBCO-AF488 labeled hMSC that are presented with azide-containing membrane fusogenic liposomes (MFL) after 30 min. incubation (Scale bar=1000 µm).

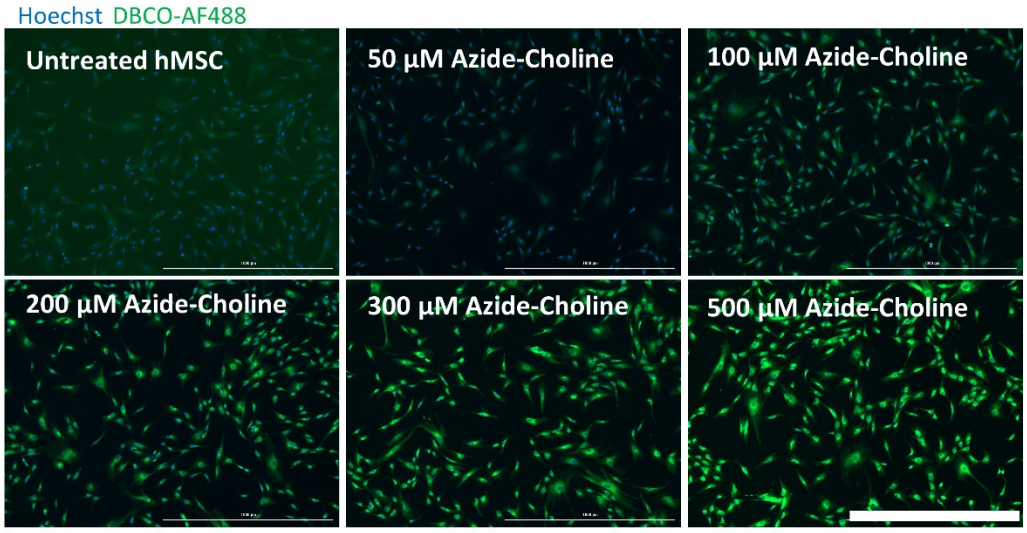

Figure S2 Fluorescent images of DBCO-AF488 labeled hMSC that are incubated with azido-choline (50-500 µM) after 2-day incubation (Scale bar=1000 µm).